Reliability Analysis of Industrial Physical Assets

MAXIM BALITKI
(Licenciado em Engenharia Mecânica)

Dissertação para obtenção do grau de Mestre em Engenharia Mecânica, na Área de Especialização de Manutenção e Produção

Orientador:
Doutor José Augusto da Silva Sobral

Júri:
Presidente: Doutor Mário José Gonçalves Cavaco Mendes
Vogais:
Doutor Daniel Augusto Estácio Marques Mendes Gaspar
Doutor José Augusto da Silva Sobral

Dezembro de 2025

Reliability Analysis of Industrial Physical Assets

MAXIM BALITKI
(Licenciado em Engenharia Mecânica)

Dissertação para obtenção do grau de Mestre em Engenharia Mecânica, na Área de Especialização de Manutenção e Produção

Orientador:
Doutor José Augusto da Silva Sobral, ISEL/IPL

Júri:
Presidente: Doutor Mário José Gonçalves Cavaco Mendes, ISEL/IPL
Vogais:
Doutor Daniel Augusto Estácio Marques Mendes Gaspar, ESTG/IPV
Doutor José Augusto da Silva Sobral, ISEL/IPL

Dezembro de 2025

Acknowledgements

This thesis concludes a journey I would not have been able to complete without numerous people's support, generosity, and encouragement, to whom I will always be grateful.

I would like to provide special thanks to my parents for literally giving me everything in life, with immeasurable love and support that inspire me everything I do. I owe them everything.

To my girlfriend, Alina – thank you for your unconditional love, patience and especially for being my biggest supporter. Your support has truly been an anchor during this long process.

I would like to express my gratitude to my PhD supervisor, José Sobral, for his guidance and expertise in this area, which were invaluable to the development of this dissertation.

A special thank you to Navaltik Management (ManWinWin Software) for giving me this opportunity. Without them, this work would have never seen the light of day.

Also, I would like to express my most sincere thanks to Hugo Cardoso and João Marques for taking the time to help selecting the theme of this dissertation.

I also with to thank Pedro Martins and Paulo Lopes, who helped me to iron out all the technical issues with coding in SQL and Python in the self-created program that analyzed the time-to-failure data. Without your help, I would have not made it.

A very special thank you goes to Nuno Malhado, who collaborated on this thesis, but also actively participated in the data gathering that made this study possible. Without him, this research was not realized in the form it has taken – but more than that, without him, it does not exist.

I also would like to explicitly thank Alexandre Frazão who quietly and carefully took time to explain the operations performed by a beamhouse line. His clarity and generosity were in fact critical in my understanding of the practical context of this investigation.

To everybody who has somehow contributed to this journey – Thank you. This accomplishment and experience belong to you as much as it belongs to me.

Statement of integrity

I declare that this dissertation is the result of my personal and independent research. Its content is original, and all sources listed in the bibliographic references were consulted and are duly mentioned in the text. I further declare that all scientific and technical references relevant to the development of the work are duly cited and included in the bibliographic references.

The author

Lisbon, December 9th, 2025

Análise de Fiabilidade de Ativos Físicos Industriais

Resumo

Esta dissertação de mestrado dedica-se ao estudo e análise de fiabilidade de ativos físicos industriais, com ênfase na linha de curtume de uma empresa de produção de couro.

A investigação visa analisar e modelar a vida (e os seus parâmetros) de ativos físicos críticos via distribuições estatísticas; traçar conclusões sobre a fase de vida dos equipamentos e melhorar os indicadores de fiabilidade do sistema com auxílio a estratégias de redundância.

Através do histórico de avarias dos diversos elementos da linha de curtume, extraíram-se os tempos até às falhas (TTF) via um código escrito em Python pelo autor. Este algoritmo permite conectar-se à base de dados SQL, onde se encontra tabelado o histórico de manutenção, e efetuar os cálculos necessárias para o estudo de fiabilidade. Os dados considerados têm como data de início o ano de 2021 para as pinças de transporte, tapete transportador e máquina de dividir e 2019 para a máquina de descarna.

Foi aplicada a distribuição de Weibull de 2 parâmetros para os quatro ativos, validada pelo teste de chi-quadrado. Concluiu-se que os quatro equipamentos se encontravam na fase de vida "mortalidade infantil", apesar de, conceptualmente, ultrapassarem já esta fase. A razão para tal fenómeno pode estar escondido na possibilidade de os equipamentos estarem a resistir a esta transição (de mortalidade infantil para vida útil), devido a reparações imperfeitas.

Com respaldo a funções principais da fiabilidade, determinaram-se, para cada ativo, a probabilidade de sucesso a 50, 100, 150, 300 e 500 horas e o tempo médio entre avarias (MTBF). Na medida em que os bens, configurados em série, apresentavam valores de fiabilidade relativamente baixos, foram apresentados quatro modelos de redundância (paralelo ativo, paralelo-série, paralelo *standby* e paralelo *standby*-série), que permitiram incrementar os resultados.

Palavras-chave: Fiabilidade, curtume, distribuições de vida, MTBF, redundância

Reliability Analysis of Industrial Physical Assets

Abstract

This master's dissertation is dedicated to the study and reliability analysis of industrial physical assets, with an emphasis on the beamhouse line of a leather production company.

The research aims to analyze and model the life (and its parameters) of critical physical assets using statistical distributions; draw conclusions about the life-cycle phase of the equipment; and improve the system's reliability indicators through redundancy strategies.

Using the repair history of various elements in the beamhouse line, the times to failure (TTF) were extracted via Python code written by the author. This algorithm connects to the SQL database, where the maintenance history is stored, and performs the calculations required for the reliability study. The data considered start in 2021 for the transport clamp machine, conveyor belt and lime splitting machine, and in 2019 for the fleshing machine.

A 2-parameter Weibull distribution was applied to the four assets and validated through the chi-square goodness-of-fit test. It was concluded that the four pieces of equipment were in the infant mortality life phase, despite, theoretically, having already surpassed this stage. The reason for this phenomenon may lie in the possibility that the equipment is resisting this transition (from infant mortality to useful life) due to imperfect repairs.

Based on fundamental reliability functions, the probability of success at 50, 100, 150, 300 and 500 hours, and the mean time between failures (MTBF) were determined for each asset. Since the assets, which follow a series configuration, showed low reliability values, four redundancy models (parallel system, parallel-series, standby system and standby-series) were presented to improve the results.

Keywords: Reliability, Beamhouse line, lifetime distributions, MTBF, redundancy

List of Symbols and acronyms

Roman alphabet

A^2	*Anderson-Darling statistic test*
C	*confidence level*
D	*Kolmogorov-Smirnov test statistic*
F	*cumulative density function*
m	*mean life*
R	*reliability function*
P	*probability of any event*
t	*operating time*
Z	*number of standard deviations from the mean*

Greek alphabet

α	*confidence level complement / significance level*
β	*shape parameter*
Γ	*gamma function*
γ	*location parameter*
η	*scale parameter*
θ	*generic parameter*
λ	*failure rate*
μ	*mean value*
v	*number of degrees of freedom*
σ	*standard deviation*
Φ	*cumulative density function of a normal / lognormal distribution*
X^2	*chi-square value*

Acronyms

CDM	*Conditional Decomposition Method*
CDF	*Cumulative Density Function*
CVM	*Cramer-von Mises statistic*
EDF	*Empirical Distribution Function*
GOD	*Goodness Of Fit*
LDA	*Life Data Analysis*
MLE	*Maximum Likelihood Estimate*
MTBF	*Mean Time Between Failures*

MTTF	*Mean Time To Failure*
pdf	*Probability Density Function*
PLC	*Programmable Logic Controller*
RBD	*Reliability Block Diagram*
TTF	*Times To Failure*

Contents

List of figures

List of tables

1.Introduction

1.1 Scope

The scope of this thesis encompasses the reliability analysis of industrial physical assets, focusing on applying reliability engineering principles to determine the probability and capability of parts, components and systems to perform their required functions under specified conditions, during a determined time interval.

The analysis will be carried out on the beamhouse line of a leather producing company. The beamhouse operations include soaking, liming, and removal of extraneous tissues, such as unhairing and fleshing.

This research will study the life characteristics of the critical components that compose the beamhouse line. This includes the probability of failure and success according to the specified required functions, environmental conditions, and the mission duration; and the mean time between failures (MTBF) of the assets and the system itself.

Reliability analysis provides a systematic approach to understanding and reducing the risks associated with equipment failure. The principles of reliability may be applied systematically to enhance the performance of the longevity of the organization’s assets, by optimizing maintenance schedules, and reduce operational costs.

1.2 Motivation

As industries seek to improve productivity and competitiveness, the reliability of physical assets is critical to performing uninterrupted operational activity and to performing at optimal levels. This is especially the case in the leather industry, which is a process intensive sector, where the failure of critical assets may result in production disruptions and financial losses.

The beamhouse line is crucial to leather manufacturing and includes soaking, liming and dehairing processes required to prepare raw hides for additional treatment. Due to beamhouse’s prominence in the production process, a breakdown will delay other

downstream processes, increasing downtime and maintenance costs and thus, lowering output.

This study is further driven by a real-world application: the beamhouse line of a producing-leather company, which generously provided detailed operational data for analysis. The collaboration with this company displays the applied value of the research, as it will enable targeted, strategic improvements in reliability of their production processes. In addition, the results of this study have the capability to act as a template for reliability improvements in other industrial contexts.

From an academic perspective, this research looks into reliability engineering by exploring its applications in a relatively under-researched domain. While reliability analysis has been extensively applied in sectors such as maritime, aerospace, and automotive manufacturing, its implementation in traditional industries like leather production remains limited.

Ultimately, this research is motivated by the convergence of practical and theoretical implications: the need to determine the reliability and life-characteristics of the beamhouse line for the leather-producing company, and the opportunity to apply the reliability engineering principles to a new industrial domain.

1.3 Objectives

The primary objective of this study is to develop a mathematical and statistical model for the items of the beamhouse line and for the overall system. This model aims to characterize the life cycle of critical assets involved in the production process of a leather manufacturing company.

By employing this model, it will be possible to determine whether these assets are at the beginning of their life cycle, within their useful life, or approaching the wear out phase.

Moreover, based on the life cycle characteristics of equipment that constitutes the line, the analysis will yield insights regarding maintenance activities. In particular, it will provide guidance on the optimal frequency of predetermined maintenance activities.

Ultimately, a key goal of this thesis is to determine the reliability of the system and of each piece of equipment at 50, 100, 150, 300 and 500 hours. These results will support meaningful conclusions and help quantify the potential for performance improvement.

1.4 Document’s structure

Chapter 1 provides information regarding the objectives, goals, scope and motivation of this study.

Chapter 2 combines a number of unique reliability analysis carried out using Weibull, exponential, normal and lognormal distributions.

Chapter 3 covers, initially, the history of reliability engineering. Moreover, throughout the chapter, reliability is covered in big detail: lifetime distributions (most frequently used: exponential, Weibull, normal and lognormal distribution), confidence levels (beta-binomial, Fisher's matrix and likelihood ratio bounds) , goodness of fit (GOF) tests (chi-square, Kolmogorov-Smirnov, Cramér-von Mises, Anderson-Darling and correlation coefficient) and system's reliability (series, parallel, stand-by, complex, and *k*-out-of-*n* configurations).

Chapter 4 applies the theoretical concepts of reliability engineering to a beamhouse line of a leather-producing company, determining fundamental functions of each piece of equipment, reliability of the overall system and suggesting potential performance improvements.

2. State of the art

Reliability analysis represents the study of lifetimes that can be employed on various items and equipment. For example, a general exponential distribution was applied to electronic device [1], under different voltage levels.

The paper by Lemes *et al.* [2] demonstrates the application of exponential distribution in the reliability analysis of electronic equipment based on warranty failure data (Figure **2**.**1**), in particular telecommunication equipment motherboards . Specifically, it uses this distribution to model the time to failure for electronic components, which is common in reliability assessments due to random nature of failures. The method facilitates the estimation of the failure parameter, allowing the calculation of reliability functions.

		Month 1	Month 2	Month 3	Month 4	Month 5	Month 6
Month 1	699	0	1	3	6	6	7
Month 2	1863		3	5	13	10	6
Month 3	1214			1	6	11	8
Month 4	1582				0	2	5
Month 5	1075					0	2
Month 6	1347						0

Figure 2.1 - Monthly production lot and reported failures in the analysis period **[2]**.

Figure **2**.**1** represents the number of lots produced every month (table on the left side) and the number of reported failures (scheme on the left side), until the end of the warranty period.

Ehlich *et al.* [3] presents a case study on applying reliability measurement to a large-scale software system, specifically Remote Measurement System-Digital 1 (RMS-D1) at AT&T Bell Laboratories. The study focuses on using reliability modeling to determine when to stop testing during the system's development. The authors employed an empirical approach, analyzing failure data collected during the system's load testing phase. This involved a controlled load test simulating real-world usage patterns. They used an exponential nonhomogeneous Poisson process model to analyze the failure

data and predict future reliability. This model assumes that the failure rate decreases exponentially over time as faults are connected. The model's parameters were estimated using maximum likelihood estimation and regression analysis. The study found that the exponential model provided a reasonably good fit to the failure data, particularly after 60% of the load testing was complete. The authors used the model to estimate the failure rate at different points in the testing process and to predict the additional testing time required to reach a target reliability level (Figure **2**.**2**).

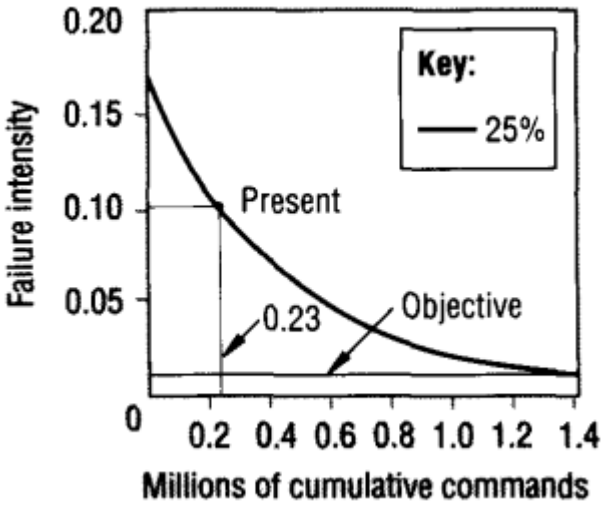

Figure 2.2 - Applying the exponential nonhomogeneous Poisson process model to RMS-D1's load test at 25% into load test, the estimated failure intensity is 0,110 failures per command executed [3].

Figure **2**.**2** displays the failure rate, measured as failures per command executed, plotted against millions of cumulative commands for the RMS-D1 system at 25% completion of its load test. The graph shows a failure intensity significantly higher than the target objective of 0,010. The observed failure intensity at this point is approximately 0,110, indicating a need for continued testing and debugging before the system reaches the desired reliability level. The visual representation clearly demonstrates the inadequacy of the system's reliability at this early stage of testing.

Ahmed *et al.* [4] presented a case study of reliability analysis of ATM machines in Sudan. Among common types of faults in ATM, this study only considered data of out of journals. The authors found that all five machines selected had a constant failure rate (Figure **2**.**3**), which meant that the times to failure (TTF) follow an exponential distribution lifetime.

Code	Masseur	Time/hour						
		0	24	48	72	96	120	144
B3	R(t)	1	0.63885	0.40813	0.26074	0.16657	0.10642	0.06798
	h(t)	0.01867	0.01867	0.01867	0.01867	0.01867	0.01867	0.01867
	Cum.h(t)	0.00	0.44808	0.89616	1.3442	1.7923	2.2404	2.6885
B5	R(t)	1.00	0.7124	0.50824	0.36233	0.25831	0.18415	0.13128
	h(t)	0.0141	0.0141	0.0141	0.0141	0.0141	0.0141	0.0141
	Cum.h(t)	0.00	0.3384	0.6768	1.0152	1.3536	1.692	2.0304
B13	R(t)	1.00	0.61819	0.38216	0.23625	0.14605	0.09028	0.05581
	h(t)	0.02004	0.02004	0.02004	0.02004	0.02004	0.02004	0.02004
	Cum.h(t)	0.00	0.48096	0.96192	1.4429	1.9238	2.4048	2.8858
B22	R(t)	1.00	0.60672	0.36811	0.22334	0.13551	0.08222	0.04988
	h(t)	0.02082	0.02082	0.02082	0.02082	0.02082	0.02082	0.02082
	Cum.h(t)	0.00	0.49968	0.99936	1.499	1.9987	2.4984	2.9981
B35	R(t)	1.00	0.67689	0.45819	0.31014	0.20993	0.1421	0.09619
	h(t)	0.01626	0.01626	0.01626	0.01626	0.01626	0.01626	0.01626
	Cum.h(t)	0.00	0.39024	0.78048	1.1707	1.561	1.9512	2.3414

Figure 2.3 - Results of reliability model test of machines (adapted from **[4]**).

Figure **2.3** shows the failure rate of the five ATM at different time periods. It is observed that over time, the hazard rate remains constant, which is characteristic of the exponential distribution. Besides that, the figure depicts the reliability function, which is decreasing over time.

Pham [5] mentions various studies where Weibull distribution was applied for reliability analysis. In particular, failure of brittle and composite materials, yield strength of steel, fatigue life of steel (Figure **2.4**); pitting corrosion in pipes, fracture strength of glass (Figure **2.5**) and adhesive wear in metals.

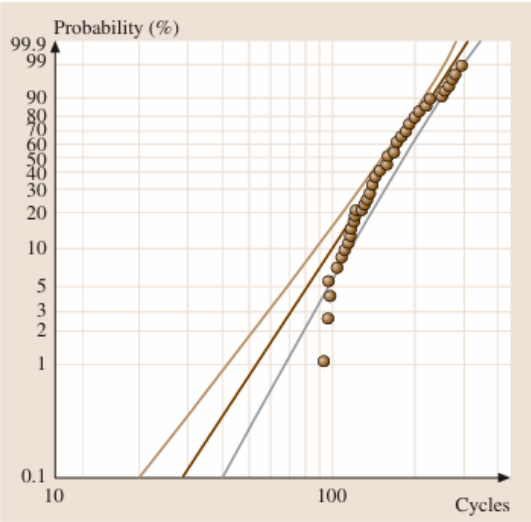

Figure 2.4 - Weibull probability plot for alloy T7987 fatigue life **[5]**.

Figure **2.4** illustrates the fit of Weibull distribution for modeling the lifetime of T7987 alloy under fatigue conditions. The investigation considered 67 specimens of the alloy that failed before having accumulated 300 thousand cycles of testing [6].

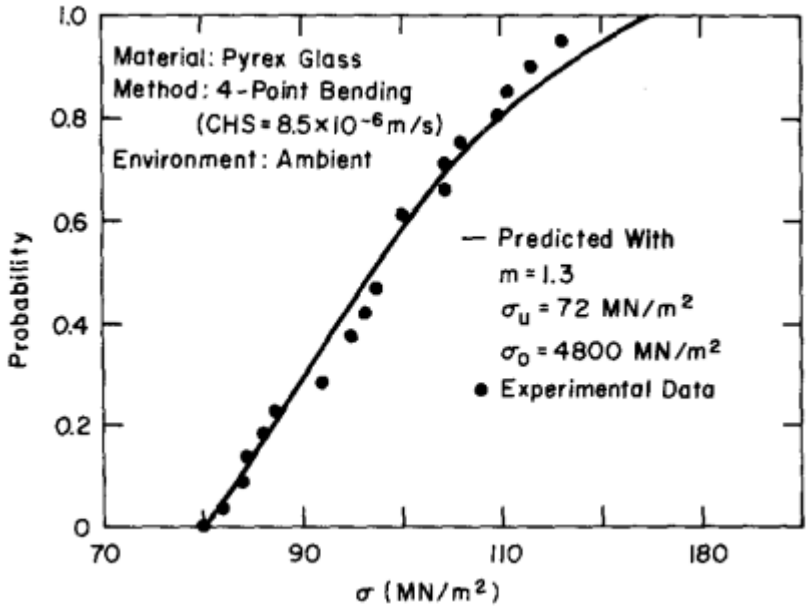

Figure 2.5 - Comparison of the experimental values of probability versus fracture stress from bend tests with those calculated using the Weibull distribution function **[7]**.

Figure **2.5** presents a validation of the Weibull distribution model for predicting fracture probability in Pyrex glass specimens subjected to bend testing. The graph plots cumulative probability of fracture against applied stress (σ) ranging from 70 to 180 MN/m^2, where experimental data points (solid circles) are compared with the theoretical Weibull distribution curve (solid line). The experimental data exhibits the characteristic S-shape behavior expected from brittle fracture statistics, with fracture probability increasing from near zero at lower stresses to approaching unity at higher stress levels. The close correspondence between experimental measurements and the Weibull prediction demonstrates the validity of using this statistical framework to model the inherent variability in glass strength due to random flaw distributions. This agreement supports the fundamental assumption that fracture initiation in brittle materials follows Weibull statistics, thereby providing confidence in the derived Weibull parameters (m – shape parameter, σ_u – characteristic parameter and σ_o – scale parameter) for subsequent analysis and engineering applications.

Furthermore, Weibull distribution has been used as a model in diverse disciplines to study many different issues, such as geophysics, food science, social science, environment, nature and medical science (Figure **2.6**) [5].

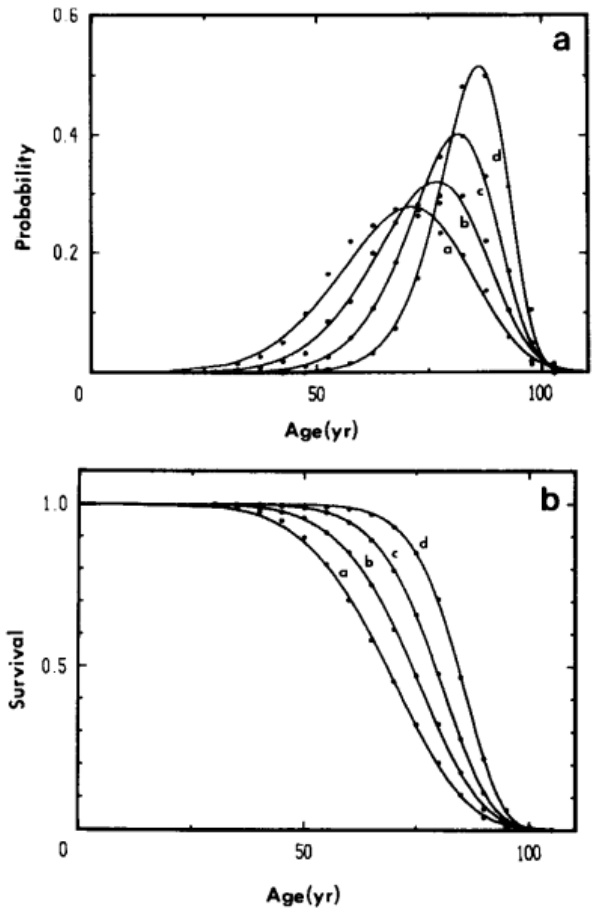

Figure 2.6 - Four population-adjusted causes of death (·) and their best fitting Weibull functions. (a) Probability density representation. (b) Survivorship representation **[8]**.

Juckett and Rosenberg [8] demonstrated that human disease-specific mortality patterns follow a discrete, integer-based Weibull law characterized by periodic clustering of shape and scale parameters, suggesting that age-related death is governed by quantized biological mechanisms rather than continuous stochastic processes across different populations and causes of death. Figure **2.6** demonstrates the effectiveness of Weibull functions in modeling cause-specific mortality distributions through two complementary visualizations. Panel (a) presents the empirical mortality data as probability density functions, where each curve represents the normalized frequency of deaths at specific ages for different disease categories, typically exhibiting unimodal, right-skewed distributions that reflect the varying age patterns of disease-specific mortality. Panel (b) transforms these same data into reliability curves, illustrating the cumulative probability of survival beyond each age and providing insight into the timing and progression of mortality risk across the lifespan.

Dolas *et al.* [9] presented a comprehensive reliability analysis of diesel engines using the two-parameter Weibull distribution, demonstrating its effectiveness as a statistical model for failure prediction and maintenance planning. The research employs maximum likelihood estimation techniques to determine the shape and scale parameters from

empirical failure data collected from twenty diesel engines under operational conditions. The study validates the Weibull model's capability to accurately represent failure patterns, enabling the derivation of critical reliability metrics including survival probability functions, failure rate functions, and unreliability estimates (Figure **2**.**7**).

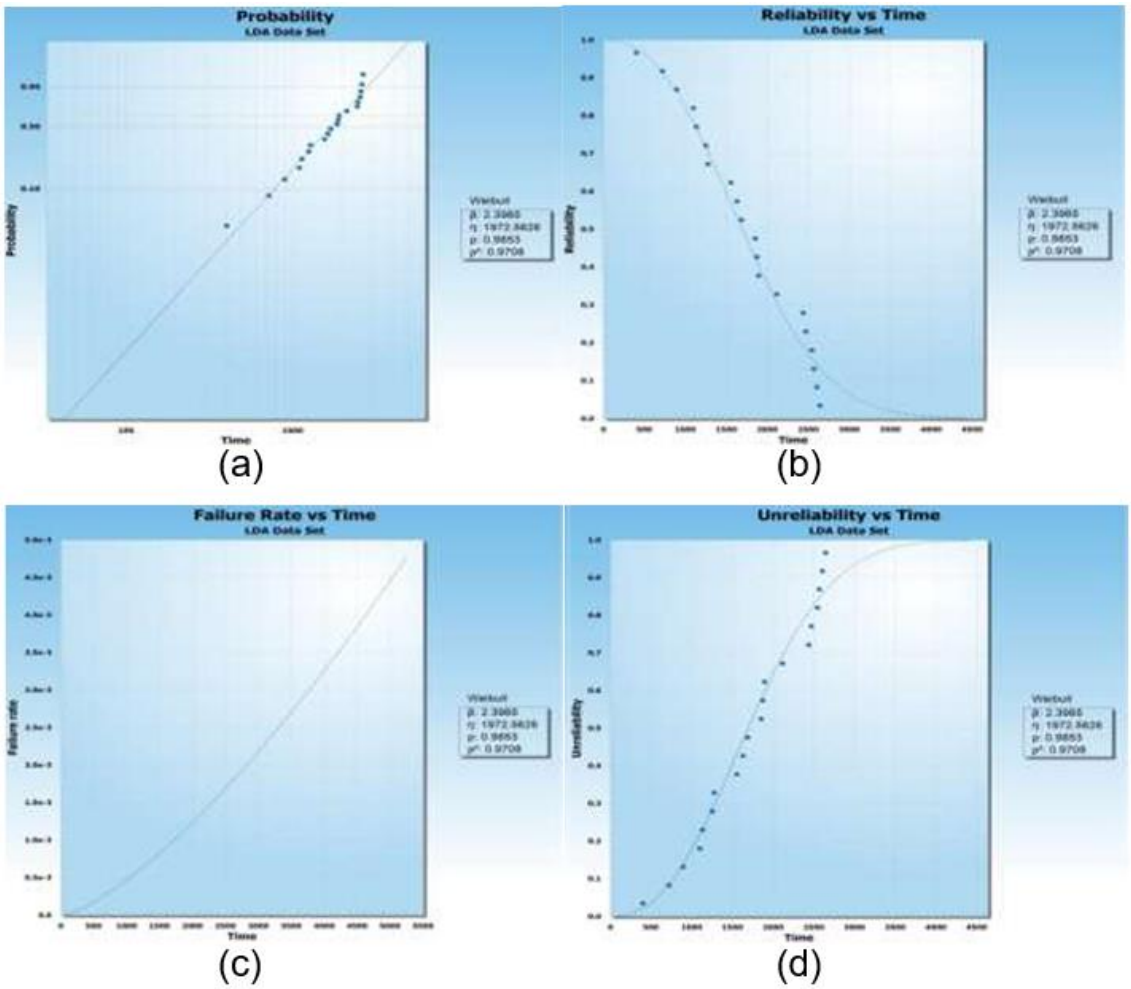

Figure 2.7 - (a) Weibull probability plot. (b) Reliability Vs Time plot. (c) Failure rate Vs Time plot. (d) Unreliability Vs Time plot **[9]**.

The four graphs illustrated in Figure **2**.**7** provide a comprehensive visual validation of the Weibull distribution's applicability to diesel engine failure analysis. Figure **2**.**7** (a) displays the Weibull probability plot, where empirical failure data points align approximately along a straight line against the theoretical Weibull distribution. Figure **2**.**7** (b) illustrates the reliability versus time relationship, showing a monotonically decreasing curve that represents the probability of engine survival without failure, starting from unity and asymptotically approaching zero as operational time increases. Figure **2**.**7** (c) presents the failure rate over time, revealing the temporal evolution of failures, or wear-out patterns characteristic of aging systems. Figure **2**.**7** (d) complements the reliability analysis by depicting unreliability versus time, showing an increasing curve that approaches unity, representing the cumulative probability of failure occurrence.

Abramovich and Baburin [10] have looked into failure statistic data of power supply systems' elements for gas pumping compressor stations. The authors have applied the Weibull distribution to determine the life parameters.

Clement and Lasky [11] have presented a study comparing various solder alloys, used in electronics, applying Weibull distribution. Specifically, focusing on lead-free solders such as SAC105, SAC305 and SACM against traditional tin-lead (SnPb) solder (Figure **2.8**).

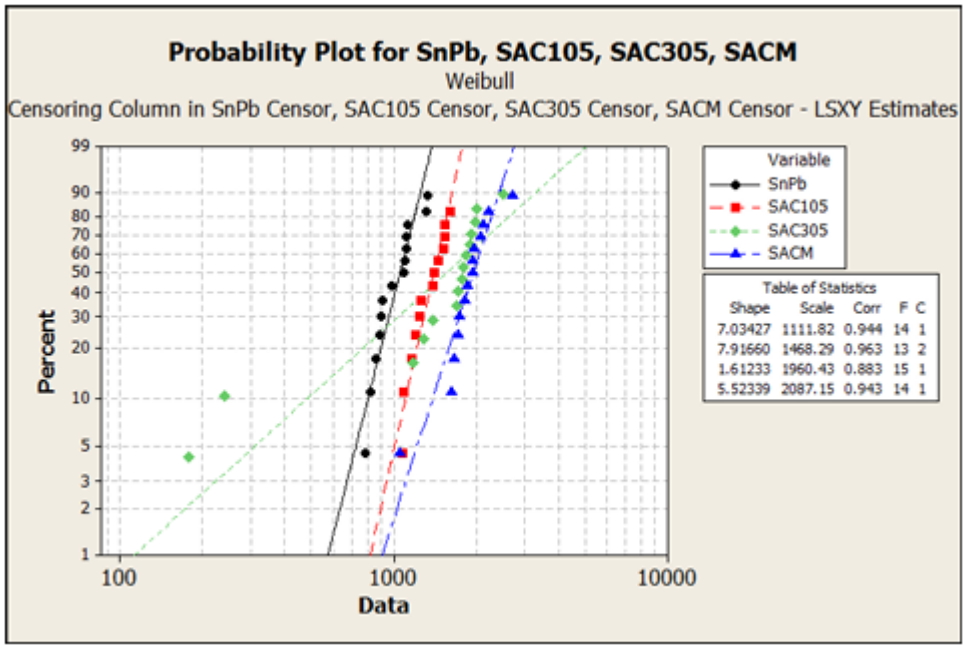

Figure 2.8 - Probability plot for all four variables **[11]**.

Figure **2.8** exhibits Weibull probability plot for all four solder alloys. The plot presents the cumulative failure probabilities of each material under thermal cycling stress, with reliability curves fitted using LSXY estimation methods. The x-axis represents the number of cycles to failure, plotted on a logarithmic scale, while the y-axis indicates the cumulative percentage of failed samples. Among the materials tested, SACM demonstrates the highest scale parameter (η = 2087,15), indicating the longest expected life before failure. It also shows a relatively high shape parameter (β = 5,52), suggesting a predictable wear-out failure pattern. SnPb and SAC105 also exhibit high β values (7,03 and 7,92, respectively), indicating strong reliability and consistency in failure behavior. In contrast, SAC305 has a significantly lower shape parameter (β = 1,61), which implies a higher variability in failures and potential influence from early-life failures.

Reliability analysis of aviation equipment is another example of application of Weibull distribution [12]. This research presents a case study that demonstrates the practical application of Weibull distribution to real-world failure data from aviation equipment,

providing insights into reliability characteristics and maintenance planning. Additionally, the study compares Lognormal and Weibull distributions (Figure **2.9** and Figure **2.10**, respectively) as potential models for analyzing fault data in aviation equipment. Weibull distribution demonstrated flexibility and ability to model varied failure rates, which makes it more suitable for analyzing fault characteristics in aviation equipment.

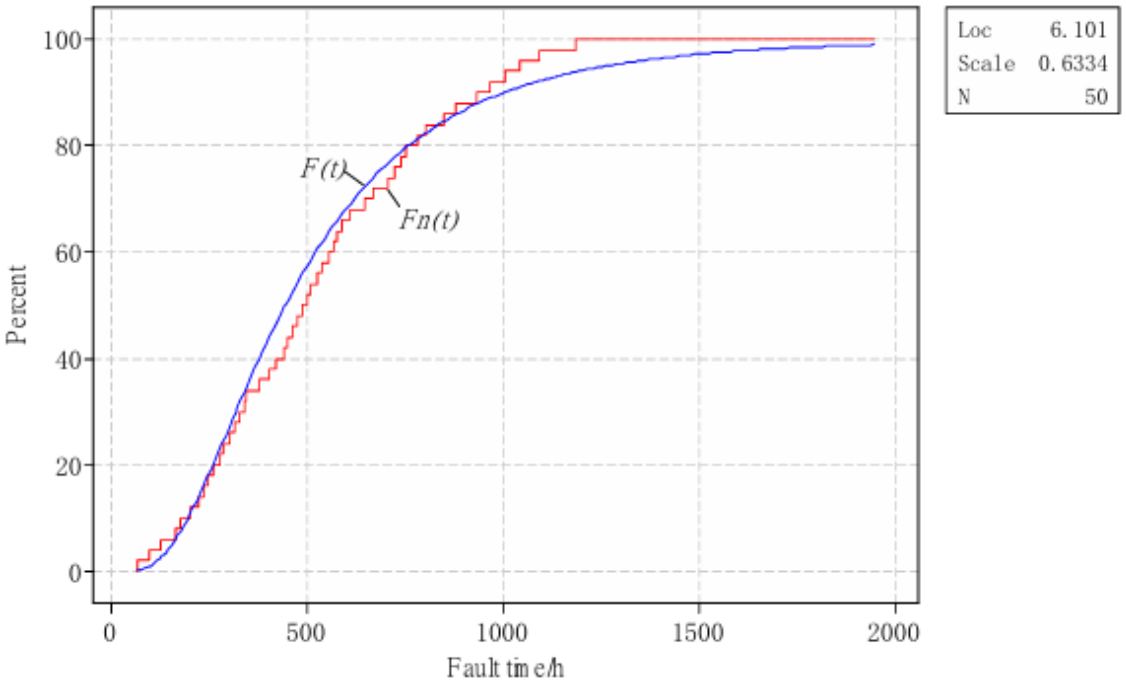

Figure 2.9 - Lognormal empirical cumulative distribution function of fault time **[12]**.

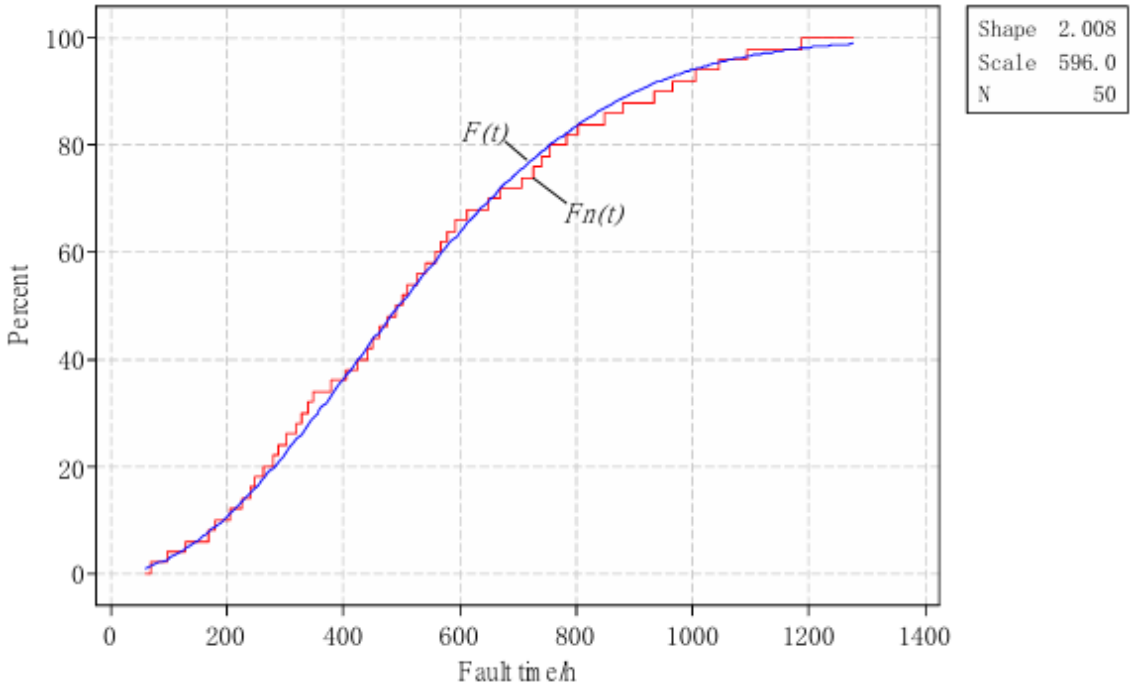

Figure 2.10 - Weibull empirical cumulative distribution function of fault time **[12]**.

Figure **2**.**9** and Figure **2**.**10** present the empirical cumulative distribution function, denoted $F_n(t)$, compared with the fitted theoretical distribution function $F(t)$, for modeling the fault time (in hours) of aviation equipment. Figure **2**.**9** corresponds to the Lognormal distribution, while Figure **2**.**10** illustrates Weibull distribution fit to the same dataset of 50 observations. The lognormal model approximates the general trend of the empirical data, but exhibits visible deviations, especially in the upper tail (above, approximately 1000 hours), where it tends to overestimate the cumulative failure probability. In contrast, the Weibull distribution remains consistently close in both the central and tail regions, indicating that the Weibull distribution effectively captures both the average failure behavior and the variability in early and late failures.

Artyushenko and Bruskov [13] have carried out a research about the application of Weibull distribution on spacecrafts, as it allows to better control the dynamic of parameters change.

Kleyner and Sandborn [14] utilized reliability principles to forecast a model warranty for electronic products of the automotive sector. The study combines various lifetime distributions to model the typical automotive product failure behavior, represented by the bathtub curve. The Weibull distribution is particularly well-suited for capturing the early-life (infant mortality) phase (Figure **2**.**11**) due to its flexibility in modeling decreasing failure rates, whereas the exponential distribution effectively characterizes the constant hazard rate observed during the useful life period. The authors emphasize that although the Weibull distribution is frequently supported as the best-fit model for pre-warranty failure data, in some cases, other distributions like lognormal or normal may be applicable, depending on the nature of the failure data. For instance, lognormal lifetime distribution was chosen when it best represented the daily distribution mileage above 50000 miles. The obtained parameters from the data analysis helped in predicting expected warranty returns and understanding the failure rate trends over time.

Figure **2**.**11** depicts the decline in failure rates during the initial period of product's lifecycle, highlighting the effective applicability of the Weibull distribution with a shape parameter less than one to model the infant mortality phase. The data suggests that this early phase lasts approximately 8 to 18 months, after which plateaus. The figure underpins the importance of distinguishing between the early failure period and the steady-state phase in warranty modeling, advocating for the piecewise statistical approach that combines Weibull for early life and exponential distribution for the subsequent phase.

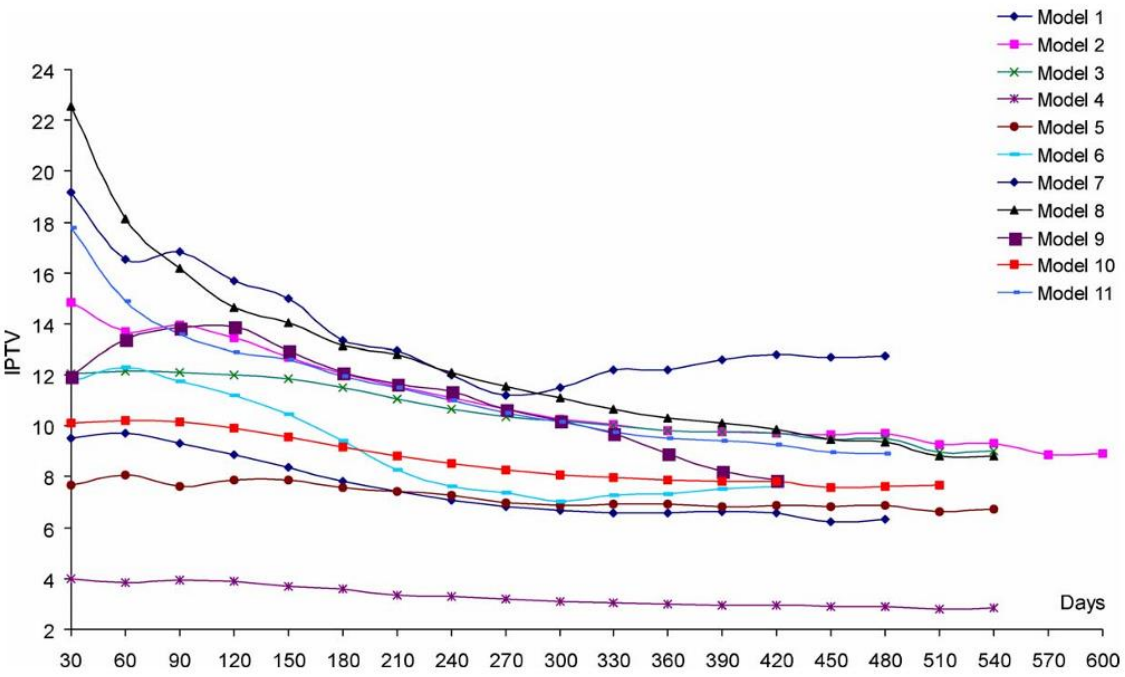

Figure 2.11 - Failure rates expressed in incidents per thousand vehicles (IPTV) for selected passengers compartment mounted electronic products [14].

Another application of lognormal distribution in reliability analysis was presented by Jancić *et al.* [15], by employing it to model the reliability (Figure **2**.**12**) and lifetime of automotive components, specifically vehicle motors. The lognormal distribution is particularly well-suited for this application because it effectively captures the gradual degradation process, and the variability associated with component lifespan over time. Its ability to represent the skewed nature of failure data makes it a preferable choice over other distributions such as the normal distribution, which is less appropriate due to its assumption of symmetry. The study emphasizes that, although other models like the Weibull distribution are widely used in reliability analysis, the lognormal distribution remains advantageous for systems where the failure process is influenced by multiple small factors, which are characteristic of many mechanical components in vehicles. Figure **2**.**12** presents a graphical representation of the reliability function of a specific vehicle component, in this case a Volvo D7C 275, over its travel distance at measuring point M1. The graph illustrates how the reliability of the component decreases as the operational distance increases, providing important insights into its failure behavior over time. This reliability curve is vital for understanding the component's performance throughout its service life and enables the readers to identify the threshold distances at which maintenance or replacements may be necessary, as denoted by $R_a(t)$.

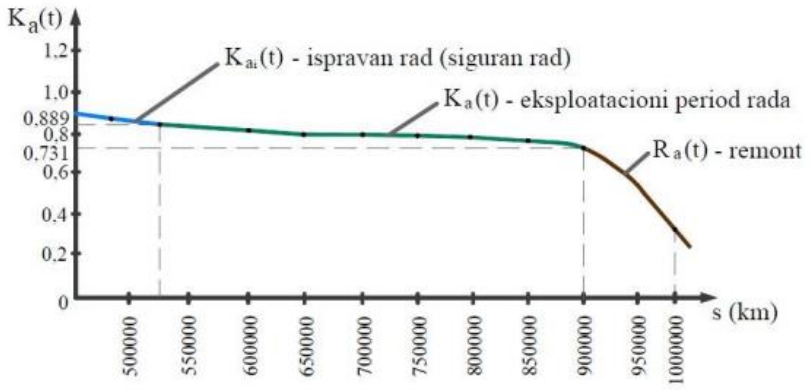

Figure 2.12 - Graph of the shown reliability value of component travel distance in the exploitation area at the measuring point M1 of motor vehicles - Volvo - D7C 275 [15].

The study carried out by Kara *et al.* [16] assesses the reliability of the Konya4 transmission line feeder by analyzing fault data collected over five years (2014-2019). To model the failure times, various lifetime distributions, including Weibull, normal, exponential and lognormal, were evaluated using GOF tests (Figure **2.13**). The results indicated that the lognormal distribution provides the most accurate fit for the fault data, primarily due to its appropriateness in modeling positively skewed failure time data common in reliability analysis. Employing suitable distribution is essential for generating reliable reliability metrics in order to minimize the number of interruptions to perform maintenance activities.

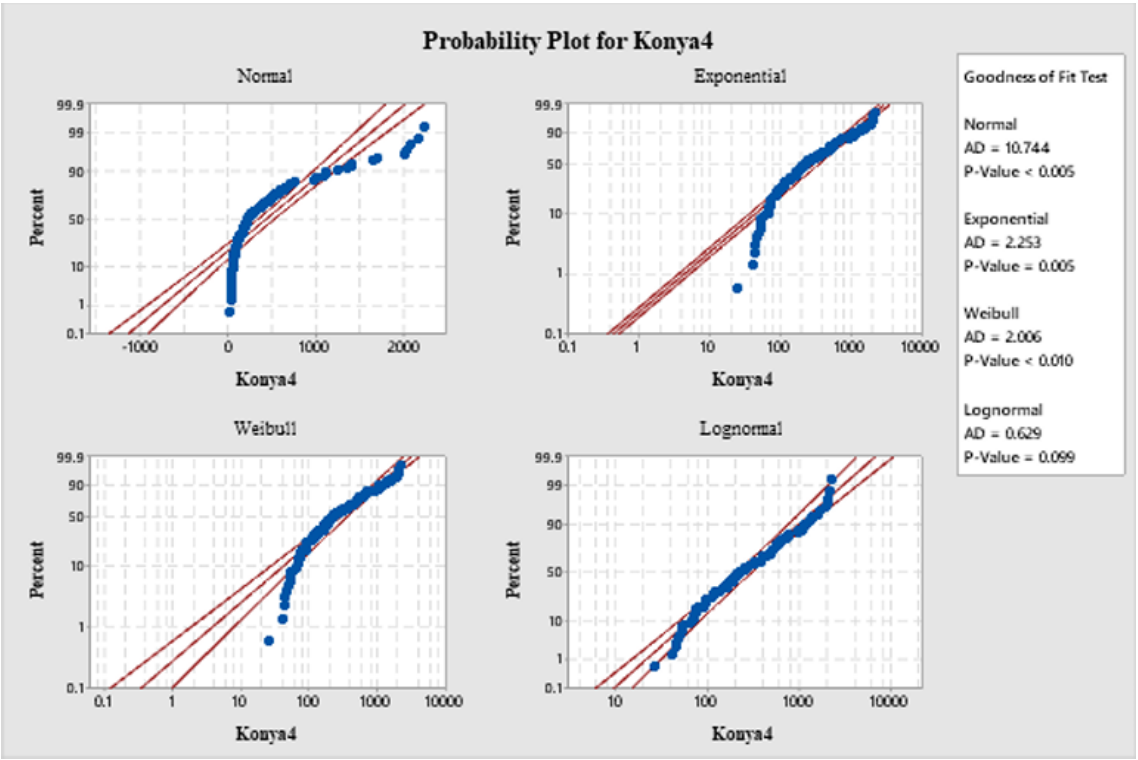

Figure 2.13 - Anderson-Darling compatibility curves of Konya4 Feeder distributions [16].

Figure **2.13** presents the Anderson-Darling compatibility curves for different candidate distributions fitted to the Konya4 feeder failure data. These curves illustrate the degree of fit between empirical data and various probability distributions within a 95% confidence interval. The figure reveals that the lognormal distribution exhibits the highest compatibility, as evidenced by its proximity to the upper boundary of the confidence region. This statistical result supports the conclusion that the lognormal lifetime distribution most accurately describes the fault occurrence times for the system.

Mikhaylov *et al.* [17] have conducted an engineering analysis of the reliability of trolleybus electrical equipment to enhance their operational longevity and ensure transportation safety. The research employed statistical methods to evaluate reliability, focusing on the reliability function and the mean time between failures (MTBF) (Figure **2.14**). The authors adopted the normal distribution function to model the lifetime of three key components: the traction electric motor, the electric power steering and the compressor.

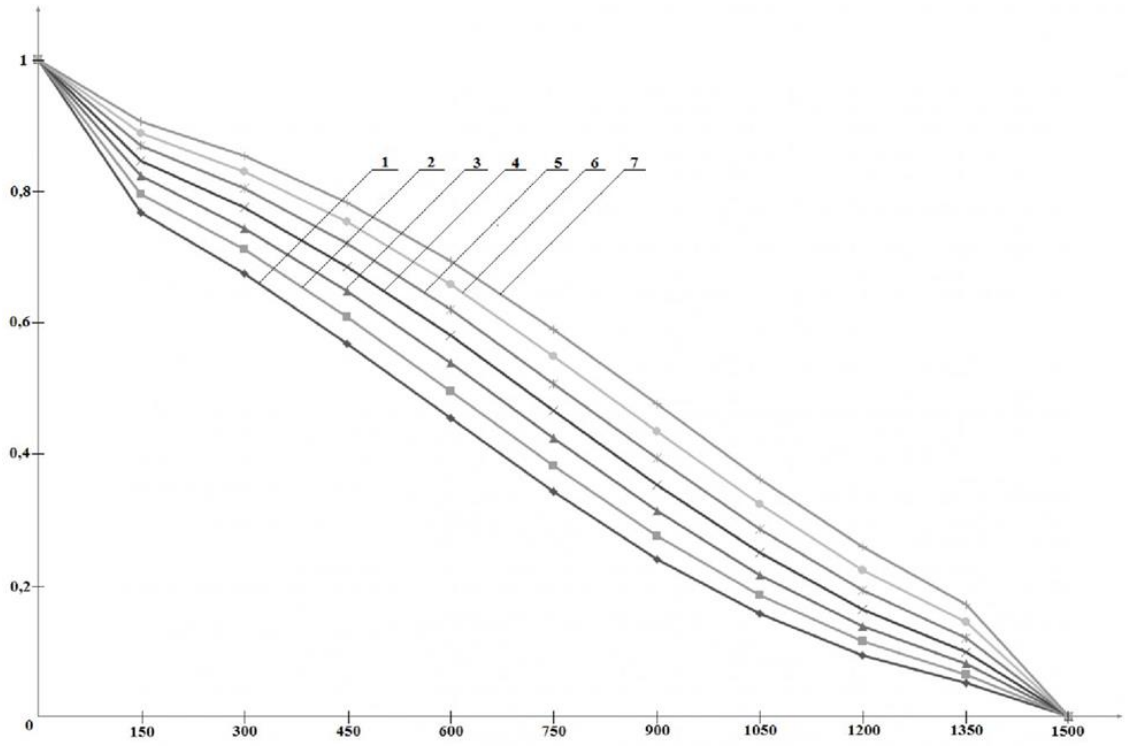

Figure 2.14 - Reliability change when MTBF increases [17].

Regarding Figure **2.14**, it illustrates the relationship between reliability function and the MTBF of different electrical components of the trolleybus, at various levels of increased lifetime. The figure presents lines showing the reliability at 0% (line 1), 5% (line 2), 10% (line 3), 15% (line 4), 20% (line 5), 25% (line 6) and 30% (line 7) increases in the average MTBF. Analysis indicates that increasing the MTBF significantly improves the probability of the system's reliability, especially at higher levels of lifetime. These results help

evaluate the influence of reliability whenever MTBF changes, which plays a crucial role in developing maintenance strategies that satisfy operational conditions during exploitation.

Anferov *et al.* [18] developed a model that uses a normal distribution (Figure **2**.**15**) for lifetime analysis to assess the operational reliability of bulldozers and other construction machinery. This model evaluates technical, organizational, and operational factors based on field test data, enabling precise forecast of work completion times and project costs.

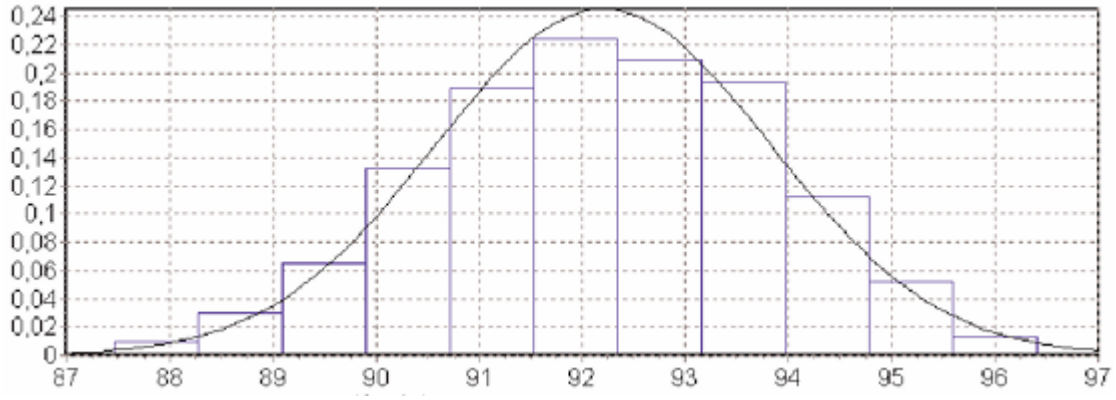

Figure 2.15 - Normal distribution lifetime of bulldozers **[18]**.

Figure **2**.**15** depicts the empirical distribution of the coefficients of usage for bulldozers, represented by a normalized histogram, overlaid with a fitted normal distribution curve. The x-axis corresponds to the coefficient of usage, defined as the percentage of time the equipment is operational during the scheduled work shifts or over the course of a year. The y-axis denotes the relative frequency. As illustrated, the distribution closely approximates a normal curve, indicating that the usage of bulldozers tends to concentrate around the mean value, approximately 92, with symmetric variability on either side.

Litvinenko *et al*. [19] presented a practical use of normal distribution for reliability analysis of electromechanical items. The results enabled to assess the basic reliability indices, as well as the peculiarities of their application in various conditions.

3. Reliability

Historically, the birth of modern reliability engineering took place in 1940s, during World War II [20]. Nevertheless, after 1960s, reliability engineering has been continuously developed [21]. Between 1960-1970, maintainability, availability and life-cycle cost gained importance. Reliability testing becomes project-specific with concepts like product assurance and cost-effectiveness emerging [22]. According to Saleh [23], in the 1970s, three major areas shaped the development of reliability engineering. First, there was an increased emphasis on system-level reliability and the safety of complex engineering systems, notably in sectors like nuclear power. Second, as software became more integral to operations, a dedicated focus on software reliability emerged. Third, an incentive program designed to reward contractors for enhancing the reliability of their products. In the 1980s, reliability shifts to consumer electronics, automotive, and telecommunications [24]. In the following years, reliability engineering has advanced significantly, driven by the need to manage increasingly complex systems and the availability of affordable computational power [25]. For instance, reliability engineering has evolved towards physics based, data-driven, and predictive approaches – such as physics of failure modes, machine learning, and prognostic systems – integrating these with human factors and analytical tools like MSS and PRA to enhance the safety, resilience, and maintenance of complex systems in industries like electronics, aerospace, and nuclear power [26].

According to NP EN 13306:2021 standard [27], reliability is an ability of an item to perform a required function under given conditions for a given time interval. In other words, reliability is defined as the probability that an item will perform its intended function without failure during specified period of time under defined operational conditions [21], [28], [29], [30], [31], [32], [33].

Kececioglu [20] defined reliability as a conditional probability at a given confidence-level, that the equipment will perform its intended functions satisfactorily or without failure, *i.e.*, within specified performance limits, at a given age, for a specified mission time, when

used in the manner and for the purpose intended while operating under specified application and operation environments with their associated stress level.

According to Birolini [22], reliability can also be defined as the ability of the item to remain functional, from a qualitative point of view. Quantitatively, reliability specifies the probability that no operational interruption will occur during the stated time interval.

Safie and Fuller [34] claim that achieving high reliability requires designing and building systems correctly. To ensure high reliability, the following steps should be taken:

- Establish reliability requirements.
- Apply both qualitative and quantitative analysis methods to verify that these requirements are met.
- Conduct thorough analysis of manufacturing, assembly and testing procedures in parallel with the design process.
- Implement concurrent engineering practices to involve all stakeholders from the outset.

3.1 Basic analytical and statistical functions

Five of the most important functions in reliability engineering are the following [20]:

- The failure probability density function.
- The failure rate function.
- The reliability function.
- The conditional reliability function.
- The mean life function.

3.1.1 Probability density function

The probability density function (pdf) is a mathematical function that describes a distribution [35]. It is the first important function in reliability engineering which has the characteristic that the area under this function's curve gives directly the probability that a component would fail during a life period from T_1 to T_2 [20]. The function *f(t)* is the pdf that the random time of failure-free operation of an object is less than *t*; namely the pdf at moment *t* [20], [28]:

$$f(t) = -\frac{d}{dt} R(t) \qquad \textbf{(3.1)}$$

Where *R(t)* is the probability that the object operates without failure during the time interval from 0 to *t*.

Additionally, pdf can be written as follows [36]:

$$\int_0^{+\infty} f(t)\, dt = 1 \tag{3.2}$$

3.1.2 Reliability function

Reliability is a function of t, so that the reliability function *R(t)* can be defined as [37], [38]:

$$R(t) = P(System\ operates\ during\ [0, t]) \tag{3.3}$$

Where P(A) denotes the probability of an event A.

The higher the item's operating time value, the lower the associated *R(t)* value tends to be, so that the value of *R(t)* decrease from 1 to 0 as *t* increases [39]. It is mathematically represented as the integral of the probability density function, *f(t)*, over time [39]:

$$R(t) = \int_t^{+\infty} f(t)\, dt \tag{3.4}$$

3.1.3 Cumulative distribution function

The probability that *x* has a value less than or equal to *x*, is referred to as the cumulative distribution function, CDF or *F* for short [36]:

$$F(x) = P\{\boldsymbol{x} \leq x\} \tag{3.5}$$

CDF represents the probability of failure by the time *t,* meaning that as time increases, *F(t)* increases from 0 to 1, indicating a higher likelihood failure, as shown in the **Figure 3.1** [39].

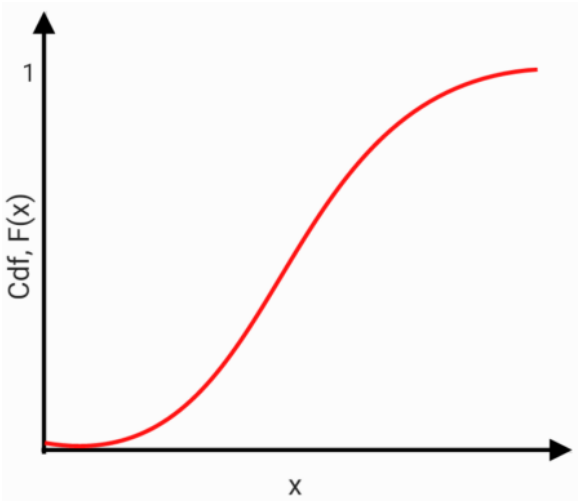

Figure 3.1 – Typical cumulative distribution function (adapted from **[40]**).

It is obvious that the CDF, *F(t)*, can be expressed in terms of its pdf, *f(t),* as [41]:

$$F(t) = \int_0^t f(\xi)\, d\xi \tag{3.6}$$

F(t) is the complement of the reliability function [39], [42]:

$$F(t) = 1 - R(t) \tag{3.7}$$

3.1.4 Conditional reliability

The notion of conditional probability captures the idea of measuring the probability of occurrence of an event, given that another event occurred [43]. To calculate conditional probability, the standard formula used is [44], [45]:

$$P(A|B) = \frac{P(A \cap B)}{P(B)} \tag{3.8}$$

This formula represents the probability of event A occurring given that event B has occurred.

The probability of failure-free operation of an object in the time interval from *t* to *t+t₀,* given failure-free operation up to time *t*, is [28]:

$$P(t; t + t_0) = \frac{P(t + t_0)}{t} \tag{3.9}$$

Another way of arriving at Equation (3.9) is to use the following equation [20]:

$$\frac{R(T_2)}{R(T_1)} = e^{-\int_{T_1}^{T_2} \lambda(T) dT} \tag{3.10}$$

3.1.5 Failure rate

$\lambda(t)dt$ represents the failure probability in the interval *t, t+dt* assuming that the equipment survives until time *t*; therefore according to conditioned probability formulations [28], [42]:

$$\lambda(t) = \frac{f(t)}{R(t)} \tag{3.11}$$

Substituting Equation (3.1) in (3.11) leads to [30], [42]:

$$-\lambda(t) = \frac{dR(t)}{dt} \frac{1}{R(t)} \tag{3.12}$$

It is well known that the failure rate function can be interpreted as the probability of failure in an infinitesimal unit interval of time [46]. It provides a measure of the changes in the probability of failure over the lifetime of a component, often exhibiting a bathtub shape (Figure **3**.**2**) [31].

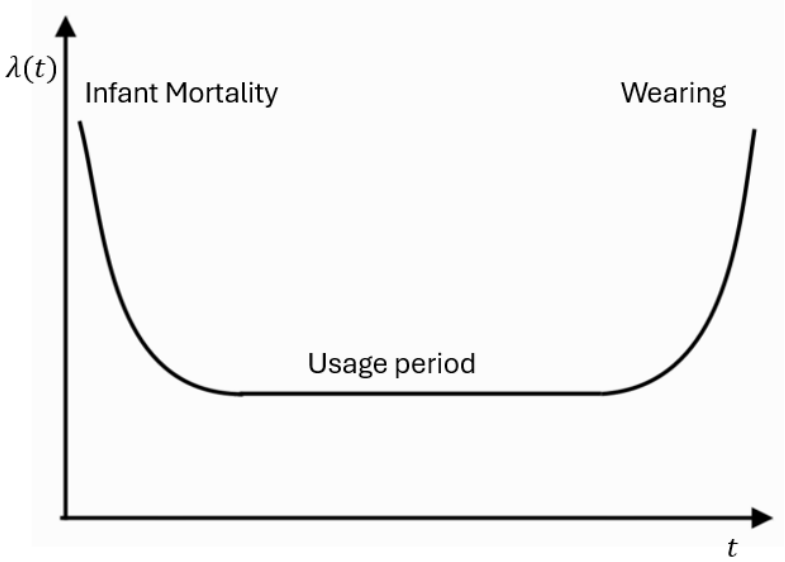

Figure 3.2 - The bathtub curve (adapted from **[46]**).

The Figure **3.2** illustrates three regions, infant mortality (decreasing failure rate), useful life (constant failure rate), and wear out (increasing failure rate) [47]. The figure shows an early failure period with a high failure rate that weeds out defective items, followed by a nearly constant failure-rate period with a low failure rate based on statistical failures, and followed by a wear-out failure-rate period, *i.e.*, a rapidly rising failure rate, as the lives of components expire [48].

3.1.6 Mean life

Mean life corresponds to the average time that the units in population are expected to operate before failure [49]. This metric is often referred to as “mean time to failure” (MTTF) or “mean time between failure” (MTBF) [49].

MTBF is the expected time between two successive failures of a repairable system [28], [50], [51], [52].

MTBF is the expected time to failure for non-repairable systems, representing the mean of the failure time distribution [28], [50], [53].

The mean life *m* is defined as the first moment of the failure density function [45], [54]:

$$m = \int_0^{+\infty} t \cdot f(t)\, dt \tag{3.13}$$

The MTTF or the mean operating time of an object up to failure, T_1, is [28]:

$$T_1 = \int_0^{+\infty} R(x)\, dx \tag{3.14}$$

Where T_1 is the mean value of the random operating time object.

The MTBF is the mean time to failure-free operation of an object as a whole from the moment of completion of the (*j-1*)st renewal to the *j*th failure [28]:

$$T_j = \int_0^{+\infty} R_j(x)\, dx \tag{3.15}$$

Where T_j is the expected mean value of the random length of time of failure-free operation of the object from the moment of renewal after failure (*j-1*) to failure *j*.

3.1.7 Relationships between basic functions

The following relationships can readily be derived from previous equations [28], [45]:

$$R(t) = e^{-\int_0^t \lambda(x)\, dx} \tag{3.16}$$

$$R(t) = 1 - F(t) \tag{3.17}$$

$$F(t) = 1 - e^{-\int_0^t \lambda(x)\, dx} \tag{3.18}$$

$$f(t) = \lambda(t) \cdot e^{\int_0^t \lambda(x)\, dx} \tag{3.19}$$

$$f(t) = \frac{dF(t)}{dt} \tag{3.20}$$

3.2 Lifetime distributions

In reliability engineering various types of statistical distributions are applied. This chapter will reference the most commonly used and most widely applicable distributions for life data analysis [49].

3.2.1 Weibull distribution

The Weibull distribution is arguably the most popular statistical distribution used by reliability engineers [30], [40], [55]. It has the great advantage in reliability work that by adjusting the distribution parameters it can be made to fit many life distributions [40]. The Weibull distribution is particularly suitable for failure cases of mechanical equipment due to accumulation of wear and tear over a long period of time [56].

Its most general case, the 3-parameter Weibull pdf is defined by [49], [57]:

$$f(t) = \frac{\beta}{\eta}\left(\frac{t-\gamma}{\eta}\right)^{\beta-1} e^{-\left(\frac{t-\gamma}{\eta}\right)^{\beta}} \tag{3.21}$$

Where:

β = shape parameter

η = scale parameter

γ = location parameter

The location parameter, γ, represents the initial period over which no failure can take place [20], as shown in the Figure **3.3**.

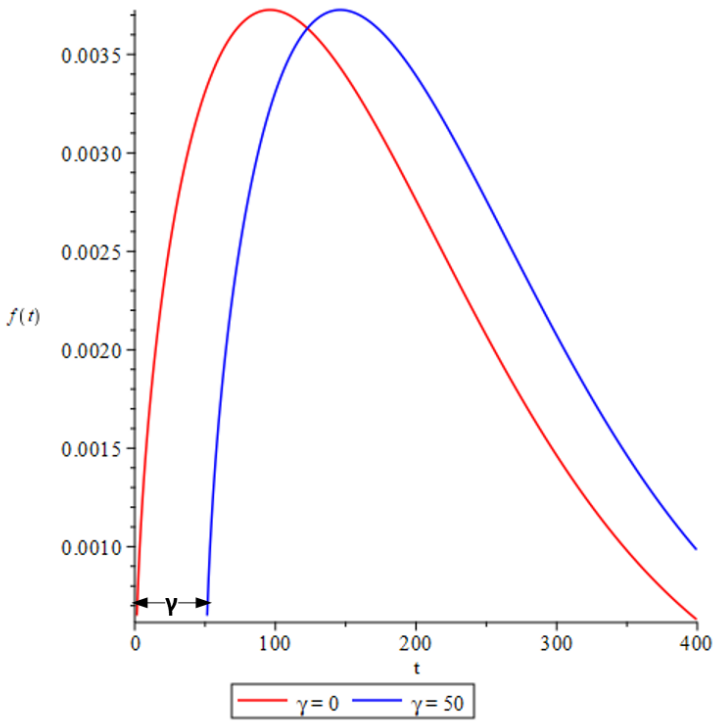

Figure 3.3 – Effect of location parameter, $\boldsymbol{\gamma}$ on Weibull pdf (adapted from **[58]**).

The shape parameter, β, controls the shape of the distribution [20]. The Figure **3.4** illustrates the shape that a pdf could assume.

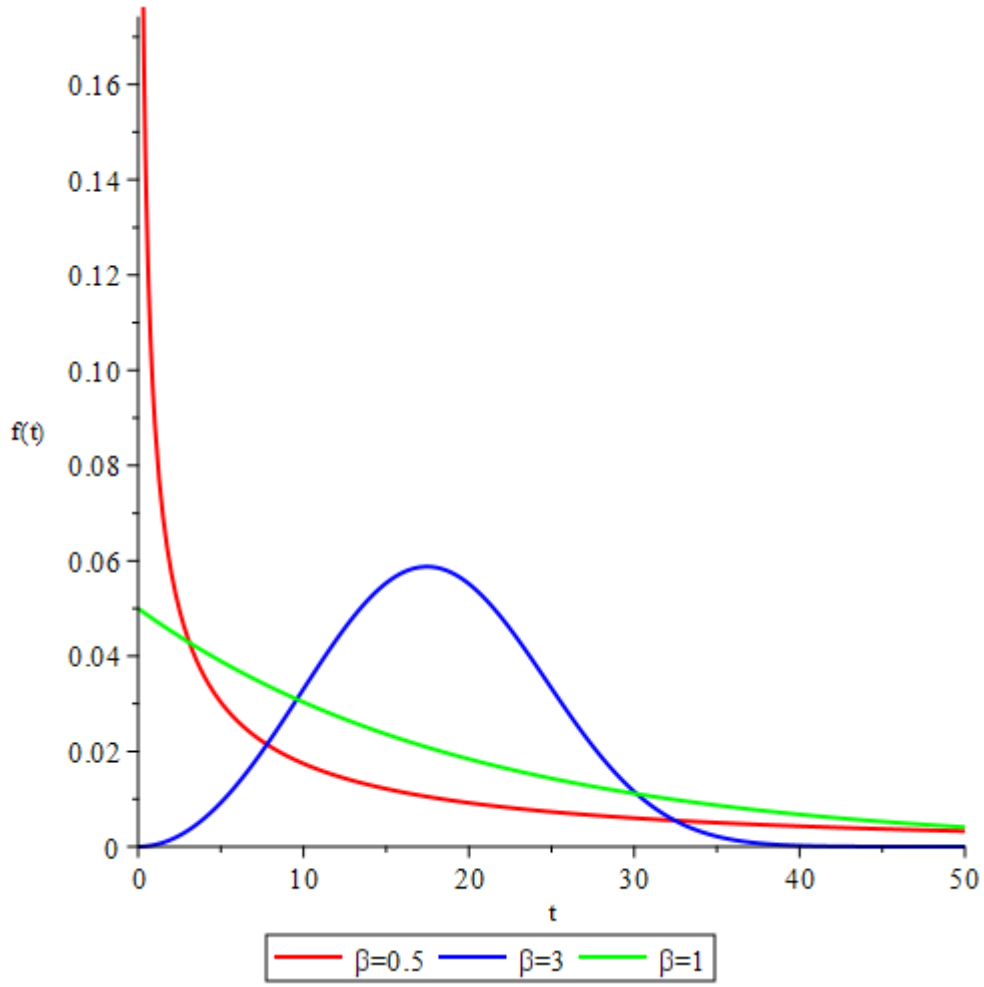

Figure 3.4 – Weibull pdf plot with varying values of shape parameter, $\boldsymbol{\beta}$ (adapted from **[58]**).

The scale parameter, η, has the same effect as when the scale of the abscissa is changed, meaning that when the parameter is decreased, the pdf gets towards its beginning point, whereas when η is increased the distribution gets stretched out away from its beginning point [20]. The Figure **3.5** illustrates exactly these tendencies.

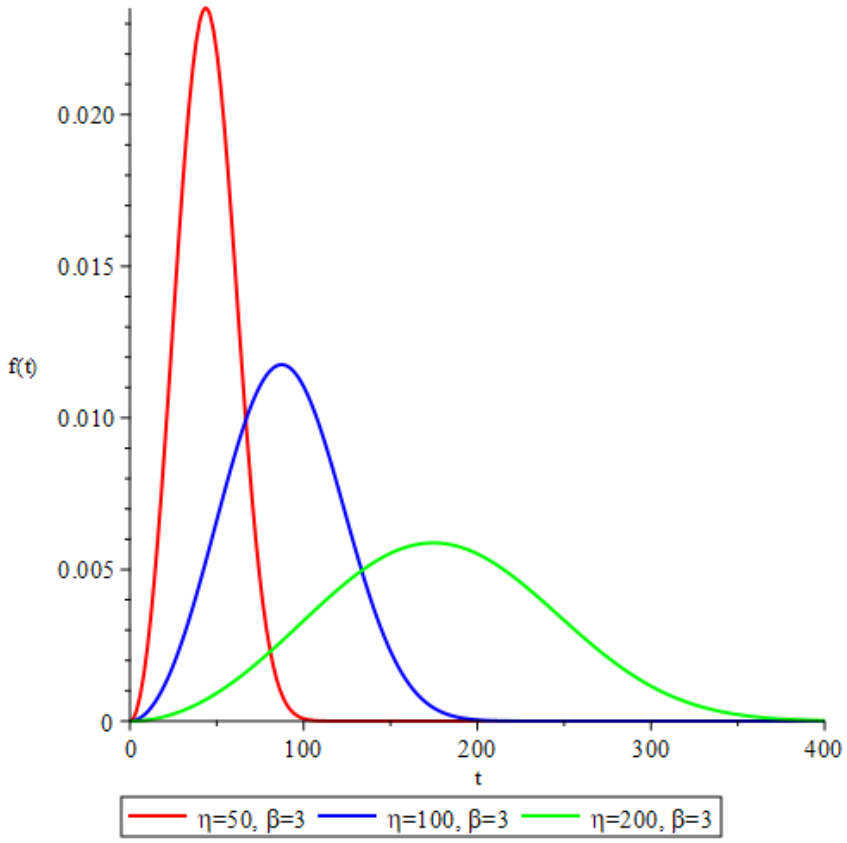

Figure 3.5 – Weibull pdf plot with varying values of scale parameter, $\boldsymbol{\eta}$ (adapted from **[58]**).

If the location parameter, γ, is assumed to be zero, then the distribution becomes the 2-parameter Weibull [45], [49], [59]:

$$f(t) = \frac{\beta}{\eta}\left(\frac{t}{\eta}\right)^{\beta-1} e^{-\left(\frac{t}{\eta}\right)^{\beta}} \tag{3.22}$$

One additional form is the 1-parameter Weibull distribution, which assumes that the location parameter, γ is zero, and the shape parameter is known as constant, or β = constant = *C,* so [49]:

$$f(t) = \frac{C}{\eta}\left(\frac{t}{\eta}\right)^{C-1} e^{-\left(\frac{t}{\eta}\right)^{C}} \tag{3.23}$$

Since the relationship between the failure rate and the time to failure can take many different forms, the analytical solution of Equation (3.16) can turn out to be extremely

complicated [42]. For a three-parameter Weibull distribution, the reliability function is written as follows [34]:

$$R(t) = e^{-\left(\frac{t-\gamma}{\eta}\right)^{\beta}} \tag{3.24}$$

The corresponding reliability function for a two-parameter Weibull distribution is [40]:

$$R(t) = e^{-\left(\frac{t}{\eta}\right)^{\beta}} \tag{3.25}$$

The mean time of the Weibull pdf is given by [20], [49]:

$$m = \gamma + \eta \cdot \Gamma\left(\frac{1}{\beta} + 1\right) \tag{3.26}$$

For the 2-parameter case, the mean life can be reduced to [36], [40], [43]:

$$m = \eta \cdot \Gamma\left(\frac{1}{\beta} + 1\right) \tag{3.27}$$

The failure rate for two-parameter Weibull distribution can be written [56], [60]:

$$\lambda(t) = \frac{\beta}{\eta}\left(\frac{t}{\eta}\right)^{\beta-1} \tag{3.28}$$

As noted, several of the other distributions can be obtained from the Weibull distribution. Modeling other distributions can be accomplished by selecting the appropriate value of shape parameter, β [61]. The Table 3.1 matches the Weibull shape parameter to the corresponding distribution.

Table 3.1 - Weibull shape parameter and the corresponding distribution (adapted from [61]).

Shape Parameter Value	Corresponding Distribution
$\beta < 1$	Gamma (k<1)
$\beta = 1$	Exponential
$\beta = 2$	Rayleigh
$\beta = 1{,}5$	Lognormal (approximate)
$\beta = 3{,}44$	Normal (approximate)

Following Chapter 3.1.5, where failure rate was covered, the Weibull plot is first used to estimate the shape parameter, β, which defines the failure mode – infant mortality (β < 1), random failures (β = 1), or wear-out (β > 1) – as represented by the reliability bathtub curve (Figure **3.6**) [62].

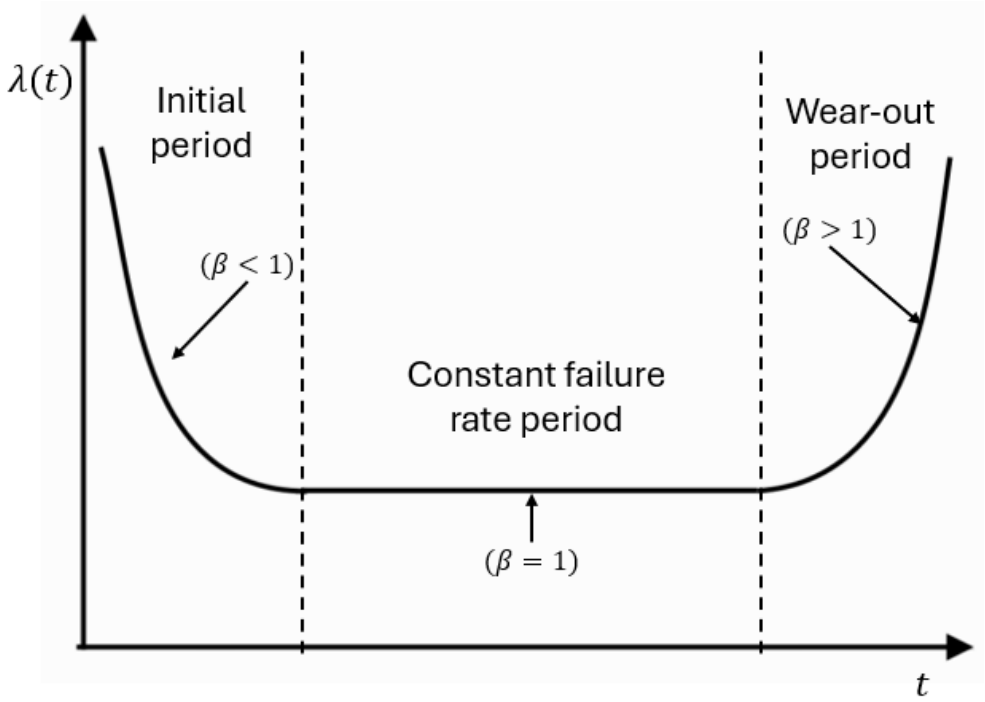

Figure 3.6 - Bathtub curve that relates Weibull shape parameter,β, (adapted from **[63]**).

Figure **3.6** illustrates three cases of the aging process. Rinne [64] describes all of them:

- β < 1: The hazard rate is monotonically decreasing and convex; the Weibull distribution reveals a delayed and negative aging process.
- β = 1: Items of this population will not undergo any aging; this case leads to the exponential distribution, which has a constant and age-independent hazard rate.
- β > 1: The failure rate is increasing monotonically (1 < β < 2) but is concave; members of such population have the property of positive aging, meaning the greater the age reached the higher the probability of an immediate failure; when β > 2, the aging is accelerated.

3.2.2 Exponential distribution

The exponential distribution is a special case of Weibull, in which the hazard function is a constant [65]. This means that exponential distribution represents typically the lifespan of a component without memory, aging nor wearing [43]. Its advantage is that it represents both phenomenologically and empirically the time-to-failure distribution of components, equipment, and system of complex nature with components and mixed life distributions [20]. An example of the application of the exponential distribution can be found in the analysis of complex electrical systems [34].

The two-parameter exponential pdf is [20]:

$$f(t) = \lambda \cdot e^{-\lambda \cdot (t-\gamma)} \tag{3.29}$$

Or it can be written in the following way [66], [67]:

$$f(t) = \frac{1}{\eta} \cdot e^{-\frac{t-\gamma}{\eta}} \tag{3.30}$$

The exponential distribution is a special case of Weibull distribution when $\beta = 1$ [68].

The CDF is given by [67]:

$$F(t) = 1 - e^{-\frac{t-\gamma}{\eta}} \tag{3.31}$$

Regarding to previous mathematical expression, Equation (3.31), the reliability function can be determined by [20]:

$$R(t) = e^{-\lambda(t-\gamma)} \tag{3.32}$$

Additionally, the scale parameter, η corresponds to [20]:

$$\frac{1}{\lambda} = m - \gamma \tag{3.33}$$

Where *m* represents the mean time between failures or to failure.

Some authors consider the general pdf expression as [1], [45], [49]:

$$f(t) = \lambda \cdot e^{-\lambda \cdot t} \tag{3.34}$$

Where location parameter, γ, is set to zero. In this regard, all previous equations will assume the following modifications. This new form is called one-parameter exponential distribution [20], [66], [67]:

The pdf is written as:

$$f(t) = \lambda \cdot e^{-\lambda \cdot t} \tag{3.35}$$

Or,

$$f(t) = \frac{1}{\eta} \cdot e^{-\frac{t}{\eta}} \tag{3.36}$$

The CDF is determined by:

$$F(t) = 1 - e^{-\frac{t}{\eta}} \tag{3.37}$$

Reliability function assumes the following formulation:

$$R(t) = e^{-\lambda t} \tag{3.38}$$

For the exponential distribution, the reciprocal of the failure rate is the mean time to failure [43]:

$$MTTF = \frac{1}{\lambda} \tag{3.39}$$

MTBF, a mean or average value, can be seen from [34]:

$$e^{-\lambda t} = e^{-\frac{t}{MTBF}} \tag{3.40}$$

For the exponential case, conditional reliability can be written as follows [20]:

$$R(T, t) = R(t) \tag{3.41}$$

The probability that a component is working at least *t*+*d* hours knowing that it already worked *t* hours is the same as the probability that it works *d* hours after its entry into service [43].

The Figure **3.7** represents the pdf of the one parameter exponential distribution, which assumes the parameter λ equal to 1, 2 and 3.

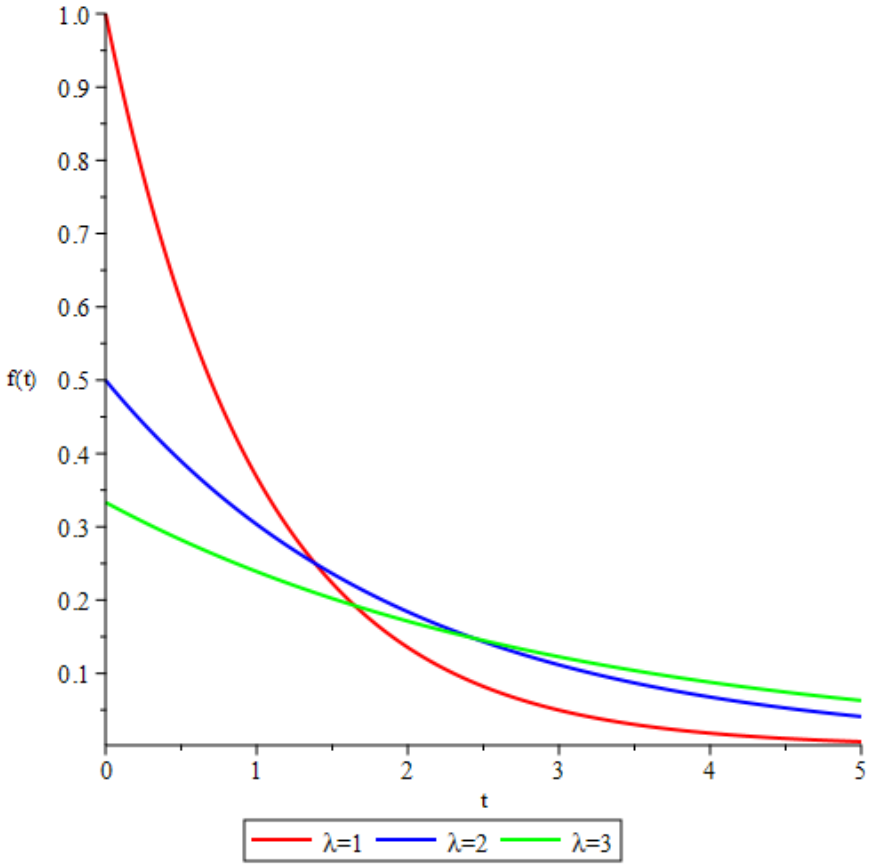

Figure 3.7 – Exponential pdf plot with varying values of λ (adapted from **[69]**).

3.2.3 Normal distribution (Gaussian distribution)

The normal distribution can be considered a good approximation to the Weibull distribution as long as its shape parameter is in the open interval (3,25;3,61) [70]. O'Connor and Kleyner [40] consider that when the $\beta = 3{,}5$, the distribution approximates to normal distribution.

The normal distribution is the best-known theoretical distribution in statistics [71]. It is commonly used for general reliability analysis, times-to-failure of simple electronic and mechanical components, equipment or systems [49]. The pdf of the normal distribution is given by [43], [72]:

$$f(t) = \frac{1}{\sigma\sqrt{2\pi}} e^{-\frac{1}{2}\left(\frac{t-\mu}{\sigma}\right)^2} \quad \textbf{(3.42)}$$

Where μ is the mean of the normal times to failure and σ is the standard deviation of the times to failure. The **Figure 3.8** represents the shape of the pdf function, over time, by applying different values of mean and standard deviation.

Similarly, the CDF corresponding to Equation (3.42) is [36]:

$$\Phi(t) = \int_{-\infty}^{t} \frac{1}{\sqrt{2\pi}\sigma} e^{-\frac{1}{2}\left(\frac{t'-\mu}{\sigma}\right)^2} dt' \quad \textbf{(3.43)}$$

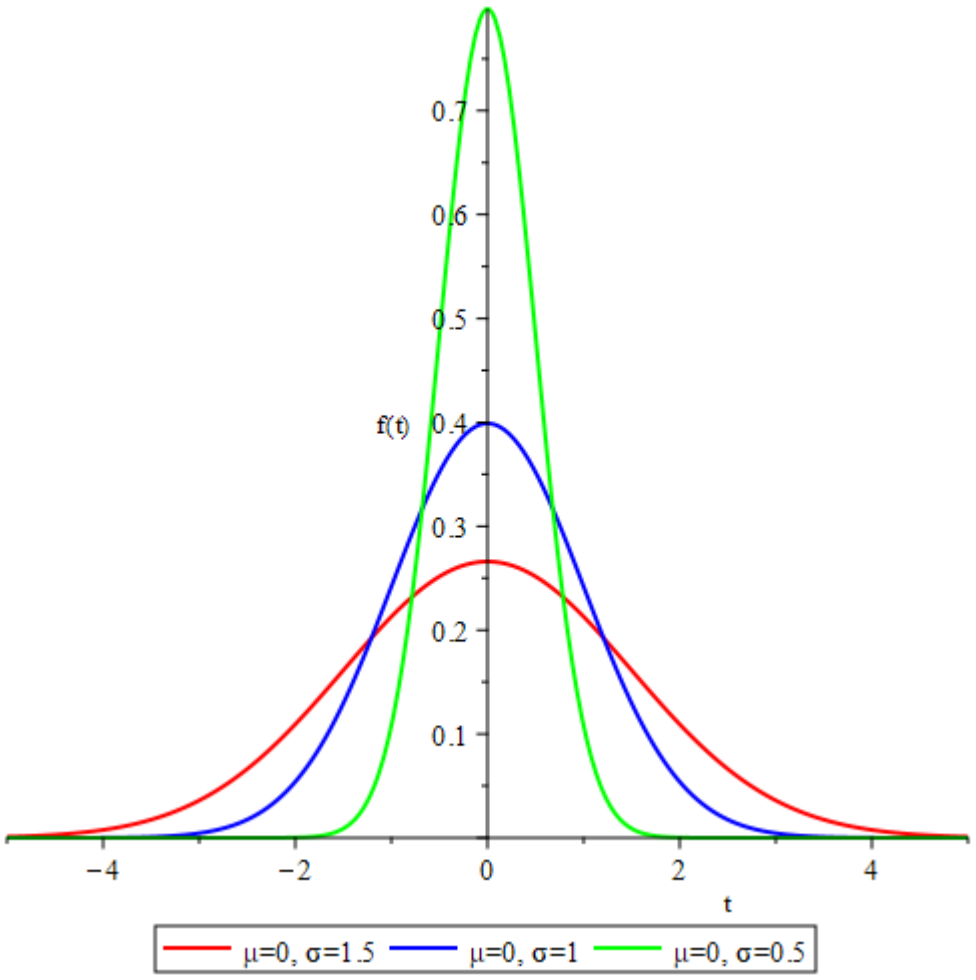

Figure 3.8 - Normal distribution (adapted from **[41]**).

The normal distribution with parameters $\mu = 0$ and $\sigma = 1$ is called the standard normal distribution [68]. In this regard, it is often beneficial to make a change of variables first in order to express *F(t)* in a standardized form [36]. This can be achieved by defining variable *Z* in terms of *t* [41]:

$$Z = \frac{t - \mu}{\sigma} \tag{3.44}$$

The scale parameter defines where the bulk of the distribution lies, meaning that in the case of the normal distribution, the scale parameter, η, is the standard deviation, σ, [20], [49]. Similarly to exponential distribution, the normal distribution does not have a shape parameter, since it has a predefined shape that does not change [49].

The instantaneous normal hazard rate is given by [20]:

$$\lambda(t) = \frac{\frac{1}{\sigma\sqrt{2\pi}} e^{-\frac{1}{2}\left(\frac{t-\mu}{\sigma}\right)^2}}{\int_t^{+\infty} \frac{1}{\sigma\sqrt{2\pi}} e^{-\frac{1}{2}\left(\frac{t-\mu}{\sigma}\right)^2} dt} \tag{3.45}$$

3.2.4 Lognormal distribution

In contemporary statistical analysis, it is recognized that certain variables within a system exhibit an exponential relationship, characterized by the equation $x = e^w$. When the exponent *w* is treated as a random variable, *x* consequently becomes a random variable of significant interest. A particularly noteworthy case arises when *w* is normally distributed. In this scenario, the distribution of *x* is identified as a lognormal distribution. This nomenclature stems from the transformation $\ln(x) = w$, indicating that the natural logarithm of *x* follows a normal distribution [73].

The lognormal distribution is a more versatile distribution than the normal distribution as it has a range of shapes, and therefore is often a better fit to reliability data, such as for populations with wear out characteristics [40].

Lognormal distribution usually fits when analyzing mechanical parts under stress rupture loading [34].

The pdf of a lognormal distribution is [74], [75]:

$$f(t) = \frac{1}{\sqrt{2\pi}\sigma' t} e^{-\frac{1}{2}\left(\frac{\ln t - \mu'}{\sigma'}\right)^2} \tag{3.46}$$

Where μ' and σ' are the mean and standard deviation of the natural logarithms of the times-to-failure. They can be obtained from applying the following mathematical expressions [76]:

$$\mu' = \frac{1}{n}\sum_{i=1}^{n} ln\,(t_i) \tag{3.47}$$

$$\sigma' = \sqrt{\frac{1}{n-1}\sum_{i=1}^{n}(ln(x_i) - \mu')^2} \tag{3.48}$$

The **Figure 3.9** illustrates the shape of the pdf function, over time, by applying different values to parameters μ and σ.

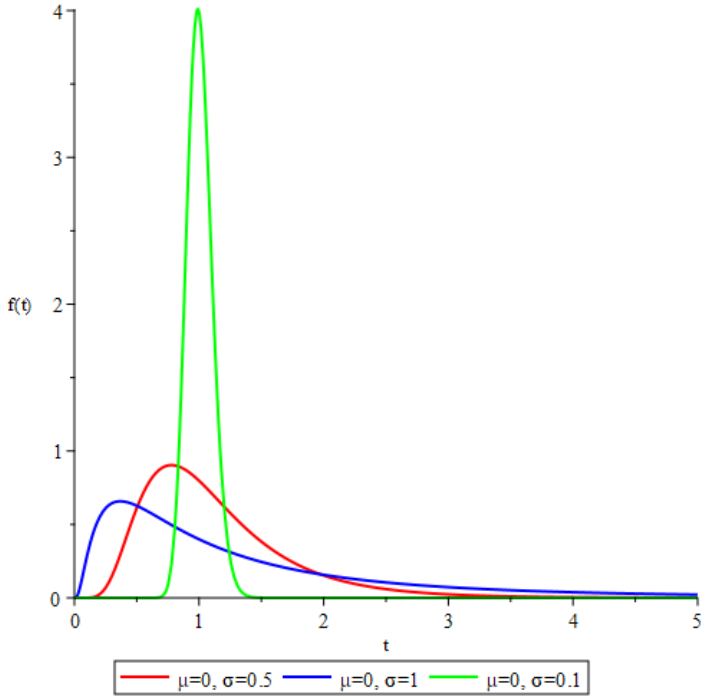

Figure 3.9 - Lognormal distribution (adapted from **[41]**).

The mean and the standard deviation are given by, respectively [20], [40]:

$$\mu = e^{\mu\prime + \frac{\sigma\prime^2}{2}} \tag{3.49}$$

$$\sigma = \sqrt{e^{2\mu' + \sigma\prime^2} - e^{2\mu' + \sigma\prime^2}} \tag{3.50}$$

The reliability mission of a time *t* is determined by [49]:

$$R(t) = \int_{ln\,t}^{+\infty} \frac{1}{\sqrt{2\pi}\sigma' t} e^{-\frac{1}{2}\left(\frac{ln\,t-\mu'}{\sigma'}\right)^2} dt \quad \textbf{(3.51)}$$

3.3 Confidence levels

A point estimate is a single value given as the estimate of a population parameter of interest [43]. In contrast, confidence intervals provide the range over which the true parameter values may exist with certain level of confidence [47]. Confidence limits may be shown with two error probabilities, ε_1 and ε_2, where ε_1 is the probability that the true value of the parameter is not less than a given lower limit, and ε_2 is the probability that the true value of the parameter is not more than a given upper limit [28]. For a same sample, the smaller the confidence range, the smaller the confidence level, and vice-versa [43], [49], [77], [78]. Most commonly, the 90%, 95%, and 99% confidence levels are used [43]. The Figure **3.10** demonstrates a Weibull line (red) and the bounds (blue) for 90% confidence.

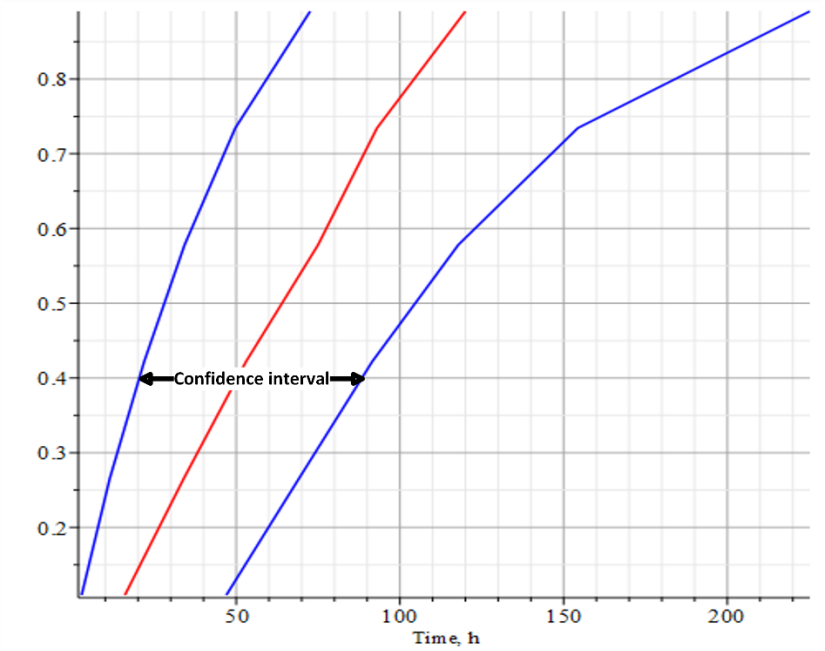

Figure 3.10 - Two-sided 90% confidence bounds (adapted from **[40]**).

3.3.1 Fisher information matrix

The Fisher matrix approach has come into more common use because it is easily adapted to the personal computer and because it provides tight confidence intervals for moderate sample sizes [79]. The lower and upper bounds are written, respectively [47], [80]:

$$\underline{\theta_C} = \hat{\theta} - \Phi^{-1}\left(\frac{1+C}{2}\right)\sqrt{[J_n(\hat{\theta})]^{-1}} \quad \textbf{(3.52)}$$

$$\overline{\theta_C} = \hat{\theta} + \Phi^{-1}\left(\frac{1+C}{2}\right)\sqrt{[J_n(\hat{\theta})]^{-1}} \quad \textbf{(3.53)}$$

Where:

$\hat{\theta}$ is the maximum likelihood estimate (MLE) of the parameter θ;

Φ is the CDF of the standard normal distribution (Z-score);

C is the confidence level;

J_n is the Fisher information matrix.

3.3.2 Likelihood ratio bounds

For small data sets, Fisher matrix bounds tend to be insufficiently conservative, whereas the likelihood ratio methods yields more conservative estimates and is therefore more appropriate [40].

Likelihood ratio confidence bounds are based on the following inequality [6], [47], [49], [77]:

$$-2 \cdot \ln\left(\frac{L(\theta)}{L(\hat{\theta})}\right) \geq \chi^2_{\alpha;k} \quad \textbf{(3.54)}$$

Where:

$L(\theta)$ is the likelihood function for the unknown parameter θ;

$L(\hat{\theta})$ is the likelihood function calculated at the estimated parameter value $\hat{\theta}$;

α is the confidence level complement $(1 - C)$.

3.3.3 Beta-binomial bounds

Type I confidence levels are confidence bounds around time for a given reliability [49]. Thus, confidence bounds can be estimated by solving the Weibull reliability equations (3.25) and CDF general equation (3.7) for time *t* [40]. *t* defines the time for upper and lower bounds.

$$t = \eta \cdot \left(\ln\left(\frac{1}{R}\right)\right)^{\frac{1}{\beta}} \quad \textbf{(3.55)}$$

For beta-binomial 90% bounds the following equations relate the 5% and 95% ranks to the Weibull line [79], [81]:

$$t_{i;0,95} = \eta \cdot \left[\ln\left(\frac{1}{1 - F_{i(0,95)}}\right)\right]^{\frac{1}{\beta}} \quad \textbf{(3.56)}$$

$$t_{i;0,05} = \eta \cdot \left[\ln\left(\frac{1}{1 - F_{i(0,05)}}\right)\right]^{\frac{1}{\beta}} \quad \textbf{(3.57)}$$

3.4 Goodness-of-fit tests

Before applying a probability model to represent the underlying population data, it is essential to assess its adequacy using a goodness-of-fit test [82]. In this regard, five tests will be presented within this chapter, which frequently appear in engineering and reliability. For a uniform approach, the following assumptions will be made:

H_0: The given data follows a specific probability distribution

H_a: The given data does not follow a specified probability distribution

3.4.1 Chi-square

The Chi-Square goodness-of-fit test, developed by Karl Pearson, is used to assess whether a set of observations follows a specific distribution – discrete or continuous – with or without known parameters, by comparing the observed frequencies to the expected probabilities [83]. The Pearson's sum is given by [83], [84], [85]:

$$\chi^2 = \sum_{i=0}^{k} \frac{(O_i - E_i)^2}{E_i} \quad \textbf{(3.58)}$$

Where O_i represents observed frequency, E_i expected frequency and k the number of different data cells or categories.

The Chi-Squared goodness-of-fit assumes non-negative values, where a value of zero denotes a perfect fit between the observed data and theoretical distribution [83]. As the statistic increases, it indicates a growing divergence, suggesting a poorer fit [83]. Adequacy is assessed by comparing the test statistics to a critical value from the chi-squared distribution table, determined by the significance level and the corresponding degrees of freedom [83], [86]. The number of degrees of freedom, *v*, is [87], [88]*:*

$$v = k - 1 \tag{3.59}$$

Where *k* is the number of classes whose contributions are summed in finding χ^2.
For testing H_0: independence with a table having *r* rows and *c* columns, the number of degrees of freedom, *v*, can be calculated by applying the following expression [89]:

$$v = (r - 1)(c - 1) \tag{3.60}$$

There are more general situations in which a degree of freedom is lost for each parameter estimated in certain chi-square random variables [90]. In this regard, the number of degrees of freedom can be obtained from [90], [91], [92]:

$$v = k - p - 1 \tag{3.61}$$

Where:

- *k* = number of classes / categories
- *p* = number of estimated parameters

3.4.2 Kolmogorov-Smirnov

The Kolmogorov-Smirnov test compares the distribution function $G_0(x)$ with the corresponding experimental quantity *S,* also called Empirical Distribution Function (EDF)*,* given by [93]*:*

$$G_0(x) = \int_{-\infty}^{x} g_0(x)\, dx \tag{3.62}$$

$$S(x) = \frac{Number\ of\ observations\ with\ x_i < x}{Total\ number} \tag{3.63}$$

The test statistic is the maximum difference *D* between the two functions, in EDF statistics [93], [94]:

$$D = \sup|G(x) - S(x)| \quad \textbf{(3.64)}$$

The Kolmogorov-Smirnov test statistic, *D*, can be written in the following way [95]:

$$D = \sup(D^+, D^-) \quad \textbf{(3.65)}$$

The quantities D^+ and D^-, respectively, denote the maximum positive and negative difference [93].

The hypothesis is accepted whenever *D* is lower than the critical value that is based on a given α and n [83].

3.4.3 Cramer-von Mises and Anderson-Darling

The two tests, Craver-von Mises and Anderson Darling are related and based on measures of disparity or divergence between the true but unknown and the hypothesized distributions [96].

The general Cramer-von Mises family of test statistics focuses on the squared differences given by [95], [96]:

$$Q = \int_{-\infty}^{+\infty} [F_n(y) - F_0(y)]^2 \Psi(y)\, dF_0(y) \quad \textbf{(3.66)}$$

Where $F_n(y)$ is the empirical distribution function, $F_0(y)$ is the hypothesized distribution and $\Psi(y)$ is an appropriate scaling function.

Additionally, Cramer-von Mises statistic can be written in the following way [97], [98]:

$$CVM = \sum_{i=1}^{n} \left(U - \frac{2i-1}{2n}\right)^2 + \frac{1}{12n} \quad \textbf{(3.67)}$$

Where:

n = number of TTF

U = Expected probability given a particular lifetime distribution (Table 3.2)

Table 3.2 - Analytical expression of *U* based on a particular lifetime distribution (adapted from [83]).

Lifetime distribution	Analytical expression of *U*
Normal	$\Phi\left(\frac{TTF_i - \bar{t}}{\sigma}\right)$
Lognormal	$\Phi\left(\frac{\ln TTF_i - \bar{t}}{\sigma}\right)$
Exponential	$1 - e^{-\frac{TTF_i}{m}}$
Weibull	$1 - e^{-\left(\frac{TTF_i - \gamma}{\eta}\right)^{\beta}}$

Where:

$\bar{t}$ = Arithmetic average of TTF

The Anderson-Darling statistic, A^2, belonging to the quadratic statistics, can be written in the following form [99]:

$$A^2 = n\int_{-\infty}^{+\infty} \frac{\big(S(x) - G(x)\big)^2}{G(x)\big(1 - G(x)\big)} dG(x) \tag{3.68}$$

Furthermore, the Anderson-Darling statistic can be written in a different form [100]:

$$A^2 = -n - s \tag{3.69}$$

Where:

$s = \sum_{i=1}^{n} \frac{(2i-1)}{n} [\ln G(Y_i) + \ln(1 - G(Y_{n+1-i}))] \cdot n$ is the random sample size and Y_i the ordered data.

Woodruff [82] proposes another form for describing the Anderson-Darling statistic:

$$A^2 = -\sum_{i=1}^{n} \left(U - \frac{2i-1}{2n}\right)^2 + \frac{1}{12n} \tag{3.70}$$

For a given level of significance, α, the hypothesis is rejected if the value of the test statistic is greater than the critical value [83], [100].

3.4.4 Correlation coefficient

Correlation coefficient is a measure of how well the linear regression model fits the data and is usually denoted by ρ [49]. In other words, it tells how strongly two variables are linearly related [100]. In general, the best fit would provide ρ closest to 1 [40]. A correlation coefficient value of zero would indicate that the data are randomly scattered and have no pattern or correlation relation to the regression line model.
The correlation coefficient can be obtained from the following formula [101]:

$$\rho = \frac{\frac{1}{n-1}\sum_{i=1}^{n}(X_i - \bar{X})(Y_i - \bar{Y})}{S_X \cdot S_Y} \tag{3.71}$$

Where S_X and S_Y represent the standard deviations for X and Y values, respectively. Additionally, the correlation coefficient can be written in a more extended form [49]:

$$\rho = \frac{\sum_{i=1}^{n} X_i Y_i - \frac{\sum_{i=1}^{n} X_i \sum_{i=1}^{n} Y_i}{n}}{\sqrt{(\sum_{i=1}^{n} X_i^2 - \frac{\left(\sum_{i=1}^{n} X_i\right)^2}{n})(\sum_{i=1}^{n} Y_i^2 - \frac{(\sum_{i=1}^{n} Y_i)^2}{n})}} \tag{3.72}$$

3.5 System's reliability

A fully satisfactory estimate of the reliability of a structure is based on a system approach [31]. In analyzing a complex system, a particular failure law may be applied to the entire system [102]. In short, the design configuration and arrangement of components used have a direct effect on the overall system performance and its reliability [103].

3.5.1 Series configuration

This is probably the most commonly occurring network in engineering systems [104]. Figure **3.11** represents a reliability block diagram (RBD) of a series configuration. This type of arrangement obliges all units to work normally for the successful operation of the whole system [104]. In other words, if any one of the components malfunctions, it will cause the assembly to fail [105].

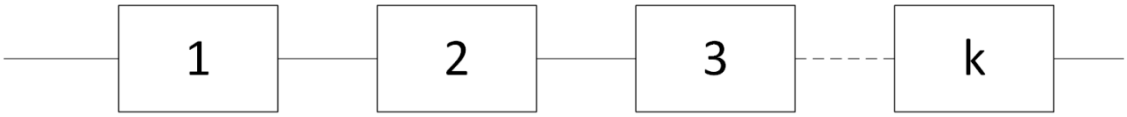

Figure 3.11 - RBD of a series configuration (adapted from **[104]**).

The series system reliability is expressed by [104], [106], [107]:

$$R_s(t) = \prod_{i=1}^{k} R_i \tag{3.73}$$

3.5.2 Parallel configuration

A parallel system is considered a configuration where the system operates continuously if at least one out of *n* components is operational, known as 1-out-of-*n* [108]. However, when one subsystem of a parallel system fails, the system will still function even if this subsystem is not repaired right away [37].

The reliability block diagram is shown in the Figure **3**.**12**.

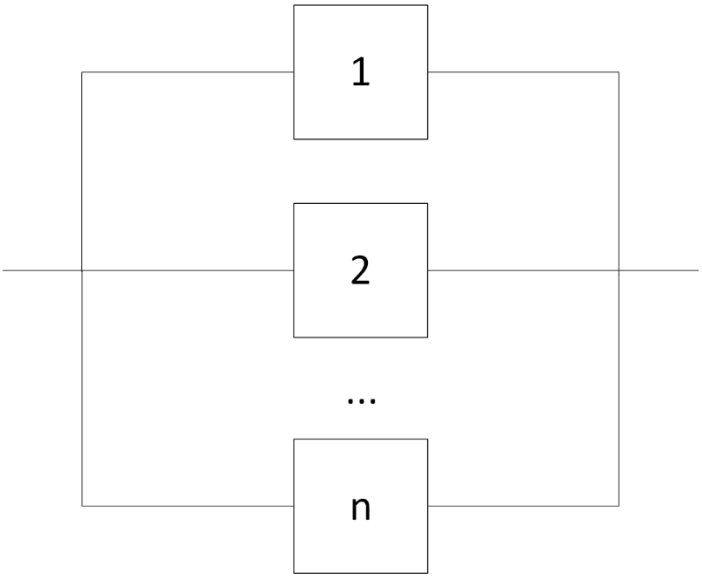

Figure 3.12 – RBD of parallel system (adapted from **[109]**).

Figure **3**.**12** illustrates a system comprising *n* components. The system is designed with redundancy, such that the functionality of the system is maintained as long as at least one of the components remains operational.

In this regard, the general expression for this active parallel redundancy is [40], [110]:

$$R = 1 - \prod_{i=1}^{n} (1 - R_i) \tag{3.74}$$

Where R_i is the reliability of the *i*th unit and *n* is the total number of units in parallel.

3.5.3 Standby configuration

A standby system is a type of reliability configuration characterized by its dual operating modes: active and sleep [111]. In the active mode, the standby system is fully operational and capable of providing its services. Conversely, in the sleep mode, the system is not actively providing services but remains ready to be activated by an external signal or input. The external signal is sensed by a sensing subsystem, which detects a break down in the active unit and commands to switch in the stand by unit [109]. This type of system is a common approach to improve system reliability [112], [113]. It is particularly relevant in contexts where energy consumption is a concern, as they can reduce power usage when not in active service [111]. Standby redundancy where one or several elements are working online while other redundant elements serve as standby spares is one of the widely-applied techniques of providing fault tolerance [114].

Additionally, this redundant configuration is used to ensure high reliability, in the long term, in the extreme environment, where it is not possible to carry out frequent maintenance and repairs [115].

The Figure **3.13** illustrates a block diagram of this type of configuration.

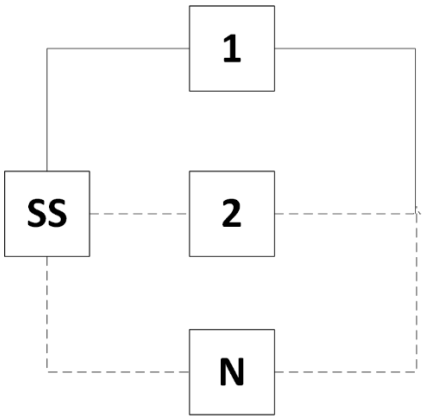

Figure 3.13 - Standby configuration RBD (adapted from **[41]**).

The block diagram above highlights that a switching device (SS) engages element no. 2 when component no. 1 experiences a failure. This same principle is applied to element no. *N*, which is activated when component (*N-1)* malfunctions.

According to Dhilon [116], when one unit is working and *k* units are in standby mode, the system reliability is given by:

$$R_{sys}(t) = \frac{\sum_{i=0}^{k}\{[\int_0^t \lambda(t)dt]^i e^{-\int_0^t \lambda(t)dt}\}}{i!} \quad \textbf{(3.75)}$$

According to Elsayed [103], the simplest nonrepairable standby system is a two-unit system that functions successfully when the primary unit does not fail, or if the primary unit fails during operating time *t* and the stand by assumes the function of the primary unit. In this regard, the reliability of the system is the sum of the probability that the primary unit does not fail until time *t* and the probability that the primary unit fails at some time τ, $0 < \tau < t$, and the standby unit functions successfully from τ to time *t* [103]:

$$R_{sys}(t) = R_1(t) + \int_{\tau=0}^{t} f_1(\tau) \cdot R_2(t-\tau) d\tau \quad \textbf{(3.76)}$$

The general reliability formula for *n* equal units in a standby configuration, assuming a perfect switching device and a exponentially distributed unit TTF is [40], [116]:

$$R_{sys} = \sum_{i=0}^{n-1} \frac{(\lambda t)^i}{i!} \cdot e^{-\lambda t} \quad \textbf{(3.77)}$$

Taking in consideration a two-unit system with similar elements, the respective reliability is given by [36]:

$$R_{sys} = (1 + \lambda t) e^{-\lambda t} \quad \textbf{(3.78)}$$

Where $\lambda_1 = \lambda_2 = \lambda$.

Accordingly, the *MTTF* of the above system is given by [41]:

$$MTTF = \frac{n}{\lambda} \quad \textbf{(3.79)}$$

Where *n* refers to the total number of active and standby rows.

In a non-perfect scenario, where switching device reliability is lower than 1, the following reliability equation can be written [32]:

$$R_{sys} = \sum_{i=0}^{n-1} \frac{(R_{SS} \cdot \lambda t)^i}{i!} \cdot e^{-\lambda t} \quad \textbf{(3.80)}$$

Where R_{SS} refers to the reliability of the switching device, and λ to the equivalent failure rate of the system.

Additionally, reliability is given by the first *n* terms of the Poisson expression [117]:

$$R_{sys} = e^{-\lambda t}\left(1 + \lambda t + \frac{\lambda^2 t^2}{2!} + \cdots + \frac{\lambda^{(n-1)} t^{(n-1)}}{(n-1)!}\right) \quad \textbf{(3.81)}$$

Considering *N* active units in one row, in perfect conditions [118]:

$$R_{sys} = \sum_{i=0}^{n-1} \frac{(N\lambda t)^i}{i!} \cdot e^{-\lambda t} \quad \textbf{(3.82)}$$

Analyzing a two-unit system using an imperfect switching device, the reliability formula could be simplified in the following way [32]:

$$R_{sys} = e^{-\lambda_1 t} + \frac{R_{SS} \cdot \lambda_1}{\lambda_1 - \lambda_2} \cdot (e^{-\lambda_2 t} - e^{-\lambda_1 t}) \quad \textbf{(3.83)}$$

3.5.4 *K*-out-of-*N* configuration

K-out-of-*N* redundancy is a *N* parallel configuration, which requires to function *K* components for system success [102]. For example, large airplanes usually have three or four engines, but two engines may be the minimum number required to provide a safe journey [103]. Figure **3**.**14** illustrates, generally, the configuration.

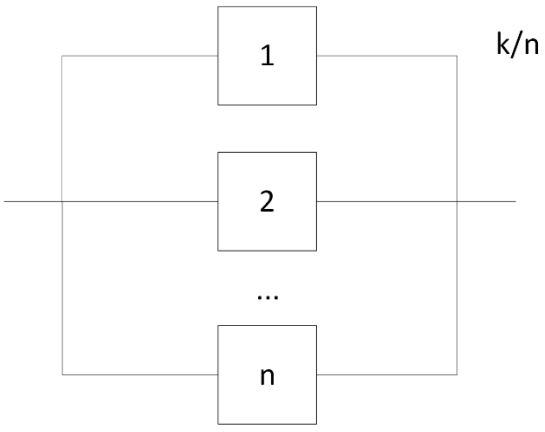

Figure 3.14 – RBD of a k-out-of-n configuration (adapted from **[110]**).

For constant failure rates of the identical units, the system's reliability can be written [102], [103], [104], [119]:

$$R_{sys} = \sum_{x=K}^{N} \left(\frac{N!}{x!\,(N-x)!} \cdot R^{x} \cdot (1-R)^{N-x} \right) \tag{3.84}$$

Pringle and Gresho [118] emphasize the importance of binomial coefficients as these coefficients are essential for calculating the systems' reliability of operational and failed components. Dragoi *et al.* [120] highlight that these coefficients help derive simple closed formulas for certain ranges of *k,* because they provide sharp bounds that are easy to calculate. They propose using Pascal's Triangle (Figure **3.15**) as an effective method for obtaining these coefficients. The binomial coefficient $\binom{n}{k}$ represents the number of ways to select *k* successes from *n* trials.

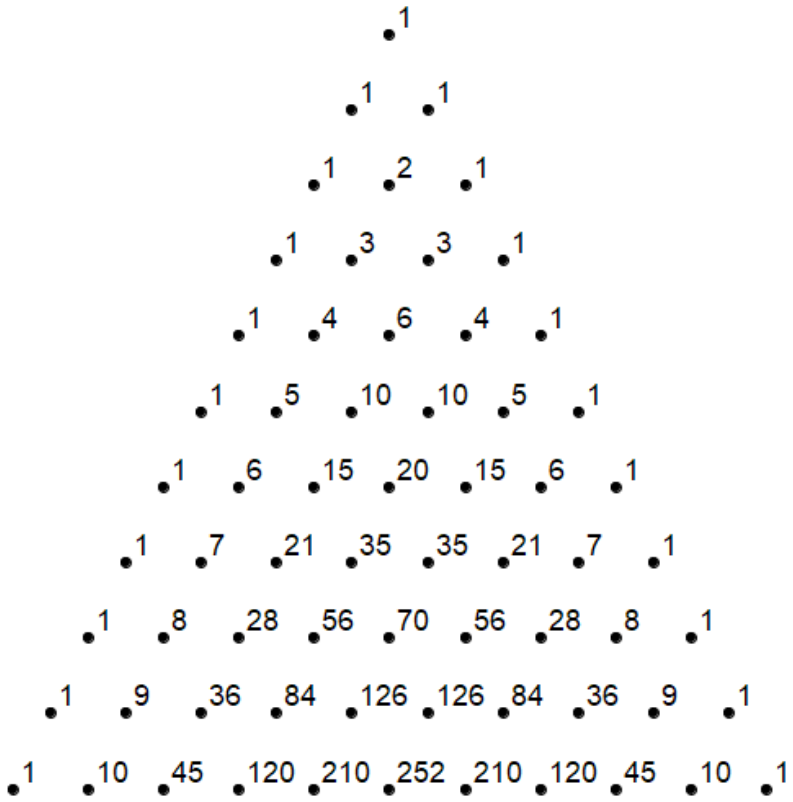

Figure 3.15 - Pascal's Triangle (adapted from [121]).

Once the coefficients are identified, they can be incorporated into the general equation of reliability system [118]:

$$R_{sys} = \sum_{M=k}^{n} \left(\binom{n}{k} R_u^M \cdot F_{at}^{n-M} \right) \tag{3.85}$$

Where *M* signifies active units, *n* indicates standby units, R_u represents the reliability of each active unit, and F_{at} denotes the failure probability of those units.

3.5.5 Complex configuration

Traditional reliability analysis often assume independent failures and constant failure rate, which can be limiting for complex industrial systems [122]. In a complex system, in many cases, it is not easy to recognize which components are in series and which are in parallel [123].

The reliability of a complex system is dictated by the Bayes' theorem: The reliability of a system is equal to the reliability of the system, given that a chosen unit, Unit A, is good times the reliability of Unit A, plus the reliability of the system, given that Unit A is bad times the unreliability of Unit A [109]. Mathematically:

$$R_{sys} = \left(R_{sys}\middle|A_G\right) \cdot R_A + \left(R_{sys}\middle|A_B\right) \cdot (1 - R_A) \quad \textbf{(3.86)}$$

This process is also known as the Conditional Decomposition Method (CDM) [124].

A complex system can be illustrated by a bridge configuration (Figure **3**.**16**), where the component *E* is neither in series nor in parallel with the others [124].

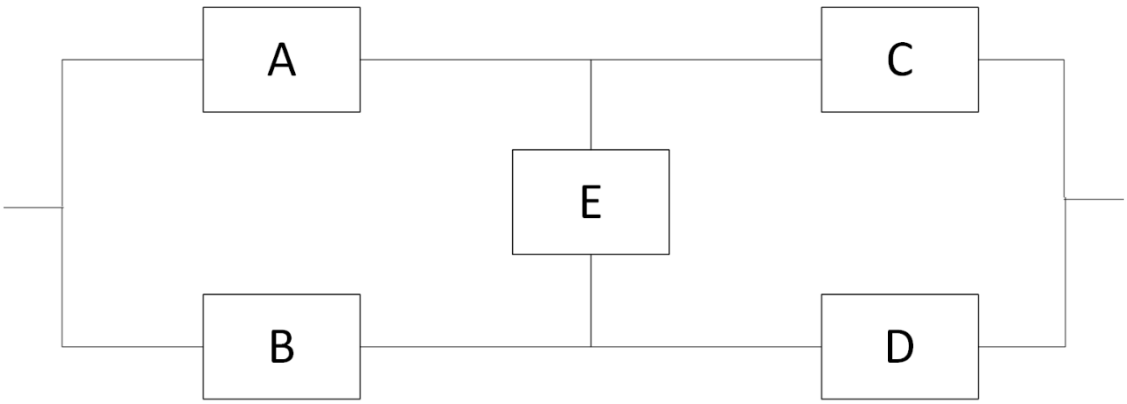

Figure 3.16 - RBD of a bridge system (adapted from [125], [126]).

According to CDM, the system is divided in two subsystems, one when *E* is considered good (Figure **3**.**17**), and other where *E* has failed (Figure **3**.**18**) [122], [127].

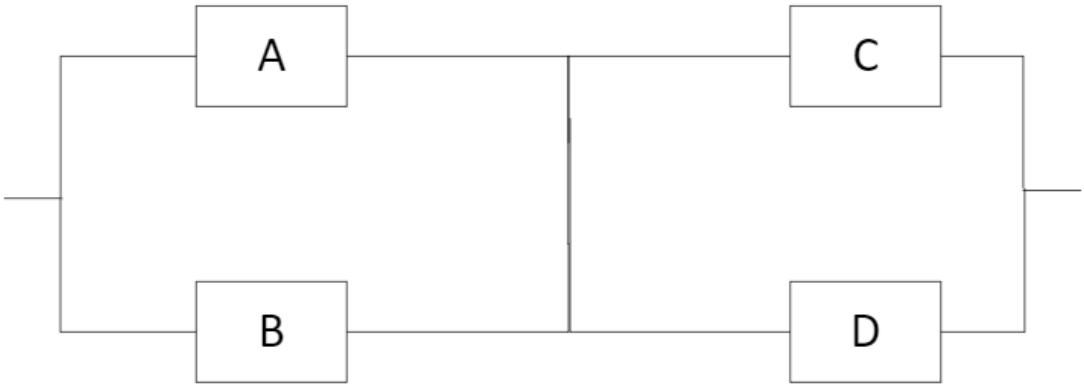

Figure 3.17 - Subsystem considering *E* "good" (adapted from [122], [127]).

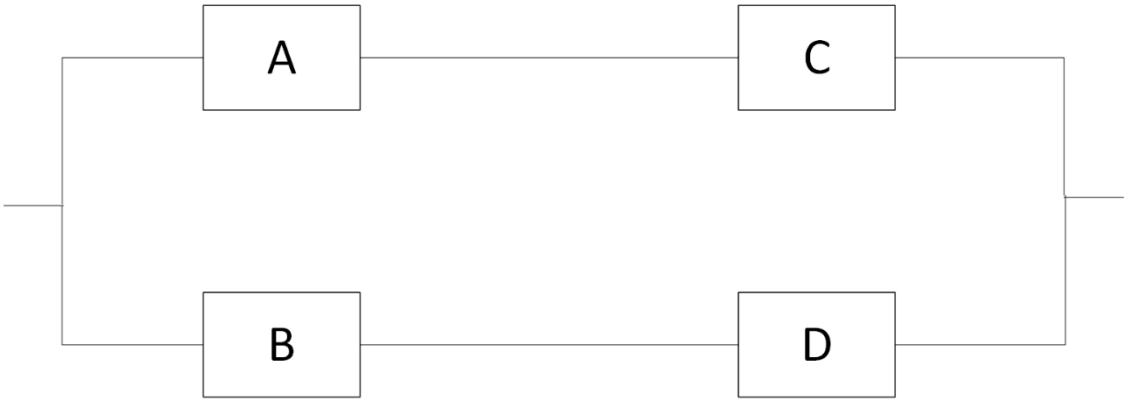

Figure 3.18 - Subsystem considering *E* "bad" (adapted from [122], [127]).

The set of subsystems above are then defined utilizing series-parallel connected configurations, which were covered in sections 3.5.1 and 3.5.2 [122].

4. Case study

Beamhouse operations comprise a series of chemical and mechanical treatments designed to cleanse and prepare raw hides for the tanning process. These operations typically include soaking, fleshing, unhairing, liming and lime splitting. Soaking serves to rehydrate the hide and eliminate curing agents and impurities – an essential step prior to mechanical processing. Fleshing, a mechanical procedure, follows and involves the removal of residual flesh, fat, and subcutaneous tissue from the inner side of the hide. Subsequently, a chemical treatment is instigated to remove hair and epidermis from the hide, effectively preparing it for tanning. Finally, the limed hide is split into two distinct layers: the top grain (upper layer), which contains the fine grain surface, and the split (lower layer), which lies beneath the grain and be further processed for various leather products. The figure below (Figure **4**.**1**) shows the beamhouse line, where the operations described above are carried out.

Figure 4.1 - Beamhouse line.

Within this chapter, each machine will be described in detail, including its technical specifications. Furthermore, a Life Data Analysis (LDA) will be conducted for every piece

of equipment. This analysis comprises the calculation of life characteristics and fundamental reliability functions. Among these, the CDF and the reliability function will be presented along with its associated confidence level. For this purpose, the beta-binomial distribution has been selected. It is important to note that this analysis considers data collected from the implementation of the ManWinWin system up to March 18th, 2025. The analysis is conducted using a self-developed program written in Python language (see Appendix A). The algorithm is able to directly connect the SQL database, where the maintenance repairs are stored, and after determining the TTF, performs the necessary calculation for the reliability analysis. The results are presented in the following sub-chapters.

To fully validate these results and assess the lifetime distribution of each machine, the Chi-Square test will be applied, assuming a significance level of 5% (see Appendix B).

Finally, the reliability of each piece of equipment and the whole system will be calculated for five different times: 50 hours, 100 hours, 150 hours, 300 hours and 500 hours.

4.1 Leather transport clamp

4.1.1 Description

Leather transport clamp (Figure **4.2**) is a machine that conveys natural hide directly to the fleshing machine. The main specifications are presented in the Table 4.1.

Figure 4.2 - Transport Clamp Machine.

Table 4.1 - Leather transport clamp technical specifications.

Manufacturer	Feltre
Model	CC Flesh
S/N	2595
Year	2017

4.1.2 Life data analysis

The following LDA is based on historical data from 2021, encompassing a total of 42 TTF instances. The Table 4.2 represents the results of the analysis.

Table 4.2 - LDA of transport clamp.

Shape parameter, β	0,80
Scale parameter, η [h]	614,62
MTBF [h]	694,43
Correlation coefficient, ρ	0,9894

Based on the life characteristics, it is possible to conclude that this machine is currently in its early failure period, as indicated by the shape parameter ($\beta < 1$). Furthermore, considering the correlation coefficient, which is very close to 1, it can be inferred that the model presents a high degree of accuracy, and the results are statistically reliable. Additionally, a Chi-Squared test has been carried out to validate the lifetime distribution. The results are presented within Table 4.3.

Table 4.3 - Chi-square test of the transport clamp lifetime distribution (Weibull - 2 parameter).

Chi-square (Observed value)	12,481
Chi-square (Critical value)	14,067
Degrees of freedom, *v*	7
P-value	0,086
Significance level, α	0,05

The following interpretation can be drawn from Table 4.3:

H_0: The sample follows a Weibull – 2 parameter distribution

H_a: The sample does not follow a Weibull - 2 parameter distribution

As the computed p-value is greater than the significance level, one cannot reject the null hypothesis H_0.

In this regard, the 2-parameter Weibull distribution formulas can be applied to determine the pdf, reliability, CDF and failure rate, depending on parameter time, *t*.

Table 4.4 - LDA functions of the transport clamp.

Pdf	$\frac{0,80}{614,62} \cdot \left(\frac{t}{614,62}\right)^{0,80-1} \cdot e^{-\left(\frac{t}{614,62}\right)^{0,80}}$
Reliability	$e^{-\left[\frac{t}{614,62}\right]^{0,80}}$
CDF	$1 - e^{-\left[\frac{t}{614,62}\right]^{0,80}}$
Failure rate	$\left(\frac{0,80}{614,62}\right) \cdot \left(\frac{t}{614,62}\right)^{0,80-1}$

Based on the fundamental functions presented in the Table 4.4, the corresponding curves will be plotted below (Figure **4.3**, Figure **4.4**, Figure **4.5**, Figure **4.6**).

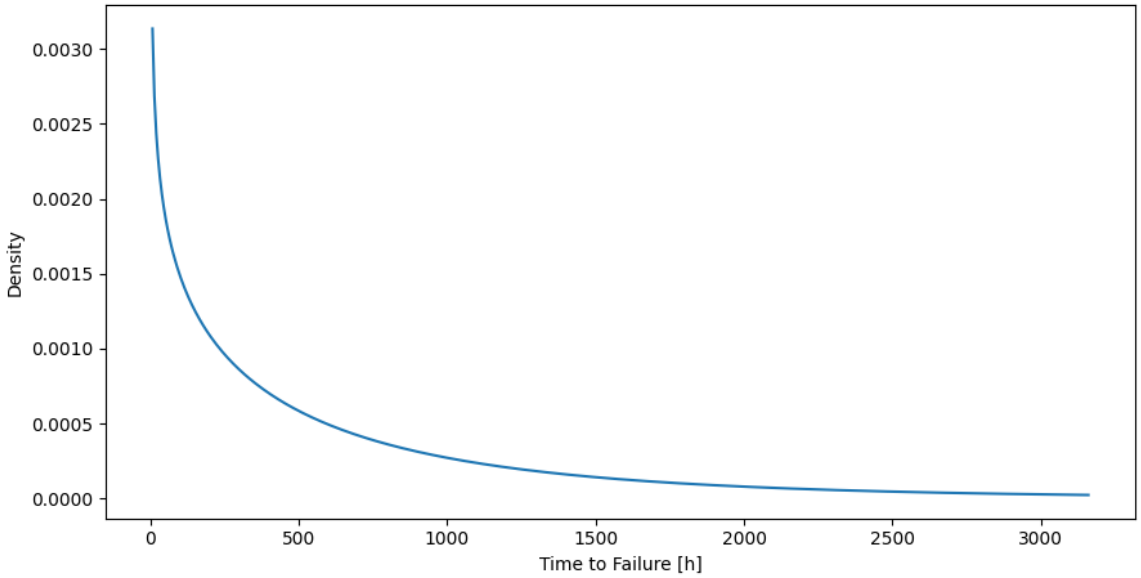

Figure 4.3 - Pdf of the transport clamp machine.

The Figure **4.3** shows the probability density function of the time to failure. Its observed decreasing curve suggests a higher probability of early failures (infant mortality), followed by a decreasing probability of failure over time. This pattern is consistent with the current piece of equipment state – infant mortality.

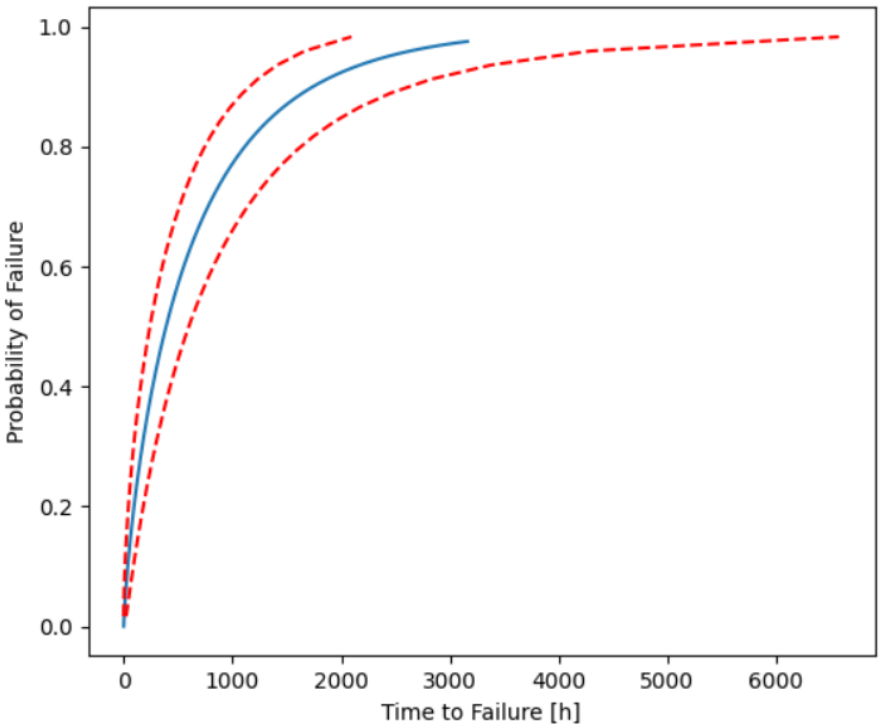

Figure 4.4 - CDF of the transport clamp with 90% confidence bounds.

The solid line in the Figure **4.4** represents a Weibull reliability model, which estimates the probability of failure at any given time. The dashed lines indicate the confidence intervals, reflecting the uncertainty involved with the model estimate. The upward, S-shaped curve indicates an increase in the probability of failure with increasing operational time.

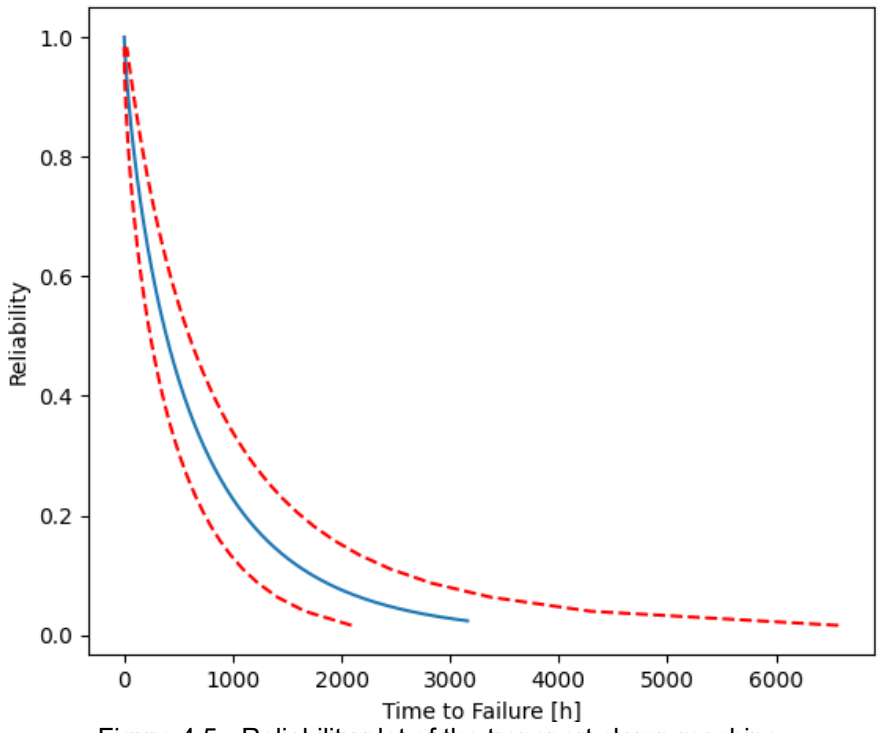

Figure 4.5 - Reliability plot of the transport clamp machine.

The reliability plot, which is illustrated by Figure **4.5**, exhibits a complementary decreasing trend to the failure probability. The confidence bounds similarly widen with time, providing important information about the precision of the reliability estimates at different time points.

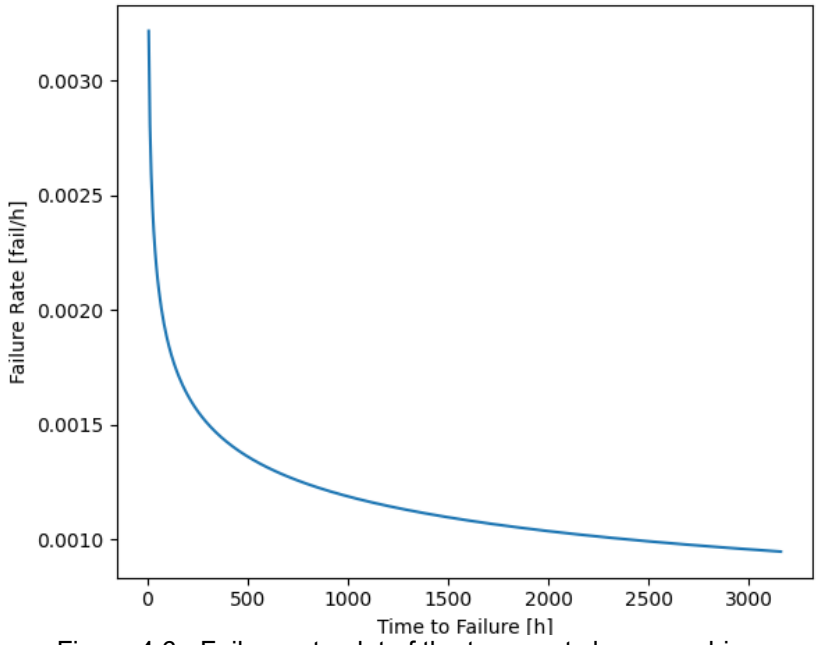

Figure 4.6 - Failure rate plot of the transport clamp machine.

The failure rate curve, represented in the Figure **4.6**, provides crucial information about the machine's aging characteristics and failure patterns. The shape of this curve indicates that the transport clamp in analysis experiences infant failures, a conclusion that was already supported by the analysis the shape parameter ($\beta < 1$).

In the end, Table 4.5 presents the reliability results of the transport clamp for the five time intervals (50 hours, 100 hours, 150 hours, 300 hours, 500 hours).

Table 4.5 - Reliability of the transport clamp at 50, 100, 150, 300 and 500 hours.

Time (h)	50	100	150	300	500
Reliability (%)	87,52	79,24	72,46	57,00	42,86

4.2 Fleshing machine

4.2.1 Description

This continuous fleshing machine (Figure **4.7**) presented in this study retains the core functionality of traditional fleshing equipment while incorporating several enhancements aimed at increasing efficiency and reducing manual intervention. Instead, it is inserted

into the feed opening to the appropriate depth, after which the machine operates autonomously, maintaining uninterrupted functionality even during the feeding phase. Proceeded hides exit from the rear of the machine, with the grain side facing upward. This output configuration is easily integrated into a linear processing system. Especially in relation to splitting machines where a more linear feed and workflow are able to be accommodated.

The machine is equipped with a fully hydraulic system for opening and closing motions, an upgrade hydraulic unit enhances the operation performance and reduces the mechanical wear on the machine. The full hydraulic unit provides electronic controlling of the conveying speeds, so they can keep accurate to achieve continuous throughput, time savings and ultimately contribute to the longevity of the system in the end.

From a structural point of view, the machine uses stainless steel protective covers, which can offer better corrosion resistance and facilitate easier cleaning – an important consideration in environments requiring high standards of hygiene and durability.

Figure 4.7 - Fleshing Machine.

The fleshing cycle begins by positioning the hide into the upper intake of the machine, starting from the head end. Once initiated by the operator, the system engages the fleshing bench, allowing the hide to be drawn into the machine. During this initial stage, the tail portion undergoes processing.

Throughout the operation, the operator oversees the hide's movement and triggers the processing of the remaining section, specifically, the neck area, at the appropriate point. As the procedure continues, the hide advances through the machine and is ultimately discharged via the front conveyor belt. It exits to the conveyor belt with the grain surface facing upwards and the tail end leading.

Schematically, these processes can be split into four phases, represented in the Figure **4.8**, Figure **4.9**, Figure **4.10** and Figure **4.11**:

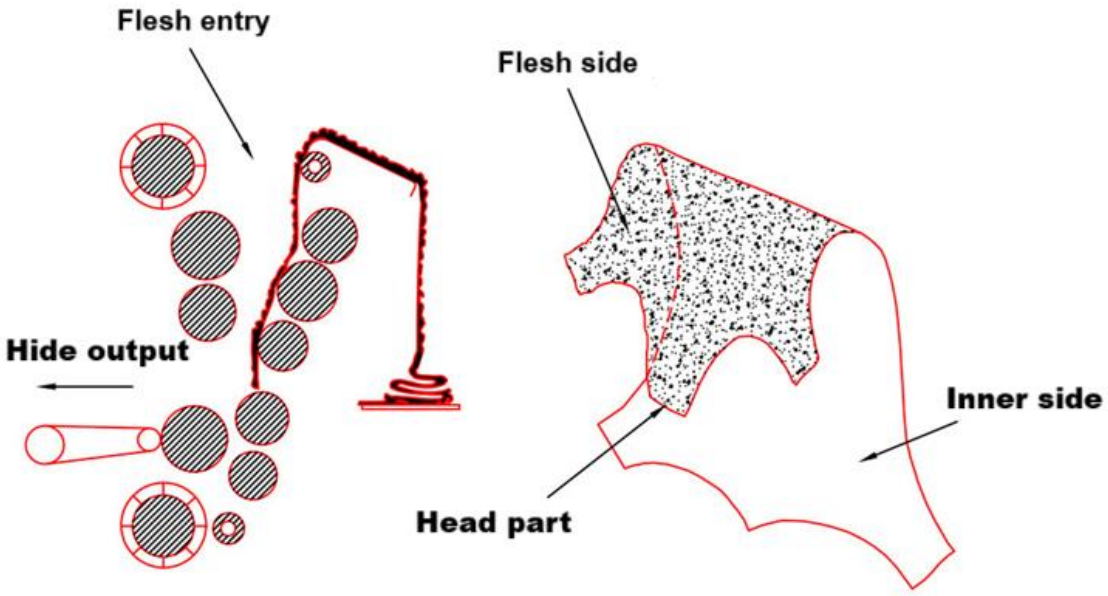

Figure 4.8 - Phase 1 of the fleshing machine (adapted from **[128]**).

In the Figure **4.8**, the hide is introduced into the machine beginning with the head section. As it advances internally, the rear portion, corresponding to the tail, is subjected to the fleshing process.

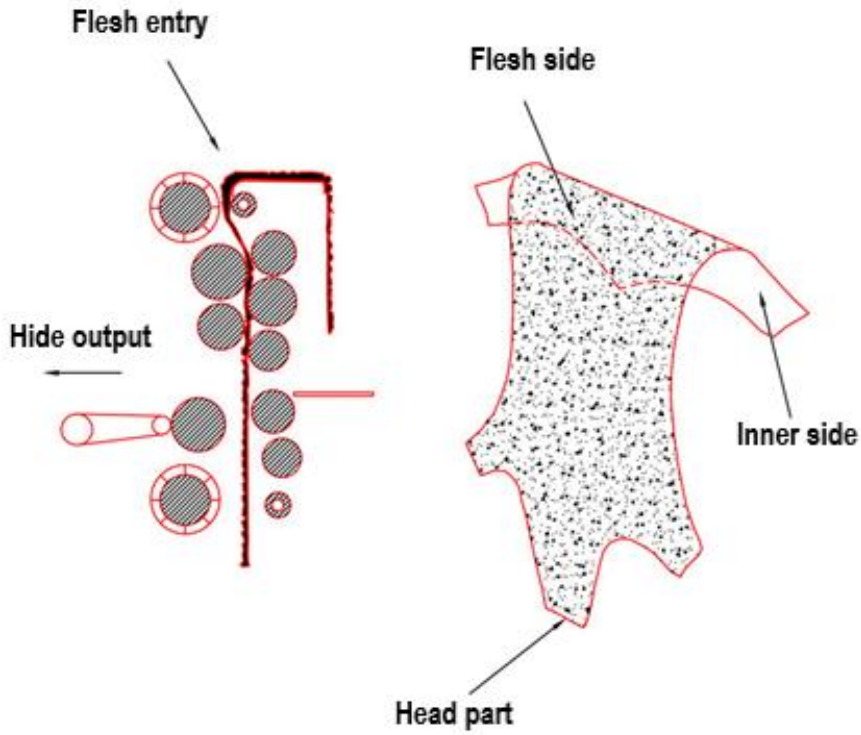

Figure 4.9 - Phase 2 of the fleshing machine (adapted from **[128]**).

In the figure above, the hide is guided downward onto the lower transport rollers, where it continues moving until the operator visually confirms the approach of the fleshy area, typically observed via the inspection area.

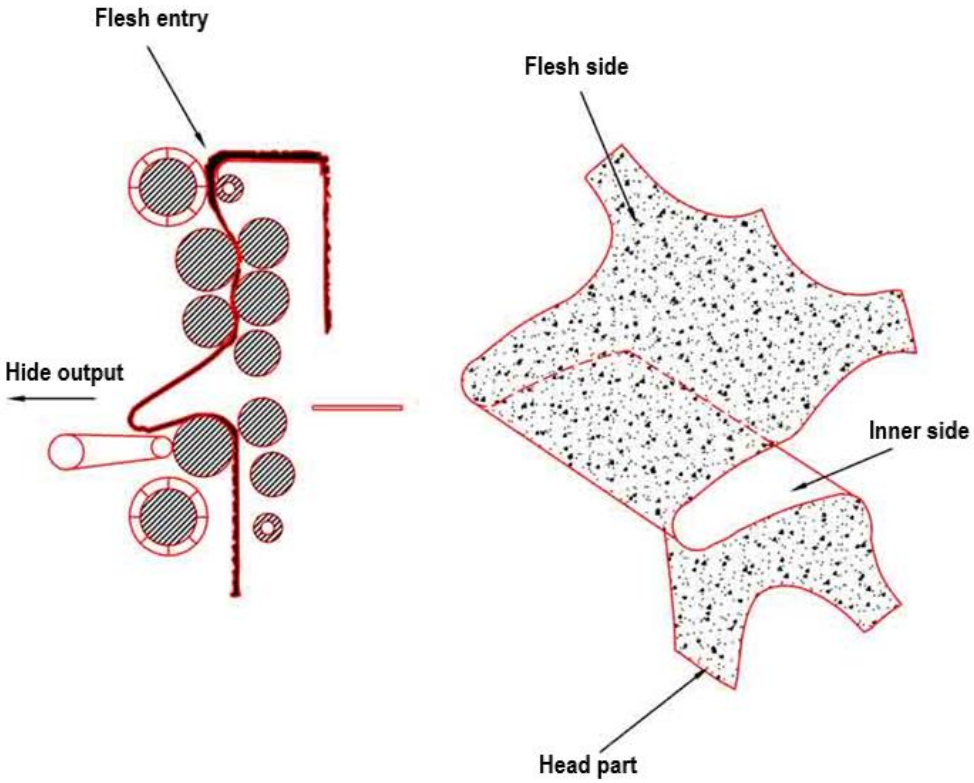

Figure 4.10 - Phase 3 of the fleshing machine (adapted from **[128]**).

The Figure **4.10** illustrates the closure of the lower transport roller.

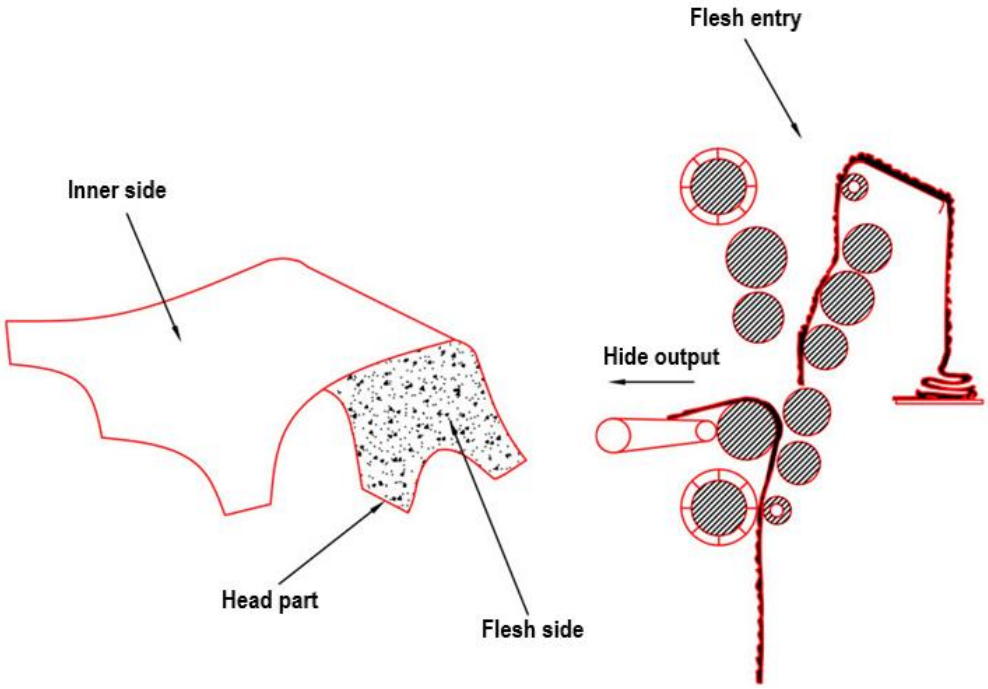

Figure 4.11 - Phase 4 of the fleshing machine (adapted from **[128]**).

The illustration above shows the process, which continues with the opening of the swinging bench in the upper section and its closure in the lower part of the machine. This transition initiates the fleshing operation for the second half of the hide, specifically the head section, within the lower processing zone. Upon completion, the fully fleshed hide is discharged via the front exit conveyor, emerging with the tail end leading and the grain surface facing upward.

Table 4.6 - Technical specifications of the fleshing machine.

Manufacturer	Persico
Model	SP34
S/N	39X42
Year	2017

4.2.2 Life data analysis

The following LDA is based on historical data from 2019, comprising a total of 321 TTF records. The results of this analysis are presented in the Table 4.7.

Table 4.7 – Life data characteristics of the fleshing machine.

Shape parameter, β	0,78
Scale parameter, η [h]	138,48
MTBF [h]	159,99
Correlation coefficient, ρ	0,9915

Based on the results of the Table 4.7, the reliability analysis reveals key insights into the fleshing machine's operational characteristics. The shape parameter, β = 0,78, indicates a decreasing failure rate over time, which is typical of early-life failures. This suggests that once the infant failures are overcomed, the system becomes increasingly reliable. The scale parameter, η = 138,48 hours, represents the characteristic life of the item, acting as a benchmark for the expected time by which approximately 63,2% of similar units would have experienced at least one failure.

Finally, a high correlation coefficient of ρ = 0,9915 underscores the excellent fit of the Weibull model to the observed data, thereby affirming the robustness of the reliability predictions. However, to fully validate this hypothesis, a chi-square test is carried out, which results are presented in Table 4.8.

Table 4.8 - Chi-square test of the fleshing machine lifetime distribution (Weibull - 2 parameter).

Chi-square (Observed value)	7,868
Chi-square (Critical value)	14,067
Degrees of freedom, *v*	7
P-value	0,344
Significance level, α	0,05

Table 4.8 allows for the following interpretation:

H_0: The sample follows a Weibull – 2 parameter distribution

H_a: The sample does not follow a Weibull - 2 parameter distribution

As the computed p-value is greater than the significance level, one cannot reject the null hypothesis H_0.

Based on the shape and scale parameters, 2-parameter Weibull distribution is applied to determine the fundamental LDA functions (Table 4.9).

Table 4.9 - LDA fundamental functions for the fleshing machine.

Pdf	$\frac{0,78}{138,48} \cdot \left(\frac{t}{138,48}\right)^{0,78-1} \cdot e^{-\left(\frac{t}{138,48}\right)^{0,78}}$
Reliability	$e^{-\left[\frac{t}{138,48}\right]^{0,78}}$
CDF	$1 - e^{-\left[\frac{t}{138,48}\right]^{0,78}}$
Failure rate	$\left(\frac{0,78}{138,48}\right) \cdot \left(\frac{t}{138,48}\right)^{0,78-1}$

Given Table 4.9, the four functions can now be plotted in function of time (Figure **4.12**, Figure **4.13**, Figure **4.14** and Figure **4.15**).

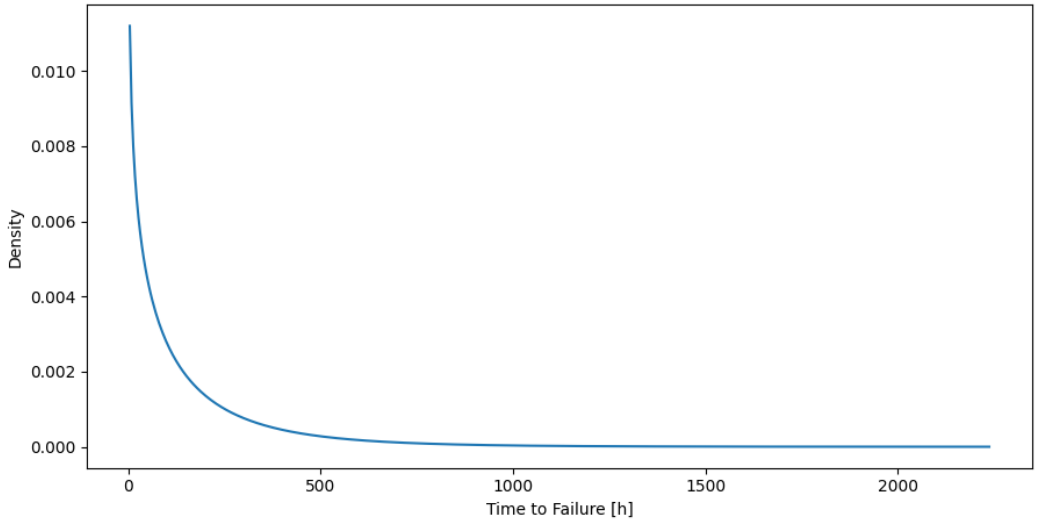

Figure 4.12 - Pdf curve of the fleshing machine.

Figure **4.12**, alike Figure **4.3**, shows a similar behavior over time. The curve shows a high probability of failure early on, which then gradually decreases in less than 250 hours. This suggests that early failures are more common, and the system becomes more reliable over time (although reliability is still decreasing - Figure **4.14**). This is consistent with an item exhibiting infant mortality.

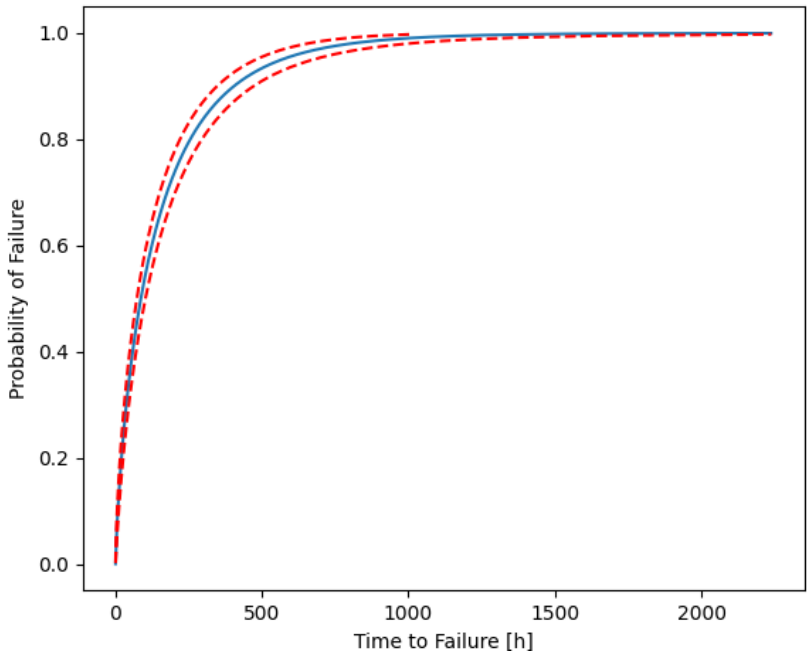

Figure 4.13 - CDF curve of the fleshing machine.

The Figure **4.13** represents the cumulative density function over time for the fleshing machine. A close inspection of the curve presents a notable increase in probability of failure, indicating a steep rise over time. Moreover, the dashed lines, marking the confidence bounds, reside remarkably close to the fitted model, indicating that the forecasts are highly reliable.

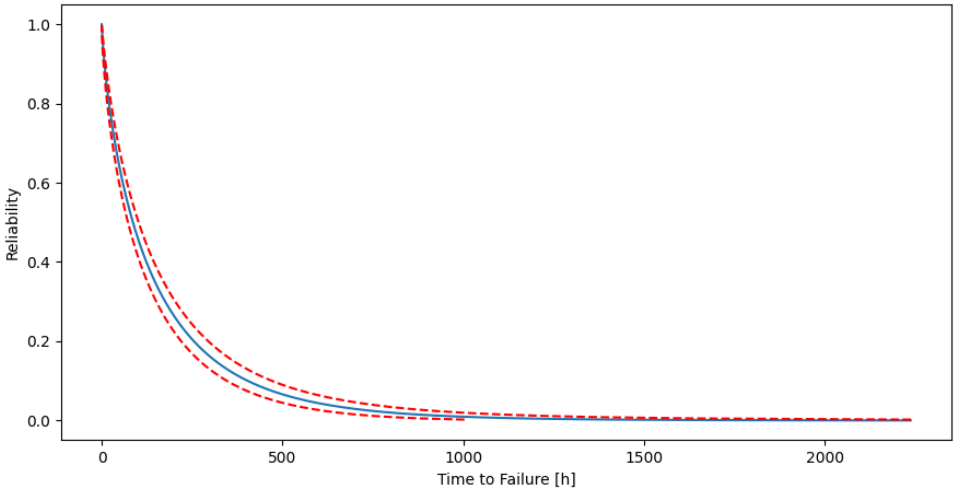

Figure 4.14 - Reliability curve of the fleshing machine.

Figure **4.14** displays behavior complementary to that shown in Figure **4.13**. Although CDF increases over time, the reliability function decreases correspondingly. Moreover, the narrow confidence bounds suggest low uncertainty, owing to the significant number of TTF analyzed and the very high correlation coefficient.

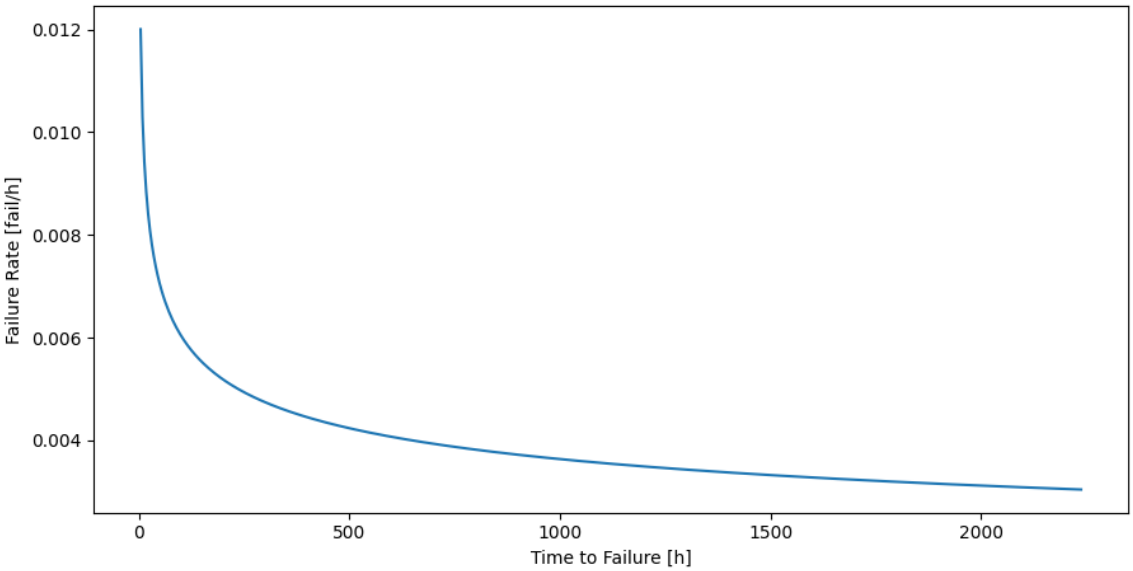

Figure 4.15 - Failure rate of the fleshing machine.

Figure **4.15** illustrates the hazard rate of the fleshing machine, which decreases over time. This indicates that the piece of equipment is becoming less prone to failure as it ages, after an initial period of higher failure probability. This is consistent with the bathtub curve failure pattern, where there is an initial high failure rate decreasing over time – infant mortality.

Ultimately, Table 4.10 demonstrates the reliability of the fleshing machine for the five time intervals.

Table 4.10 - Reliability of the fleshing machine at 50, 100, 150, 300 and 500 hours.

Time (h)	50	100	150	300	500
Reliability (%)	63,62	46,03	34,50	16,10	6,59

4.3 Belt conveyor & Cutting line

4.3.1 Description

The Trimstar cutting line (Figure **4.16**), manufactured by Feltre, is used in tannery industry for trimming and transporting leather. The main functions of the machine are managed by a programmable logic controller (PLC). The table below presents the technical specifications of this piece of equipment.

Figure 4.16 - Belt conveyor and cutting line.

Table 4.11 - Technical specifications of the cutting line.

Manufacturer	Feltre
Model	Trimstar Pro
S/N	3053
Year	2020

4.3.2 Life data analysis

The life data variables resulting from LDA are based on data from 2021, which is converted into 206 TTF. Consequently, the results are displayed in the Table 4.12.

Table 4.12 – Life data characteristics of the cutting machine.

Shape parameter, β	0,72
Scale parameter, η [h]	133,68
MTBF [h]	164,09
Correlation coefficient, ρ	0,9875

Table 4.12 presents the parameters of the Weibull distribution fitted to the TTF data. The shape parameter (β = 0,72) indicates a decreasing failure rate, given that β < 1. The scale parameter, ρ = 133,67 hours, represents the characteristic life of the cutting machine. The high correlation coefficient (ρ = 0,9875) indicates a strong fit of the Weibull distribution to the observed data, which provides means of quantifying the important reliability parameters such as MTBF. Nevertheless, the results of the chi-square goodness of fit test are presented in Table 4.13.

Table 4.13 - Chi-square test of the belt conveyor and cutting line lifetime distribution (Weibull - 2 parameter).

Chi-square (Observed value)	6,237
Chi-square (Critical value)	14,067
Degrees of freedom, *v*	7
P-value	0,512
Significance level, α	0,05

Table 4.13 suggests the following interpretation:

H_0: The sample follows a Weibull – 2 parameter distribution

H_a: The sample does not follow a Weibull - 2 parameter distribution

As the computed p-value is greater than the significance level, one cannot reject the null hypothesis H_0.

In this context, the fundamental functions are therefore presented in Table 4.14.

Table 4.14 - Life data fundamental functions of the cutting line and belt conveyor.

Pdf	$\frac{0,72}{133,68} \cdot \left(\frac{t}{133,68}\right)^{0,72-1} \cdot e^{-\left(\frac{t}{133,68}\right)^{0,72}}$
Reliability	$e^{-\left[\frac{t}{133,68}\right]^{0,72}}$
CDF	$1 - e^{-\left[\frac{t}{133,68}\right]^{0,72}}$
Failure rate	$\left(\frac{0,72}{133,68}\right) \cdot \left(\frac{t}{133,68}\right)^{0,72-1}$

Based on the expressions presented in Table 4.14, the fundamental functions are subsequently plotted in Figure **4**.**17**, Figure **4**.**18**, Figure **4**.**19** and Figure **4**.**20**.

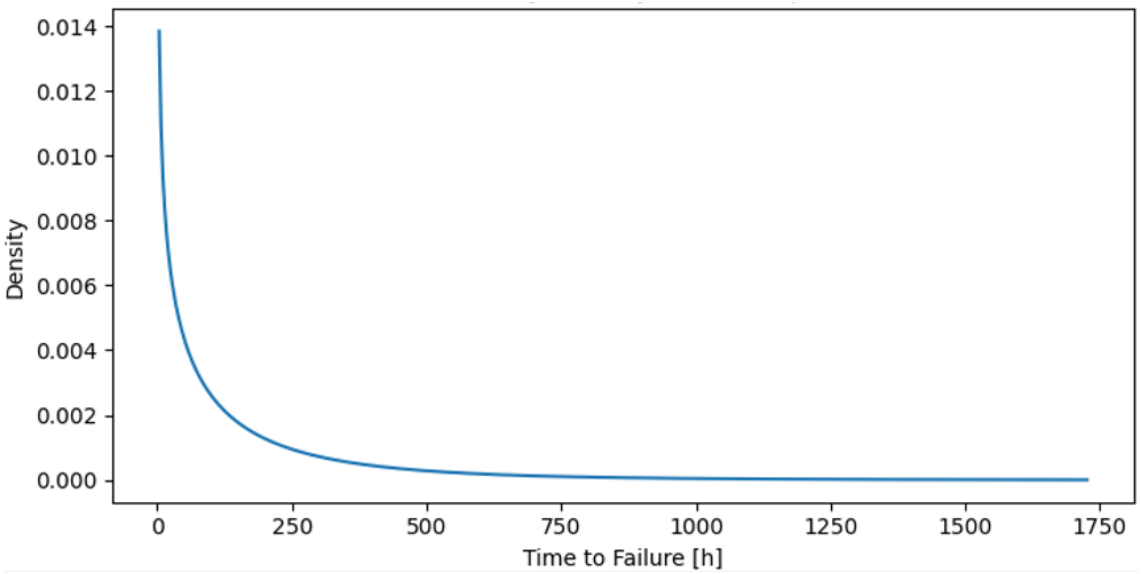

Figure 4.17 - Probability density function of the belt conveyor and cutting line.

The plot illustrated in Figure **4.17** displays the pdf model in function of time. The curve is sharply peaked near the origin, indicating that most failures occur early in the system's life. The long right tail shows that while most units fail early, a small proportion survive much longer. This distribution is typical of systems with a significant infant mortality phase, followed by a period of lower, more stable failure rates.

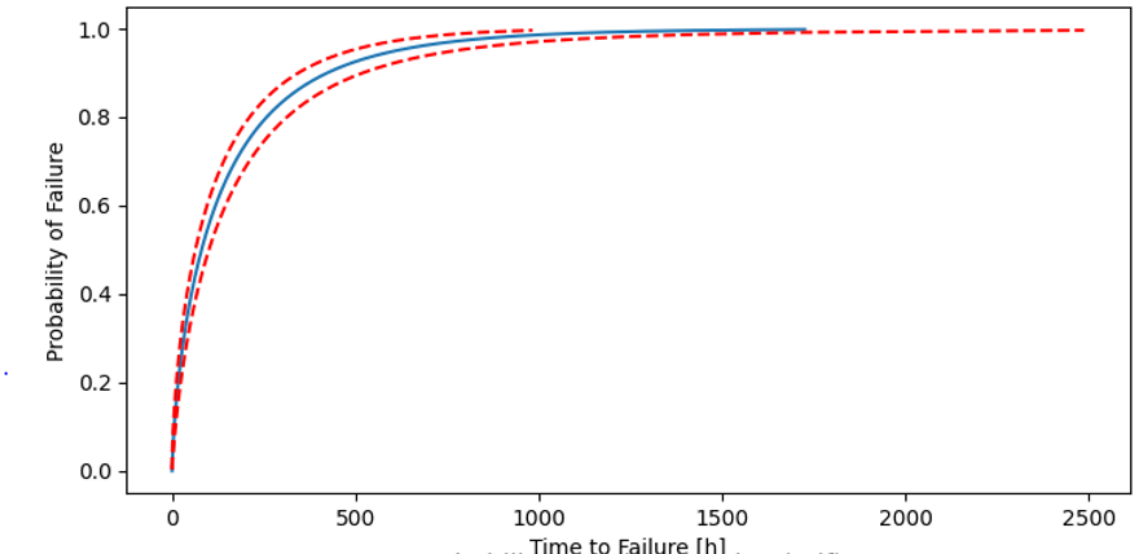

Figure 4.18 - CDF plot of the belt conveyor and cutting line vs time.

This plot, observed in Figure **4.18**, presents the cumulative probability that the belt conveyor system will have failed by a given time. The main curve (solid blue) shows a classic S-shaped growth, starting near zero and approaching one as time increases. The two dashed red lines represent confidence bounds based on sample variability. The relatively narrow band between these lines suggests a high degree of certainty in the failure probability estimates. In other words, the data gives a strong indication of the parameter's value.

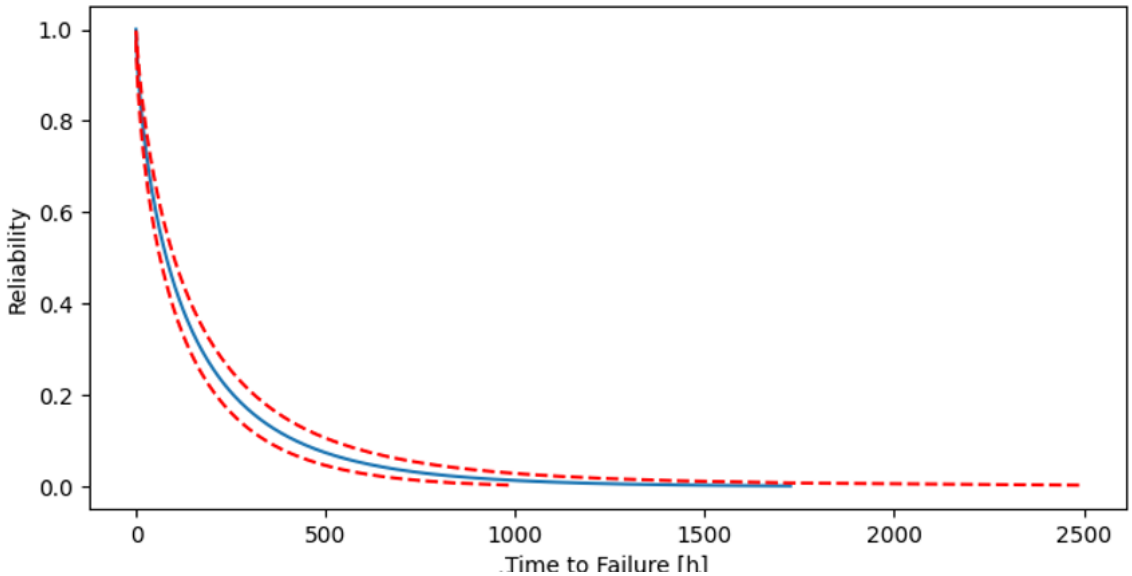

Figure 4.19 - Reliability plot of the belt conveyor and cutting line vs time, in hours.

The plot above, presented by Figure **4.19**, shows the reliability function (solid blue). The curve starts at 1 (full reliability at time zero) and decreases rapidly at first, then more slowly, approaching zero as time increases.

The rapid initial decline mirrors the early failures seen in the probability of failure plot. Similar to the CDF curve, the narrow dashed red lines indicate a high level of precision in the model's fit to the data.

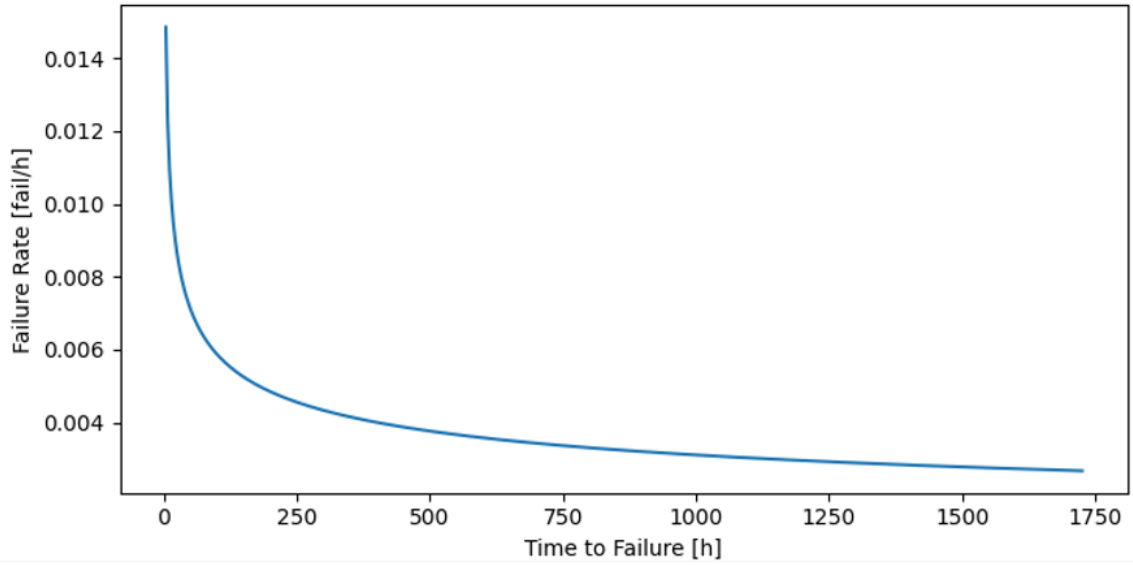

Figure 4.20 - Failure rate curve as function of time of the belt conveyor and cutting line.

The failure rate, observed in Figure **4.20**, starts high, decreases rapidly, and then stabilizes at a lower level. This is a classic shape, common in the early phase due to infant mortality. This is further supported by the shape parameter, which is lower than one ($\beta < 1$).

At last, the reliability of the conveyor belt and cutting line is highlighted at 50, 100, 150, 300 and 500 hours in Table 4.15.

Table 4.15 - Reliability of the conveyor belt and cutting line at 50, 100, 150, 300 and 500 hours.

Time (h)	50	100	150	300	500
Reliability (%)	61,22	44,46	33,73	16,61	7,44

4.4 Lime splitting machine

4.4.1 Description

This machine (Figure **4.21**), called the Predator splitter and manufactured by Alpe Spaks S.R.L Centro Spaccatrici, is intended exclusively for splitting hides into two layers: the upper layer, known as the top grain, and the lower layer, known as the split. The separation is performed by a blade along a conveyor belt. The hide must be inserted into the splitter, which is automatically fed by a bench-mounted conveyor.

Figure 4.21 - Lime splitting machine.

Table 4.16 - Technical specifications of the lime splitting machine.

Manufacturer	Alpe
Model	Predator 3100
S/N	PRE 3120013
Year	2020

4.4.2 Life data analysis

The results of the LDA below are based on data from 2021, resulting in 428 TTF. The outputs are presented in the Table 4.17.

Table 4.17 – Life data characteristics of the lime splitting machine.

Shape parameter, β	0,63
Scale parameter, η [h]	66,74
MTBF [h]	93,85
Correlation coefficient, ρ	0,9928

The Table 4.17 presents key statistical parameters for characterizing the lifetime model, using a Weibull distribution. The shape parameter, β, is 0,63, indicating a decreasing failure rate characteristic typical of early periods. The scale parameter, η, is 66,74 hours, representing the characteristic life of the lime splitting machine under study. The MTBF is calculated as 93,85 hours, providing an estimate of the expected operational time between consecutive failures. The correlation coefficient, ρ, of 0,9928 demonstrates an excellent goodness of fit between the theoretical Weibull model and empirical data. The relatively low shape parameter combined with the scale parameter indicates that failures occur more frequently in the early operational period, which is characteristic of equipment experiencing infant mortality. The high correlation coefficient (a value close to one) suggests that Weibull distribution provides an accurate representation of the failure behavior of the lime splitting machine. Nonetheless, the chi-square test is conducted to completely determine this hypothesis, which results are presented in Table 4.18.

Table 4.18 - Chi-square test of the lime splitting machine lifetime distribution (Weibull - 2 parameter).

Chi-square (Observed value)	10,589
Chi-square (Critical value)	14,067
Degrees of freedom, *v*	7
P-value	0,158
Significance level, α	0,05

The data presented in Table 4.18 support the following interpretation:

H_0: The sample follows a Weibull – 2 parameter distribution

H_a: The sample does not follow a Weibull - 2 parameter distribution

As the computed p-value is greater than the significance level, one cannot reject the null hypothesis H_0.

Based on previous conclusions, the 2-parameter Weibull distribution is suitable for modelling the lifetime behavior, which mathematical expressions are presented in Table 4.19.

Table 4.19 - Life data fundamental functions of the lime splitting machine.

Pdf	$\frac{0,63}{66,74} \cdot \left(\frac{t}{66,74}\right)^{0,63-1} \cdot e^{-\left(\frac{t}{66,74}\right)^{0,63}}$
Reliability	$e^{-\left[\frac{t}{66,74}\right]^{0,63}}$
CDF	$1 - e^{-\left[\frac{t}{66,74}\right]^{0,63}}$
Failure rate	$\left(\frac{0,63}{66,74}\right) \cdot \left(\frac{t}{66,74}\right)^{0,63-1}$

According to mathematical expressions from Table 4.19, they can now be plotted to illustrate the behavior of the model (Figure **4.22**, Figure **4.23**, Figure **4.24** and Figure **4.25**).

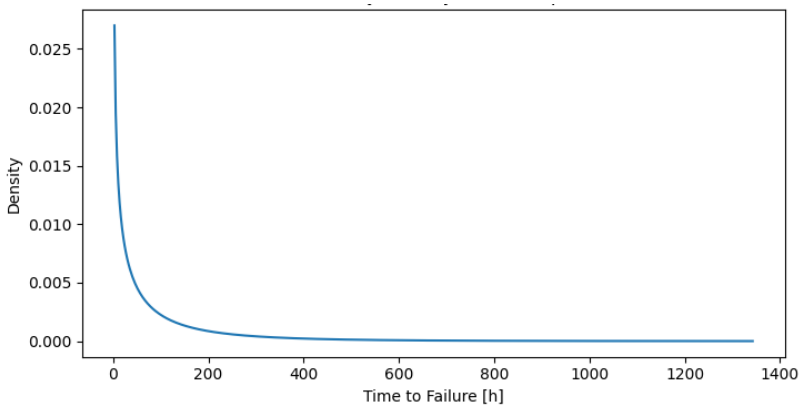

Figure 4.22 - Pdf curve of the lime splitting machine.

This plot, illustrated in Figure **4.22**, shows the pdf in terms of time, representing the instantaneous likelihood of failure occurring at a specific time. The curve has a very sharp peak at very short times, then rapidly declines to zero as time increases. This indicates that failures are most likely to occur during the burn-in period, and the chances of failure at any given time decreasing as time progresses.

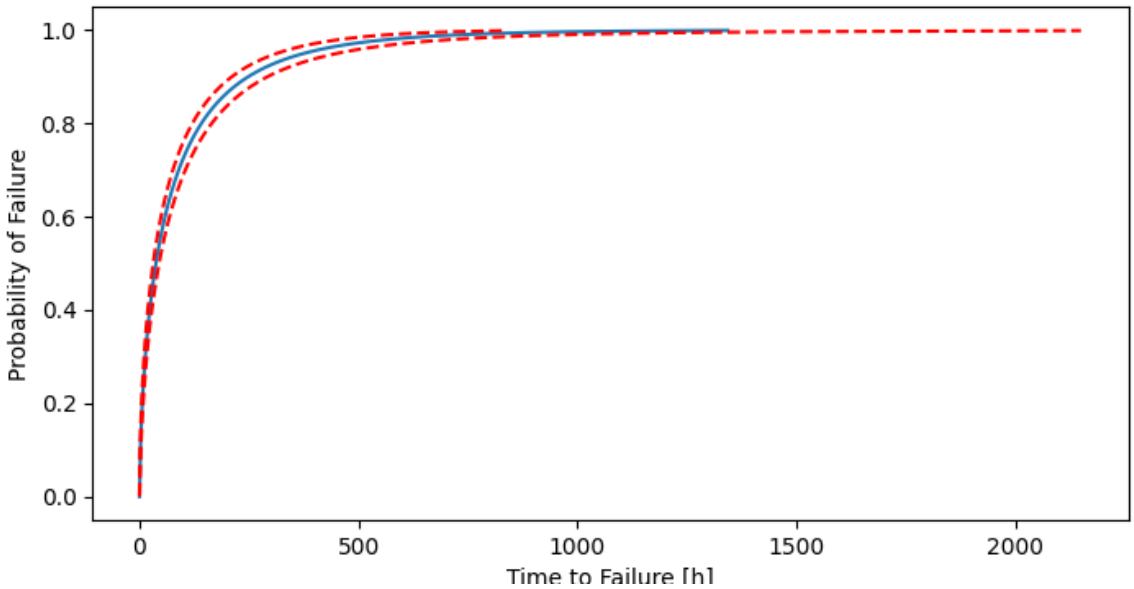

Figure 4.23 - CDF curve of the lime splitting machine.

Figure **4.23** illustrates the CDF that this machine will have failed by a given time. The curve (solid blue) exhibits a S-shaped growth, starting at zero and asymptotically approaching a probability of one as time increases. The confidence bounds (red dashed lines) are extremely close to the CDF curve, indicating a high level of certainty for a specific probability of unsuccess.

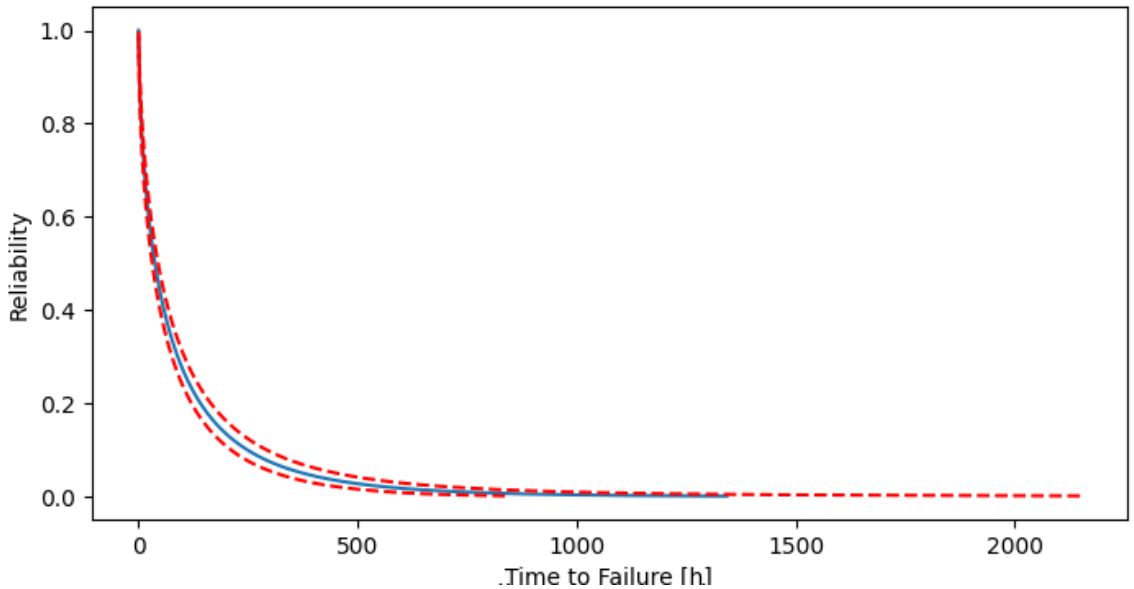

Figure 4.24 - Reliability plot of the lime splitting machine.

The plot, presented in Figure **4.24**, outlines the reliability function, which is the probability that the lime splitting machine survives up to a given time without failure. The curve (solid blue) starts at a reliability of one and decreases rapidly towards zero as time increases. Within 250 hours of operation, the reliability of the lime splitting machine falls below 20%.

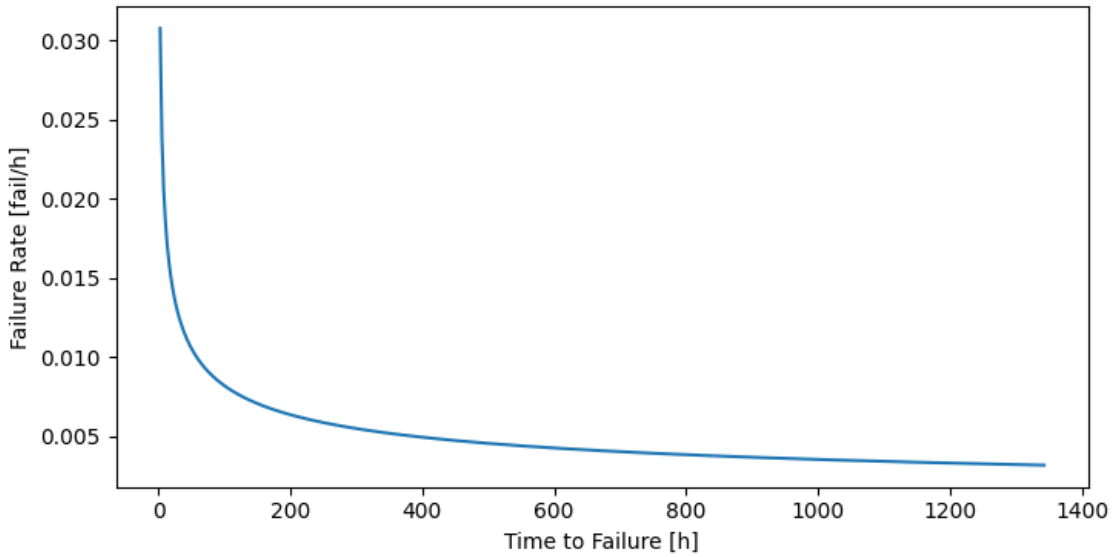

Figure 4.25 - Hazard rate of the lime splitting machine.

The hazard rate function in terms of time is given in Figure **4.25**. The failure rate is at its highest at the very beginning, and it decreases monotonically as time increases, approaching a low value at longer times. This type of behavior is typical for systems that exhibit early failures due to infant failures.

As a final point, Table 4.20 shows the probability of success for the five time intervals: 50 hours, 100 hours, 150 hours, 300 hours, and 500 hours.

Table 4.20 - Reliability of the lime splitting machine at 50, 100, 150, 300 and 500 hours.

Time (h)	50	100	150	300	500
Reliability (%)	43,49	27,47	18,81	7,48	2,78

4.5 System's reliability

The beamhouse line combines, mainly, the function of the four machines presented in Chapters 4.1, 4.2, 4.3 and 4.4. The four machines operate in series as illustrated by the RBD in the Figure **4.26**, and independently of each other.

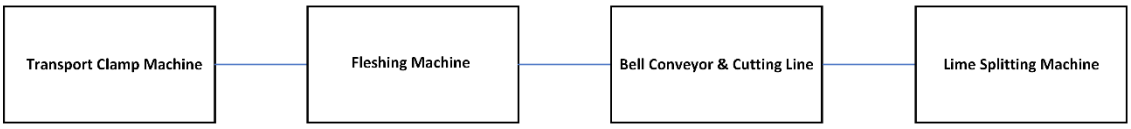

Figure 4.26 - Beamhouse line RBD in a series configuration.

Figure **4.26** represents the RBD of the system under analysis. The items are arranged in a series configuration, corresponding to the sequential steps of the production process, starting with the leather transport clamp machine and ending with the lime splitting machine. The system is considered operational as long as all components are

functioning; it fails when any single component ceases to operate. Consequently, the reliability equations presented in the Chapter 3.5.1 will be applied in this section to calculate the overall system reliability (Table 4.21). MTBF is calculated with the help of Equation (3.15).

Table 4.21 - Overall beamhouse line reliability.

Time (h)	50	100	150	300	500
Reliability (%)	14,82	4,45	1,59	0,114	0,00584
Probability of Failure (%)	85,18	95,55	98,41	99,89	99,99
MTBF (h)	25,05				

The data from Table 4.21 indicates a high probability of failure within a relatively short timeframe. For instance, at 50 operating hours, the reliability is only 14,82%, implying an 85,18% probability of failure. This probability increases sharply as operating time increases, reaching 99,99% at 500 hours. The MTBF for the beamhouse line is recorded as 25,05 hours. This metric signifies, on average, the expected operating time before a failure occurs. The relatively low MTBF value, coupled with the low and rapid decrease of reliability, suggests that the beamhouse line is prone to frequent breakdowns. Therefore, the system improvement is presented in the next section.

4.6 System's reliability improvement

In this section, several alternative configurations, such as parallel and standby setups, are presented as potential improvements to the current setup. Complex and *k*-out-of-*n* systems will not be simulated, as they are not physically applicable in this context.

4.6.1 Parallel configuration

Within this section several redundant parallel configurations (Figure **4.27**) will be presented for comparison with the overall reliability of the current system.

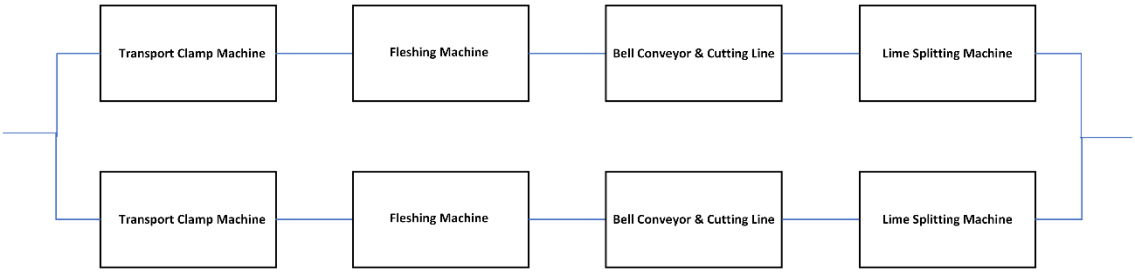

Figure 4.27 - Beamhouse line RBD in a parallel configuration.

Figure **4.27** illustrates two lines that are working simultaneously. The system fails only when the two lines stop operating. In this regard, since the series configuration reliability has already been determined for the various time periods, the RBD can be simplified as demonstrated in Figure **4.28**.

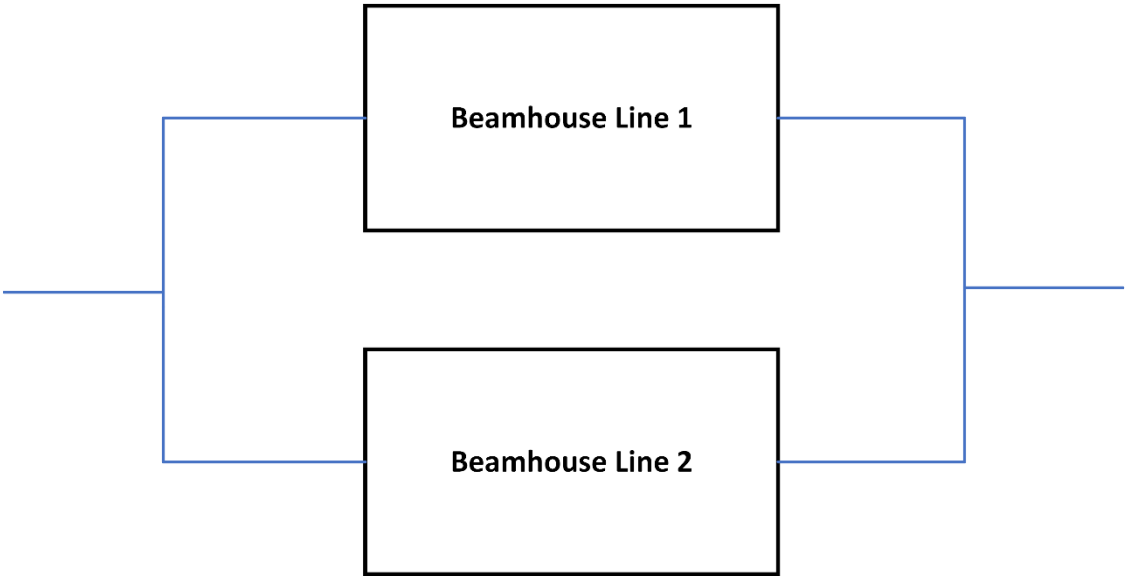

Figure 4.28 - Beamhouse line RBD in a parallel configuration (simplified).

Applying Equation (3.74) to the configuration illustrated in Figure **4.28**, the following results are obtained (Table 4.22).

Table 4.22 - Overall system reliability in a parallel configuration.

Time (h)	50	100	150	300	500
Reliability (%)	27,45	8,71	3,15	0,228	0,0117
Probability of Failure (%)	72,55	91,29	96,85	99,77	99,99
MTBF (h)	40,78				

Analysis of Table 4.22 reveals a modest increase in overall system reliability. While reliability at 50 operating hours improved from 14,82% to 27,45%, the overall reliability remains low, despite that the improvement increases over time (Table 4.23). Comparing with Table 4.21, the parallel configuration manages to maintain a reliability level approximately twice as high at each interval, which represents a substantial improvement, even though both systems exhibit a sharp decline in reliability over time.

Consequently, the unreliability is consistently lower in the parallel configuration during the initial and intermediate stages. At 50 hours the probability of failure is 72,55% for the parallel system, in contrast to 85,18% for the beamhouse line. This difference persists

up to 300 hours. However, both systems converge to a probability of failure of 99,99% at 500 hours, indicating that in the long run, even parallel redundancy can not prevent an eventual near certainty of failure.

The MTBF is a crucial metric that corroborates the superiority of the parallel configuration. The parallel system shows an MTBF of 40,78 hours, which is higher than the 25,05 hours of the series system.

Moreover, the greatest advantage of this type of configuration is that it escalates production capacity through improved reliability, making it a suitable option for organizations that seek both objectives.

Table 4.23 - Reliability improvement by comparing the series beamhouse line system and in a parallel configuration.

Time (h)	50	100	150	300	500
Reliability Improvement (%)	+12,63	+4,26	+1,56	+0,114	+0,00586
MTBF Improvement (h)	+15,73				

As observed in Table 4.23, the improvement of reliability increases over time, but the growth is each time less.

In this context, it is possible to determine the number of beamhouse lines required to guarantee, for example, 90% reliability at 50 operating hours under the same conditions:

$$R_{sp50} = 0{,}90 = 1 - 0{,}8517^{n} \leftrightarrow n \cong 14{,}35 \ \rightarrow n = 15\ lines, n \in \mathbb{N}$$

Where R_{sp50} corresponds to the reliability at 50 operating hours when the system follows a parallel configuration.
Assuming the leather producing company operates 15 beamhouse lines simultaneously, the resulting reliability is presented in Table 4.24.

Table 4.24 - System reliability overall for 15 beamhouse lines in a parallel configuration.

Time (h)	50	100	150	300	500
Reliability (%)	90,99	49,52	21,32	1,70	0,0876
Probability of Failure (%)	9,01	50,48	78,68	98,30	99,91
MTBF (h)	113,85				

The analysis of Table 4.24 reveals a significant enhancement when compared to the current system reliability overall. Table 4.21, representing the initial system configuration, shows a rapid decline in reliability over time, with a reliability, for example, of 4,45% at 100 operating hours and 1,59 % at 150 hours. In contrast, Table 4.24, illustrating the performance after improvement, demonstrates a substantial improvement (Table 4.25). While reliability still decreases with operating time, the decline is considerably less steep. At 100 hours, the reliability has increased to 49,52%, and at 150 hours, it reaches 21,32%.

Consequently, the probability of failure is drastically mitigated in the fifteen-line parallel configuration, particularly during the initial phases of operation. At 50 hours, the unreliability for the parallel system is a mere 9,01%, in stark opposition to 85,18% for the single line. By 100 hours, the parallel system's probability of failure is 50,48%, whereas the single line has already reached 95,55%. At 150 hours, the probability of failure for the parallel system is 78,66%, still substantially lower than the single line's 98,41%. Although the probability of failure approaches unity for both systems at very extended operating times, the parallel configuration undeniably affords a considerably longer operational period.

The MTBF provides the most compelling quantitative evidence of improvement. The system incorporating fifteen parallel lines exhibits an MTBF of 113,85 hours, which represents an increase of over fourfold compared to the 25,05 hours of a single beamhouse line.

Table 4.25 - Reliability improvement by comparing the beamhouse line in a series configuration and in a parallel configuration with 15 lines.

Time (h)	50	100	150	300	500
Reliability Improvement (%)	+76,17	+45,07	+19,73	+1,59	+0,082
MTBF Improvement (h)	+88,8				

A comparison of the reliability improvements, shown in Table 4.23 and Table 4.25, highlights significant gains resulting from the simulated system improvement. Notably, the reliability improvement decreases significantly as time increases on both configurations. This indicates that the benefit of redundancy strategy is very high at short operating times, and marginal as time increases.

An alternative to fully parallel configuration is to implement partial redundancy by equipping only selected elements with backup systems. This approach is more cost-effective, as it avoids the need to duplicate the entire beamhouse line. However, this

configuration is expected to offer lower overall system reliability compared to a fully parallel setup. Despite this, it still provides a significant reliability improvement over a traditional single-line (series) configuration.

In this context, a parallel-series configuration (Figure **4.29**) is proposed as a viable solution for the current beamhouse system.

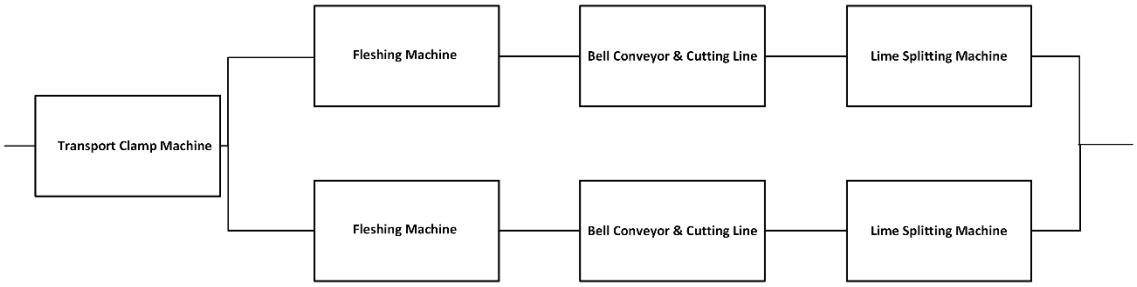

Figure 4.29 - RBD of the Parallel-Series configuration.

Figure **4.29** represents a configuration that consists of a system that commences with a transport clamp machine, which operates in series with the rest of the configuration. This implies that a failure of this initial machine would lead to the failure of the entire system, regardless of the status of subsequent components. However, this decision was based on the fact that the transport clamp machine is the most reliable item among the four pieces of equipment.

Following the transport clamp machine, the system branches into two identical processing lines, arranged in parallel. Each of these parallel lines consists of three machines connected in series: a fleshing machine, followed by a bell conveyor, and finally a lime splitting machine.

For the system to continue operating past the transport clamp machine, only one of the two lines needs to be functional.

In this regard, reliability is calculated based on Equations (3.73) and (3.74) and presented in Table 4.26.

Table 4.26 - System reliability overall of the parallel-series configuration.

Time (h)	50	100	150	300	500
Reliability (%)	27,14	8,66	3,14	0,228	0,0117
Probability of Failure (%)	72,86	91,34	96,86	99,77	99,99
MTBF (h)	40,33				

Table 4.26 and Table 4.22 reveal remarkably similar reliability metrics. Both the reliability and probability of failure values are nearly identical across all time intervals, converging completely at longer operational durations. The MTBF also shows a marginal difference

between (40,78 hours versus 40,33) (Table 4.27). This striking similarity indicates that implementing either a fully parallel system or the proposed parallel-series system would result in comparable performance. Therefore, the parallel-series setup may serve as a viable and more cost-effective alternative to the fully parallel system.

Table 4.27 - Reliability improvement comparing the fully parallel configuration to the proposed parallel-series system.

Time (h)	50	100	150	300	500
Reliability Improvement (%)	+0,31	+0,05	+0,01	+0,0	+0,0
MTBF Improvement (h)	+0,45				

Table 4.27 presents a comparison of the overall reliability between the proposed parallel-series system and a fully parallel setup. As anticipated, the reliability values of the parallel-series system are slightly lower than those of the fully parallel configuration. However, the differences are minimal across all evaluated criteria, reinforcing the notion that the parallel-series setup represents a viable and a more cost-effective alternative to the fully parallel system.

4.6.2 Standby configuration

In this section, an alternative redundant configuration will be presented as a possible solution for system improvement - standby configuration (Figure **4.30**).

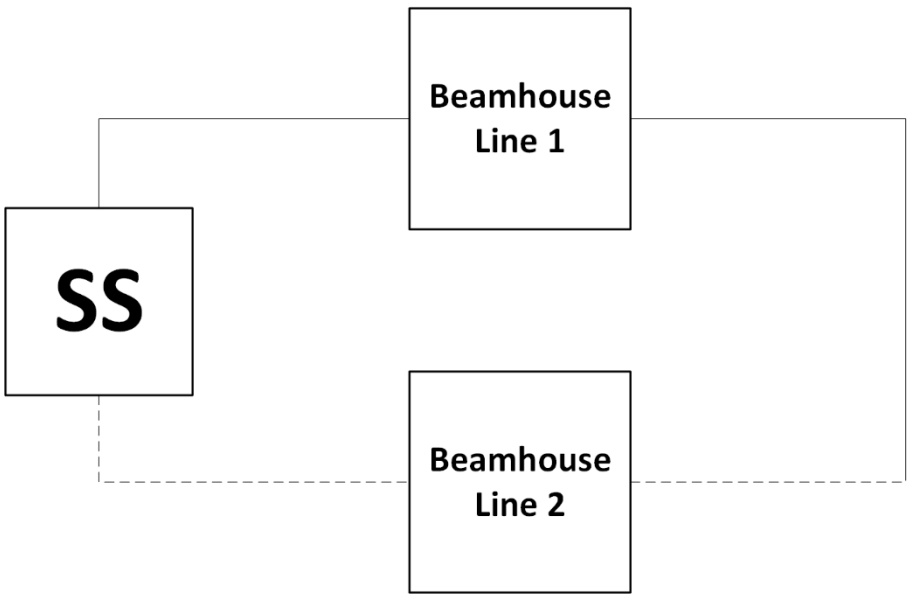

Figure 4.30 - Standby configuration of two beamhouse lines.

Figure **4.30** depicts two beamhouse lines in a standby configuration. The design incorporates line 1 as the operating unit (active unit), while line 2 is viewed as the standby unit, meaning that the second line is engaged only when there is a failure in the first. To facilitate automatic switchover, a switching device (SS) is incorporated into the system. This device is responsible for detecting a failure and seamlessly redirecting operations to the available (standby) line.

For purposes of the current simulation, it is assumed that the switching device operates 100% reliability. Under this assumption, Equation (3.76) becomes applicable. However, to apply this equation appropriately, a few assumptions must be established:

- R_1 represents the reliability of the active beamhouse line and is calculated using Equation (3.73), which corresponds to the reliability of a series system.
- $f_1(t)$ denotes the pdf of the active beamhouse line, which can be obtained using Equation (3.1).
- R_2 is the reliability of the standby beamhouse line, which is assumed to be identical to that of the active line.

Based on these assumptions, Equation (3.76) can be reformulated as follows:

$$R_{sys}(t) = R_1(t) + \int_{\tau=0}^{t} -\frac{d}{d\tau} R_1(\tau) \cdot R_1(t-\tau) d\tau$$

Calculating the reliability of the standby system at different operating hours, the corresponding results are presented in the table below (Table 4.28).

Table 4.28 - Standby system reliability overall with two beamhouse lines (one active and one standby).

Time (h)	50	100	150	300	500
Reliability (%)	35,66	12,99	5,07	0,403	0,0207
Probability of Failure (%)	64,34	87,01	94,93	99,60	99,98
MTBF (h)	50,08				

Table 4.28, in terms of reliability, demonstrates superior performance compared to a single line (Table 4.21), particularly in the initial phases (Table 4.29). At 50 hours, the standby system exhibits a reliability of 35,66%, which is more than double the 14,82% of a single line. This advantage, while significant, diminishes over time but remains evident: at 100 hours, the standby system's reliability is 12,99% versus 4,45% for the single line; at 150 hours, it is 5,07% compared to 1,59%. As operating time extends to 300 and 500

hours, both systems experience a sharp decline in reliability, converging towards extremely low values.

Correspondingly, the probability of failure is reduced in the standby system. The unreliability at 50 hours is 64,34%, a substantial improvement over the 85,18 for a single line. This reduction in failure probability is sustained throughout the time periods under consideration: 87,01% versus 95,55% at 100 hours, and 94,93% versus 98,41% at 150 hours. Looking at common failure probabilities of near certainty at 300 hours and 500 hours for both systems, the standby configuration provides a robust margins of operational time before facing unacceptable failure probabilities.

The MTBF provides a quantitative measure of this improvement. The standby system boasts an MTBF of 50,08 hours, which is approximately double the 25,05 hours of a single beamhouse line.

Table 4.29 - Reliability improvement by comparing the beamhouse line in the series configuration and in the standby configuration.

Time (h)	50	100	150	300	500
Reliability Improvement (%)	+20,84	+8,54	+3,48	+0,289	+0,0149
MTBF Improvement (h)	+25,03				

Table 4.29 quantifies the substantial reliability gains achieved by implementing a standby redundancy strategy. The data reveals a progressive and significant increase in reliability, with the standby system showing a 20,84% improvement at 50 hours, relative to a single-line series configuration. However, this enhancement is consequently lower over the time. In addition, the MTBF has increased 25,03 hours, meaning that it nearly doubled. These results highlight the potential of standby redundancy to significantly increase system reliability and operational longevity. On the other hand, this configuration does not permit to increase the production capacity, through reliability improvement, similarly to the parallel configuration.

Similar to the previous section, the following approach presents a combination of standby and series configurations (Figure **4**.**31**). This method does not require duplication of the entire beamhouse line, so it is empirical to note that while the trade-off of reliability will be less that the fully standby independent configuration, it can still add a significant addition to reliability overall.

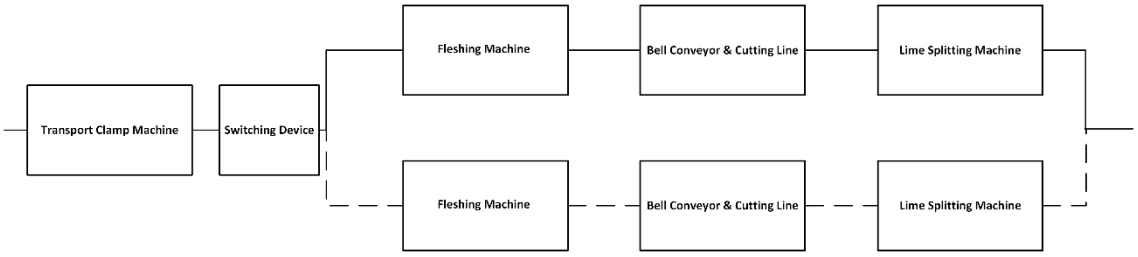

Figure 4.31 - RBD of a combination of standby and series systems.

Figure **4.31** illustrates a sophisticated mixed system configuration that strategically combines series components with a standby redundancy arrangement. This diagram visually delineates a system where both transport clamp machine and switching device are arranged in series, signifying that a failure in either would halt the entire process. However, it is assumed that the reliability of the switching device remains 100% over the time. In this regard, the overall system reliability results are presented in the following table (Table 4.30).

Table 4.30 - Reliability overall of a combination of series and standby systems.

Time (h)	50	100	150	300	500
Reliability (%)	34,48	12,53	4,90	0,392	0,0204
Probability of Failure (%)	65,52	87,47	95,10	99,61	99,98
MTBF (h)	48,71				

Table 4.30 represents the results of a mixed system combining a standby configuration in a series setup with transport clamp machine. Comparing Table 4.28 and Table 4.30, in both combinations, reliability decreases significantly as operational time increases. However, the standby system shows slightly higher reliability values at nearly every time checkpoint – 35,66% versus 34,48% at 50 hours, 12,99% versus 12,53% at 100 hours and 5,07% versus 4,90% at 150 hours. At 300 and 500 hours, both systems exhibit extremely low reliability (approaching zero), though the standby system continues to marginally outperform.

Conversely, the probability of failure naturally mirrors these trends. At 50 hours, the failure probability for the standby system is 64,34%, compared to 65,52% for the combined system. At 100 and 150 hours, the combined system again, as anticipated, shows slightly worse performance, with failure probabilities of 87,47% and 95,10%, respectively, versus 87,01% and 94,93% for the standby system. By 300 and 500 hours, the difference becomes almost negligible (both greater than 99,60%), indicating that long-term reliability is poor regardless of the system configuration, and intervention would be necessary before such durations.

The MTBF achieves a value of 50,08 hours when the system is configured in standby, whereas the combined system reports 48,71 hours. Though the difference is modest, it confirms that slightly superior reliability of the standby configuration in the observed scenarios (Table 4.31).

Table 4.31 - Reliability improvement when comparing the standby system to the mixed system (standby and series).

Time (h)	50	100	150	300	500
Reliability Improvement (%)	+1,18	+0,46	+0,17	+0,01	+0,00
MTBF Improvement (h)	+1,37				

Table 4.31 highlights the incremental reliability improvement observed when comparing the pure standby system to the mixed system. The improvements across all time intervals remain below 2%, with the highest gain of 1,18% at the 50-hour mark. The MTBF also shows a modest improvement of +1,37 hours. The results show that although the standby system achieves slightly better performance, the differences are minimal. This suggests that, depending on cost and operational constraints, the mixed system may be a more cost-effective alternative compared to a completely redundant (standby) system.

5. Final remarks and conclusions

This master thesis has taken me on a real walk through what keeps factories on their feet. Rather than drawn in theory, I followed reliability engineering all the way to the floor of a leather plant, where I shadowed its beamhouse line and heard the clatter of the machines doing their jobs. My purpose was a simple one: to take the heavy theory around reliability engineering and contrast it with actual field conditions; capturing the length of time equipment survives (or failures), the pattern of failures, and most incredibly, how things could be improved. I now realize how important it is to link technical knowledge and theoretical concepts with real-life challenges to derive value.
Ultimately, I hope this work acts as more than some interesting figures, numbers and formulas on reliability, but as a small step towards smarter maintenance, less downtime and improved support for the management and human resources that work on these systems.

One of the key takeaways is the importance of employing lifetime distributions to accurately model and predict the failure behavior of the equipment. These models provide valuable insights into whether assets are in their early, useful or wear-out phases, enabling maintenance teams to optimize intervention frequencies and therefore prevent unexpected downtimes. This means that the preventive maintenance frequencies should be synchronized with the asset's life phase. For example, ideally the preventive maintenance should be carried out when the item enters the wear-out period ($\beta > 1$).

During the initial analysis of the transport clamp, fleshing machine, belt conveyor and lime splitting machine (Table 4.2, Table 4.7, Table 4.12, Table 4.17, respectively), all components exhibited a shape parameter less than one ($\beta < 1$), despite not being factory new. This result typically indicates a decreasing failure rate over time, commonly associated with early-life failures or infant mortality. According to Bazovsky [129], in the case of nonperfect repair the failure rate stabilization process may assume a damped oscillatory character. In other words, despite maintenance efforts, the failure rate can initially increase before stabilizing. Corset *et al.* [130] state that corrective maintenance

actions are assumed to restore the system to a like-new state. This suggests that repairs may reintroduce early-life failures (infant mortality) characteristics. Dhillon [131] explains that some of the reasons for failures in burn-in period include substandard workmanship and parts, poor manufacturing methods, human error, inadequate quality control, and unsatisfactory debugging. Summarizing, this unexpected pattern suggested that failure behavior in these systems was not purely the result of aging or usage, but potentially influenced by maintenance practices, repair quality, or even flawed assumptions about the post-repair condition of the assets.

Subsequently, the analysis of the beamhouse line revealed a concerning reality. As shown in Table 4.21, the system, when left in its original configuration, demonstrated a low level of resilience, with a MTBF of just 25,05 hours. This figure clearly indicated that, without intervention, the system was prone to frequent disruptions – a serious risk for continuity of production.

This finding served as a turning point in the study, prompting a closer look at redundancy strategies – particularly parallel, standby and mixed configurations. The implementation of a parallel system, whose results are presented in Table 4.22, offered a better outcome. It provided the system with an increased buffer against failure (Table 4.23), nearly doubling the MTBF to 40,78 hours. This highlights the immediate, tangible benefits of having a reliable backup.

The analysis was taken a step further from the initial findings and extended into a system of 15 beamhouse lines in a parallel arrangement (Table 4.24). The MTBF was improved to 113,85 hours, and reliability at critical time points saw gains exceeding 1000%. This improvement emphasizes the gains that can be derived from large-scale redundancy in any critical industrial environment. In addition, to the reliability of operations, the redundancy. In addition to the reliability in operations, the redundancy of parallel arrangements will deliver real economic and productivity gains, which is an effective approach to maximizing both uptime and the lifespan of the system.

A mixed configuration, combining parallel and series networks, where transport clamp machine is placed in series with a parallel block of two processing lines (each line consisting of a fleshing machine, belt conveyor, and lime splitting machine) also contributed to positive results. This parallel-series structure produced an MTBF of 40,33 hours, very close to the fully parallel system. As Table 4.26 and Table 4.27 show, reliability varied little over any of the time windows tested, and the gains stayed below 1.15% at all points. This small edge, combined with lower cost and space demand, confirms that the parallel-series layout can replace full parallel schemes when budgets or room constrain total duplication.

Also, in parallel, the standby redundancy configuration (Table 4.26), with its own resilience, was assessed. The MTBF improved to 50,08 hours, once again proving that it is better with redundancies than having no redundancy at all with a single-line configuration. One standby redundancy (one active line and one standby) has proved to be more effective than parallel redundancy, by comparing the MTBF values and reliability at 50, 100, 150, 300 and 500 hours. However, the implementation of the standby setup requires investment in acquiring and programming the switching device, which detects the failure and swaps the production process to the available line.

The analysis of the combination of standby and series configurations significantly enhances the reliability of the system when compared to a simple series configuration. However, as demonstrated these results are slightly lower when compared to the fully standby system. The advantage of this type of setup, similar to parallel-series system, is the cost-effectiveness, since there is no necessity in duplicating all the assets.

In comparing the standby versus the parallel configurations, it is evident that both types of arrangement provide greater reliability than using a single series system. However, in all the simulations presented, the standby setups have demonstrated better results. Parallel network requires the duplication of the beamhouse line, guaranteeing production continuity whenever at least one line remains functional. The greatest advantage of this configuration is that the production capacity increases through reliability improvement, which makes a highly suitable option for companies that pursue both goals. Contrary, the standby system provides the best reliability and MTBF improvement, however the standby unit is idle until the active line fails. Additionally, the standby configuration requires acquisition and programming of the switching device in order to commute between available lines. At the same time, a parallel system is less reliable and less expensive compared to a standby system, the last one is a trade-off between reliability and cost.

The implementation of any of those possibilities would give the leather-producing organization a more reliable system, reducing downtimes and disruptions. Any of these possibilities have their own requirements, which should be taken into consideration during the decision-making process, including investment, human resources and physical space. As demonstrated in this study, the beamhouse line exhibits highly unreliable behavior even during moderate operational periods. The overall reliability of the beamhouse line is largely influenced by the reliability of each physical asset studied during the thesis (transport clamp, fleshing machine, belt conveyor and lime splitting machine). In this regard, I consider it of paramount importance to increase the reliability of each element of the beamhouse line. To achieve this, it is imperative to implement a robust maintenance plan (ideally to be carried out when the piece of equipment reaches a shape parameter greater than one, $\beta > 1$) and maintain the items at their useful life (β

= 1); frequent inspections; and potentially a reevaluation of component durability or system design. From an organizational perspective, this translates into reduced downtime and minimized production losses and associated costs, and production continuity, guaranteeing prosperity and competitiveness of the enterprise.

A possible direction for future research could involve improving the individual reliability of the items by applying all necessary technical and qualitative actions that would assist the physical assets to resist less and more effectively transit to their useful life. Additionally, a careful analysis of the raw data, taking into the account detailed maintenance historical records, could further guarantee the quality and robustness of the investigation.

References

[1] S. Ali, S. Ali, I. Shah, G. F. Siddiqui, T. Saba, and A. Rehman, “Reliability Analysis for Electronic Devices Using Generalized Exponential Distribution,” *IEEE Access*, vol. 8, pp. 108629–108644, 2020, doi: 10.1109/ACCESS.2020.3000951.

[2] D. V. Lemes, É. P. Felix, and G. F. M. Souza, “Reliability analysis of electronic equipment based on warranty failure database,” *ABCM Symp. Ser. Mechatron.*, vol. 3, pp. 395–404, 2008.

[3] W. K. Ehrlich, K. S. Lee, and R. H. Molisani, “Applying reliability measurement: a case study,” *IEEE Softw.*, no. 7(2), pp. 56–64, 1990, doi: 10.1109/52.50774.

[4] I. A. M. Ahmed, A. M. A. Hamdi, and A. H. Abdelateef, “Modeling Reliability for Exponential Distribution Using Maximum Likelihood Method (Case study: A.T.M in Sudan),” *J. Math. Stat. Sci.*, no. 5, pp. 192–209, 2018.

[5] H. Pham, Ed., *Springer Handbook of Engineering Statistics*. London: Springer, 2006.

[6] W. Q. Meeker and L. A. Escobar, *Statistical methods for reliability data*. in Wiley series in probability and statistics. Applied probability and statistics section. New York: Wiley, 1998.

[7] M. K. Keshavan, G. A. Sargent, and H. Conrad, “Statistical analysis of the Hertzian fracture of pyrex glass using the Weibull distribution function,” *J. Mater. Sci.*, vol. 15, no. 4, pp. 839–844, Apr. 1980, doi: 10.1007/BF00552092.

[8] D. A. Juckett and B. Rosenberg, “Periodic Clustering of Human Disease-Specific Mortality Distributions by Shape and Time Position, and a New Integer-Based Law of Mortality,” *Mech. Ageing Dev.*, vol. 55, no. 3, pp. 255–291, 1990, doi: doi.org/10.1016/0047-6374(90)90153-7.

[9] D. R. Dolas, M. D. Jaybhaye, and S. D. Deshmukh, “Reliability Analysis using Weibull Distribution,” *Int. Proc. Econ. Dev. Res.*, vol. 75, no. 29, pp. 144–148, 2014, doi: 10.7763/IPEDR.

[10] B. N. Abramovich and S. V. Baburin, “Анализ надежности систем электроснабжения [Analysis of power supply systems’ reliability],” presented at the Совпременные Образовательные Технологии в Подготовке Специаоистов для Минерально-Сырьевого Комплекса [Modern educational technologies in the training of specialists for the mineral resource complex], Saint Petersburg: Санкт-Петербургский горный университет [St. Petersburg Mountain University], Sept. 2018, pp. 839–849.

[11] N. L. Clement and R. C. Lasky, “Weibull Distribution and Analysis: 2019,” in *2020 Pan Pacific Microelectronics Symposium (Pan Pacific)*, HI, USA: IEEE, Feb. 2020, pp. 1–5. doi: 10.23919/PanPacific48324.2020.9059313.

[12] Y. Yang, J. Li, and C. Xu, “Reliability Data Analysis of Aviation Equipment Based on Weibull Distribution,” in *2022 4th International Conference on Frontiers Technology of Information and Computer (ICFTIC)*, Qingdao, China: IEEE, Dec. 2022, pp. 342–345. doi: 10.1109/ICFTIC57696.2022.10075118.

[13] V. M. Artyushenko and A. A. Bruskov, “Применение Распределения Вейбулла для Оценок Надежности Космических Аппаратов [Application of Weibull Distribution for Assessments of Space Car Reliability,” *Вестник Воронежского*

Государственного Университета Серия Систеиный Анализ И Информационные Технологии Bull. Voronezh State Univ. Ser. Syst. Anal. Inf. Technol., no. 2, pp. 89–102, 2024, doi: 10.17308/sait/1995-5499/2024/2/89-102.
[14] A. Kleyner and P. Sandborn, "A warranty forecasting model based on piecewise statistical distributions and stochastic simulation," *Reliab. Eng. Syst. Saf.*, vol. 88, no. 3, pp. 207–214, June 2005, doi: 10.1016/j.ress.2004.07.016.
[15] N. Janjić, B. Savić, D. Mikić, N. Stanković, and D. Petrović, "Application of Model of Reliability on Machine Systems Based on Lognormal Statistical Distribution," presented at the 13th International Scientific Conference, Novi Sad, Serbia: MMA 2018, 2018, pp. 121–125.
[16] Y. Kara, M. R. Canal, İ. Sefa, and F. E. Boran, "Selecting and Analyzing Appropriate Probability Distributions for Reliability of Electrical Transmission Lines," *Gazi Üniversitesi Fen Bilim. Derg. Part C Tasar. Ve Teknol.*, vol. 9, no. 1, pp. 108–121, Mar. 2021, doi: 10.29109/gujsc.868923.
[17] I. Mikhaylov, O. Muravlev, and A. Fedyanin, "Инженерный Анализ Эксплотуационной Надежности Электрического Оборудования Троллейбуса [Engineering Analysis of Operational Reliability of Trolley's Electrical Equipment]," *Вестник Кузбасского Государственного Технического Университета Bull. Kuzbass State Tech. Univ.*, no. 3 (115), pp. 85–92, 2016.
[18] V. N. Anferov, S. M. Kuznetsov, and S. I. Vasil'yev, "Оценка надежности работы бульдозеров [Assessment of bulldozers operation reliability]," *Системы Методы Технологии Syst. Methods Technol.*, no. 3 (19), pp. 16–21, 2013.
[19] R. S. Litvinenko, P. P. Pavlov, and A. E. Auhadeev, "Практическое Применение Нормального Закона Распределения в Теории Надежности Технических Систем [The Practical Application of the Normal Distribution in the Theory of Reliability of Technical Systems]," *Известия Высших Учебных Заведений Электромеханика News High. Educ. Inst. Electromechanics*, no. 4, pp. 96–99, 2016.
[20] D. Kececioglu, *Reliability Engineering Handbook, Volume 1*, vol. 1, 2 vols. DEStech Publications Inc., 2002.
[21] R. Kang, *Belief Reliability Theory and Methodology*. Singapore: Springer Singapore, 2021. doi: 10.1007/978-981-16-0823-0.
[22] A. Birolini, *Reliability Engineering: Theory and Practice*. Berlin, Heidelberg: Springer Berlin Heidelberg, 2017. doi: 10.1007/978-3-662-54209-5.
[23] J. H. Saleh and K. Marais, "Highlights from the early (and pre-) history of reliability engineering," *Reliab. Eng. Syst. Saf.*, vol. 91, no. 2, pp. 249–256, Feb. 2006, doi: 10.1016/j.ress.2005.01.003.
[24] J. McLinn, "A Short History of Reliability," *NASA*, Apr. 2010, Accessed: Nov. 14, 2024. [Online]. Available: https://extapps.ksc.nasa.gov/Reliability/Documents/History_of_Reliability.pdf
[25] E. Zio, "Reliability engineering: Old problems and new challenges," *Reliab. Eng. Syst. Saf.*, vol. 94, no. 2, pp. 125–141, Feb. 2009, doi: 10.1016/j.ress.2008.06.002.
[26] A. K. M. Nor, S. R. Pedapati, and M. Muhammad, "Reliability engineering applications in electronic, software, nuclear and aerospace industries: A 20 year review (2000–2020)," *Ain Shams Eng. J.*, vol. 12, no. 3, pp. 3009–3019, Sept. 2021, doi: 10.1016/j.asej.2021.02.015.
[27] IPQ, *NP EN 13306:2021 - Manutenção – Terminologia de manutenção*, Monte Da Caparica., 2021.
[28] I. Ushakov, *Handbook of Reliability Engineering*. John Wiley & Sons, Inc., 1994.
[29] B. S. Dhillon, Ed., *Applied Reliability and Quality: Fundamentals, Methods and Procedures*. in Springer Series in Reliability Engineering. London: Springer London, 2007. doi: 10.1007/978-1-84628-498-4.
[30] T. Nakagawa, *Maintenance Theory of Reliability*. in Springer Series in Reliability Engineering. London: Springer London, 2005. doi: 10.1007/1-84628-221-7.
[31] E. Nikolaidis, D. M. Ghiocel, and S. Singhal, Eds., *Engineering Design Reliability Handbook*. USA: CRC Press, 2005.
[32] Y. Liu, *Reliability Theory Based on Uncertain Lifetimes*. Singapore: Springer Singapore, 2021. doi: 10.1007/978-981-16-0995-4.

[33] H. Pham, *Statistical Reliability Engineering: Methods, Models and Applications*. in Springer Series in Reliability Engineering. Cham: Springer International Publishing, 2022. doi: 10.1007/978-3-030-76904-8.
[34] F. M. Safie and R. P. Fuller, “NASA applications and lessons learned in reliability engineering,” in *2012 Proceedings Annual Reliability and Maintainability Symposium*, Jan. 2012, pp. 1–5. doi: 10.1109/RAMS.2012.6175423.
[35] “Introduction to Life Data Analysis,” *Hottinger Bruel Kjaer Inc*, 2024, [Online]. Available: https://help.reliasoft.com/reference/life_data_analysis/lda/introduction_to_life_data_analysis.html
[36] E. E. Lewis, *Introduction to Reliability Engineering*, 2nd Edition. John Wiley & Sons, Inc., 1996.
[37] H. Pham, Ed., *Handbook of Reliability Engineering*, 1st ed. 2003. London: Imprint: Springer, 2003. doi: 10.1007/b97414.
[38] J. Xue and K. Yang, “Dynamic reliability analysis of coherent multistate systems,” *IEEE Trans. Reliab.*, no. 44, pp. 683–688, 1995, doi: https://doi.org/10.1109/24.476002.
[39] R. K. D. Santos, J. R. Mangabeiro, and V. V. F. Grubisic, “Modeling and reliability analysis of aircraft components and systems: a case study,” *Prod. Manag. Dev.*, vol. 18, no. 1, pp. 100–109, 2020, doi: 10.4322/pmd.2019.023.
[40] P. D. T. O’Connor and A. Kleyner, *Practical Reliability Engineering*, 5th ed. John Wiley & Sons, Inc., 2012.
[41] M. Modarres, M. Kaminskiy, and V. Krivtsov, *Reliability Engineering and Risk Analysis: A Practical Guide*. New York, USA: Marcel Dekker, Inc., 1999.
[42] A. C. Márquez, *The Maintenance Management Framework: Models and Methods for Complex Systems Maintenance*. in Springer Series in Reliability Engineering. London: Springer London, 2007. doi: 10.1007/978-1-84628-821-0.
[43] A. B. Rauzy, *Model-Based Reliability Engineering*. 2022.
[44] J. Zhao, S. Anuj, and D. Osherson, “On the provenance of judgements of conditional probability,” *Cognition*, no. 113, pp. 26–36, 2009, doi: https://doi.org/10.1016/j.cognition.2009.07.006.
[45] “Reliability Engineering,” in *Lees’ Loss Prevention in the Process Industries*, Elsevier, 2012, pp. 131–203. doi: 10.1016/B978-0-12-397189-0.00007-0.
[46] M. Finkelstein, Ed., *Failure Rate Modelling for Reliability and Risk*. in Springer Series in Reliability Engineering. London: Springer London, 2009.
[47] A. O’Connor, M. Modarres, and A. Mosleh, *Probability Distributions Used in Reliability Engineering*. Maryland, USA: Center for Risk and Reliability, 2016.
[48] M. H. Weik, “bathtub curve,” in *Computer Science and Communications Dictionary*, Boston, MA: Springer, 2000, p. 110.
[49] Reliasoft, “Introduction to Life Data Analysis,” *Hottinger Bruel Kjaer Inc*, 2024, Accessed: Apr. 05, 2025. [Online]. Available: https://help.reliasoft.com/reference/life_data_analysis/lda/introduction_to_life_data_analysis.html
[50] *Reliability terminology*, BS 4200-2, 1970.
[51] M. Noor M, K. Kadigarma, H. Jamaluddin E, and M. Rahman M, “Method of Predicting Estimating and Improving Mean Time Between Failures in Reducing Reactive Work in Maintenance Organization,” 2009.
[52] N. Chauhan and N. Pancholi, “Guidelines to Understanding to estimate MTBF,” *International Journal for Scientific Research and Development*, pp. 521–523, 2013.
[53] M. Krasich, “How to estimate and use MTTF/MTBF would the real MTBF please stand up?,” presented at the 2009 Annual Reliability and Maintainability Symposium, 2009, pp. 353–359. doi: https://doi.org/10.1109/RAMS.2009.4914702.
[54] B. S. Dhillon, *Reliability, Quality, and Safety for Engineers*. Boca Raton, FL: CRC Press, 2005.
[55] H. Pham, Ed., *Reliability modeling, analysis and optimization*. in Series on quality, reliability and engineering statistics, no. vol. 9. Hackensack, NJ: World Scientific, 2006.

[56] L. Chen, Y. Liang, Z. Yang, and H. Dui, “Reliability analysis and preventive maintenance of rehabilitation robots,” *Reliab. Eng. Syst. Saf.*, vol. 256, p. 110704, Apr. 2025, doi: 10.1016/j.ress.2024.110704.
[57] X. Yang, L. Xie, B. Wang, J. Chen, and B. Zhao, “Inference on the high-reliability lifetime estimation based on the three-parameter Weibull distribution,” *Probabilistic Eng. Mech.*, vol. 77, p. 103665, July 2024, doi: 10.1016/j.probengmech.2024.103665.
[58] “Weibull Distribution Characteristics - ReliaWiki.” Accessed: Jan. 06, 2025. [Online]. Available: https://www.reliawiki.com/index.php/Weibull_Distribution_Characteristics
[59] F. El Bouanani and D. B. Da Costa, “Accurate Closed-Form Approximations for the Sum of Correlated Weibull Random Variables,” *IEEE Wirel. Commun. Lett.*, vol. 7, no. 4, pp. 498–501, Aug. 2018, doi: 10.1109/LWC.2017.2789280.
[60] G. J. Hahn and S. S. Shapiro, *Statistical Models in Engineering*. in Wiley Series on Systems Engineering and Analysis. John Wiley & Sons, Inc., 1967.
[61] R. J. Sadlon, “Mechanical Applications in Reliability Engineering: NPS,” Defense Technical Information Center, Fort Belvoir, VA, Aug. 1993. doi: 10.21236/ADA363860.
[62] R. B. Abernethy, J. E. Breneman, C. H. Medlin, and G. L. Reinman, “Weibull Analysis Handbook,” West Palm Beach, Florida, AFWAL-TR-83-2073, 1983.
[63] J. Møltoft, “Behind the ‘Bathtub’- Curve: A New Model and its Consequences,” *Microelectron. Reliab.*, vol. 23, no. 3, pp. 489–500, 1983, doi: 10.1016/0026-2714(83)91178-2.
[64] H. Rinne, *The Weibull Distribution: A Handbook*. Giessen, Germany: CRC Press, 2008.
[65] S. Zacks, *The Career of a Research Statistician*. in Statistics for Industry, Technology and Engineering. USA: Birkhäuser, 2020.
[66] E. A. Elgmati and N. B. Gregni, “Quartile Method Estimation of Two-Parameter Exponential Distribution Data with Outliers,” *Int. J. Stat. Probab.*, vol. 5, no. 5, p. 12, Aug. 2016, doi: 10.5539/ijsp.v5n5p12.
[67] K. Balasubramanian and N. Balakrishnan, “Estimation for one- and two-parameter exponential distributions under multiple type-II censoring,” *Stat. Pap.*, vol. 33, no. 1, pp. 203–216, Dec. 1992, doi: 10.1007/BF02925325.
[68] J. L. Devore, *Probability & Statistics for Engineering and the Sciences*, 8th ed. Boston, USA: Cengage Learning, 2012.
[69] T. Berhane, N. Shibabaw, and T. Kebede, “Pricing weather derivative using Markov Chain Analogue Year daily rainfall model,” *SN Appl. Sci.*, vol. 2, no. 4, p. 715, Apr. 2020, doi: 10.1007/s42452-020-2500-2.
[70] S. Dubey, “Normal and weibull distributions,” *Nav. Res. Logist. Q.*, vol. 14, pp. 69–79, 1967, doi: 10.1002/NAV.3800140107.
[71] D. Altman and J. Bland, “Statistics notes: The normal distribution,” *BMJ*, vol. 310, p. 298, 1995, doi: 10.1136/BMJ.310.6975.298.
[72] K. Krishnamoorthy, *Handbook of statistical distributions with applications*. in Statistics, no. 188. Boca Raton, Fla.: Chapman & Hall/CRC, 2006.
[73] D. C. Montgomery, *Introduction to Statistical and Quality Control*, 7th ed. Arizona State University: John Wiley & Sons, Inc., 2013.
[74] Y.-G. Zhao, X.-Y. Zhang, and Z.-H. Lu, “A flexible distribution and its application in reliability engineering,” *Reliab. Eng. Syst. Saf.*, vol. 176, pp. 1–12, Aug. 2018, doi: 10.1016/j.ress.2018.03.026.
[75] L. Kounis, Ed., *Reliability and Maintenance - an Overview of Cases*. London, UK: IntechOpen, 2020. doi: 10.5772/intechopen.77493.
[76] R. S. Litvinenko, P. P. Pavlov, and R. G. Idiyatullin, “Practical application of continuous distribution laws in the theory of reliability of technical systems,” *Dependability*, vol. 16, no. 4, pp. 17–23, Jan. 2016, doi: 10.21683/1729-2646-2016-16-4-17-23.
[77] M. Ben-Daya, S. O. Duffuaa, A. Raouf, J. Knezevic, and D. Ait-Kadi, Eds., *Handbook of Maintenance Management and Engineering*. London: Springer London, 2009. doi: 10.1007/978-1-84882-472-0.

[78] E. Tipton, A. M. Kuyper, D. Sass, and K. G. Fitzgerald, *Introduction to Statistics and Data Science*. Department of Statistics and Data Science: Northwestern University Libraries, 2025. Accessed: Feb. 20, 2025. [Online]. Available: https://nustat.github.io/intro-stat-data-sci/
[79] J. McLinn, *Practical Weibull Analysis Techniques*, Fifth Edition. Minnesota: The Reliability Division of ASQ, 2010.
[80] W. Nelson, *Applied Life Data Analysis*. in Wiley publication in applied statistics. Applied probability and statistics section. John Wiley & Sons, Inc., 1982.
[81] R. B. Abernethy, *The New Weibull Handbook*, Fifth Edition. USA, 2006.
[82] B. W. Woodruff and A. H. Moore, "Application of Goodness-of-Fit Tests in Reliability," in *Handbook of Statistics*, vol. 7, Elsevier, 1988, pp. 113–120. doi: 10.1016/S0169-7161(88)07009-9.
[83] F. de S. Fernandes, "Testes de Ajuste a Distribuições Estatísticas e Métodos para Estimação dos Parâmetros em Análises de Fiabilidade [Goodness-of-Fit tests for Statistical Distributions and Parameter Estimation Methods in Reliability Analysis]," Instituto Superior de Engenharia de Lisboa (ISEL), 2013.
[84] V. Voinov, N. Balakrishnan, and M. S. Nikulin, *Chi-squared goodness of fit tests with applications*. Amsterdam: Elsevier/AP, 2013.
[85] B. Illowsky and S. L. Dean, *Introductory statistics*, 2e ed. Houston, Texas: OpenStax, Rice University, 2023.
[86] M. Mahbobi and T. K. Tiemann, *Introductory business statistics with interactive spreadsheets: using interactive Microsoft Excel templates*, 1st Canadian edition. Victoria, B.C.: BCcampus, 2015.
[87] G. W. Snedecor and W. G. Cochran, *Statistical Methods*, Eighth Edition. Iowa, USA: Iowa State University Press, 1989.
[88] D. S. Moore, G. P. McCabe, and B. A. Craig, *Introduction to the Practice of Statistics*, Sixth Edition. New York, USA: W. H. Freeman and Company, 2009.
[89] A. Agresti and B. Finlay, *Statistical Methods for the Social Sciences*, Fourth Edition. USA: Pearson Education International, 2009.
[90] R. V. Hogg, E. A. Tanis, and D. L. Zimmerman, *Probability and statistical inference*, Ninth edition. Boston: Pearson, 2015.
[91] J. A. Rice, *Mathematical statistics and data analysis*, 3rd ed. in Duxbury advanced series. Belmont, CA: Thomson/Brooks/Cole, 2007.
[92] N. R. Mann, R. E. Schafer, and N. D. Singpurwalla, *Methods for Statistical Analysis of Reliability and Life Data*. in Wiley Series in Probability and Mathematical Statistics. John Wiley & Sons, Inc., 1974.
[93] G. Bohm and G. Zech, *Introduction to Statistics and Data Analysis for Physicists*, 4th ed. WORLD SCIENTIFIC, 2010. doi: 10.1142/14343.
[94] S. M. Ross, *Introduction to Probability and Statistics for Engineers and Scientists*, 5th ed. San Diego: Elsevier Science & Technology, 2014.
[95] R. B. D'Agostino and M. A. Stephens, Eds., *Goodness-of-Fit Techniques*, vol. 68. in Statistics: Textbooks and Monographs, vol. 68. New York, USA: Marcel Dekker, Inc., 1986.
[96] A. Lisnianski and I. Frenkel, Eds., *Recent Advances in System Reliability: Signatures, Multi-state Systems and Statistical Inference*. in Springer Series in Reliability Engineering. London: Springer London, 2012. doi: 10.1007/978-1-4471-2207-4.
[97] M. Krit, "Goodness-of-fit tests in reliability: Weibull distribution and imperfect maintenance models," General Mathematics [math.GM], Université de Grenoble, 2014. Accessed: May 08, 2025. [Online]. Available: https://theses.hal.science/tel-01126901v1
[98] M. A. Stephens, "EDF Statistics for Goodness of Fit and Some Comparisons," *J. Am. Stat. Assoc.*, vol. 69, no. 347, pp. 730–737, 1974.
[99] N. Balakrishnan, E. Cramer, and D. Kundu, *Hybrid Censoring Know-How*, 1st Edition. Academic Press, 2023.
[100] K. M. Ramachandran and C. P. Tsokos, *Mathematical statistics with applications in R*, 2nd edition. Amsterdam Boston: Elsevier, Academic Press is an imprint of Elsevier, 2015.

[101] A. F. Sieger and M. R. Wagner, Eds., *Practical Business Statistics*, Eight Edition. Academic Press, 2022.
[102] C. E. Ebeling, *An Introduction to Reliability and Maintainability Engineering*. USA: McGraw-Hill, 2003.
[103] E. A. Elsayed, *Reliability Engineering*, Third Edition. in Wiley Series in Systems Engineering and Management. USA: Wiley, 2021.
[104] B. S. Dhillon, *Maintainability, Maintenance, and Reliability for Engineers*, 0 ed. CRC Press, 2006. doi: 10.1201/9781420006780.
[105] R. F. Stapelberg, *Handbook of Reliability, Availability, Maintainability and Safety in Engineering Design*. London: Springer London, 2009. doi: 10.1007/978-1-84800-175-6.
[106] P. Barringer, "Process and Equipment Reliability," *Maint. Reliab. Technol. Summit Chic.*, pp. 1–11, 2004.
[107] A. Kelly and M. J. Harris, *Management of Industrial Maintenance*. UK: Butterworth & Co Ltd, 1978.
[108] R. Akhil Vijayan, P. S. Arya, and M. Rangaswamy, "Strategic Maintenance Approaches for Enhanced Reliability in Parallel System," *J. Indian Soc. Probab. Stat.*, Jan. 2025, doi: 10.1007/s41096-024-00226-4.
[109] D. Kececioglu, *Reliability Engineering Handbook, Volume 2*, vol. 2, 2 vols. DEStech Publications Inc., 2002.
[110] X. Xiong, Y.-L. Wu, and W.-B. Jone, "Reliability Model for MEMS Accelerometers," in *Novel Algorithms and Techniques In Telecommunications, Automation and Industrial Electronics*, T. Sobh, K. Elleithy, A. Mahmood, and M. A. Karim, Eds., Dordrecht: Springer Netherlands, 2008, pp. 261–266. doi: 10.1007/978-1-4020-8737-0_47.
[111] S. Distefano, "Reliability of Standby Systems," in *Bio-Inspired Computing and Applications*, vol. 6840, D.-S. Huang, Y. Gan, P. Premaratne, and K. Han, Eds., in Lecture Notes in Computer Science, vol. 6840. , Berlin, Heidelberg: Springer Berlin Heidelberg, 2012, pp. 267–275. doi: 10.1007/978-3-642-24553-4_37.
[112] S. Wang, Y. Yao, D. Ge, Z. Lin, J. Wu, and J. Yu, "Reliability evaluation of standby redundant systems based on the survival signatures methods," *Reliab. Eng. Syst. Saf.*, vol. 239, p. 109509, Nov. 2023, doi: 10.1016/j.ress.2023.109509.
[113] A. Alkaff, M. N. Qomarudin, E. Purwantini, and S. E. Wiratno, "Dynamic reliability modeling for general standby systems," *Comput. Ind. Eng.*, vol. 161, p. 107615, Nov. 2021, doi: 10.1016/j.cie.2021.107615.
[114] G. Levitin, H. Jia, Y. Ding, Y. Song, and Y. Dai, "Reliability of multi-state systems with free access to repairable standby elements," *Reliab. Eng. Syst. Saf.*, vol. 167, pp. 192–197, Nov. 2017, doi: 10.1016/j.ress.2017.05.003.
[115] W. Wang, J. Xiong, and M. Xie, "Cold-standby redundancy allocation problem with degrading components," *Int. J. Gen. Syst.*, vol. 44, no. 7–8, pp. 876–888, Nov. 2015, doi: 10.1080/03081079.2015.1028541.
[116] B. S. Dhillon, *Engineering Maintenance: A Modern Approach*, 1st ed. CRC Press, 2002. doi: 10.1201/9781420031843.
[117] D. J. Smith, *Reliability, Maintainability and Risk*, Seventh Edition. UK: Elsevier, 2005.
[118] R. S. Pringle and P. M. Gresho, "A Comprehensive Reliability Analysis of Redundant Systems," *J Spacecr.*, vol. 4, no. 5, pp. 631–638, 1967.
[119] L. Lu and G. Lewis, "Configuration determination for k-out-of-n partially redundant systems," *Reliab. Eng. Syst. Saf.*, vol. 93, no. 11, pp. 1594–1604, 2008, doi: https://doi.org/10.1016/j.ress.2008.02.009.
[120] V. Dragoi, V. Beiu, and S. Cowell, "Tight Bounds on the Coeffcients of Consecutive k-out-of-n: F Systems," Springer, 2020. doi: 10.1007/978-3-030-53651-0_3.
[121] V. A. Uspensky, *Pascal's Triangle*. in Certain Applications of Mechanics to Mathematics. Moscow: Mir Publishers, 1976.
[122] J. G. Torres-Toledano and L. E. Sucar, "Bayesian Networks for Reliability Analysis of Complex Systems," in *Progress in Artificial Intelligence — IBERAMIA 98*, vol. 1484, H. Coelho, Ed., in Lecture Notes in Computer Science, vol. 1484. , Berlin,

Heidelberg: Springer Berlin Heidelberg, 1998, pp. 195–206. doi: 10.1007/3-540-49795-1_17.
[123] H. Bruel and K. Inc, *System Analysis Reference*. UK: HBK UK Ltd, 2024.
[124] S. Janardhanan, S. Badnava, R. Agarwal, and C. Mas-Machuca, “PyRBD: An Open-Source Reliability Block Diagram Evaluation Tool,” in *2024 IEEE International Workshop Technical Committee on Communications Quality and Reliability (CQR)*, Seattle, WA, USA: IEEE, Sept. 2024, pp. 19–24. doi: 10.1109/CQR62340.2024.10705890.
[125] N. H. Zavieh, M. A. Ardakan, and H. Davari-Ardakani, “A new model for the reliability-redundancy allocation problem under the K-mixed redundancy strategy,” *J. Stat. Comput. Simul.*, vol. 92, no. 17, pp. 3542–3560, Nov. 2022, doi: 10.1080/00949655.2022.2072844.
[126] Z. Xie, C. Zhang, H. Ouyang, S. Li, and L. Gao, “Self-adaptively commensal learning-based Jaya algorithm with multi- populations and its application,” *Soft Comput.*, vol. 25, pp. 15163–15181, 2021, doi: 10.1007/s00500-021-06445-2.
[127] “Reliability of Complex Systems,” in *Block 4 - Reliability Theory*, vol. 4, 4 vols., New Delhi: Indira Gandhi National Open University, 2023.
[128] “Continuous Fleshing Machine– Costruzioni Meccaniche Persico s.r.l.” Accessed: Apr. 20, 2025. [Online]. Available: https://www.cmpersico.com/en/products/continuous-fleshing-machine/
[129] I. Bazovsky, *Reliability Theory and Practice*. Englewood Cliffs, New Jersey: Prentice-Hall, Inc., 1961. [Online]. Available: https://babel.hathitrust.org/cgi/pt?id=mdp.39015000449549&seq=11
[130] F. Corset, M. Fouladirad, and C. Paroissin, “Imperfect and worse than old maintenances for a gamma degradation process,” *Appl. Stoch. Models Bus. Ind.*, vol. 40, no. 3, pp. 620–639, May 2024, doi: 10.1002/asmb.2849.
[131] B. S. Dhillon, *Engineering Maintainability: How to Design for Reliability and Easy Maintenance*. Houston, Tex: Gulf Pub. Co, 1999.
[132] D. C. Montgomery, G. C. Runger, and N. F. Hubele, *Engineering Statistics*, Fifth Edition. Arizona State University: John Wiley & Sons, Inc., 2011.
[133] W. C. Navidi, *Statistics for engineers and scientists*, 3rd ed. New York: McGraw-Hill, 2011.
[134] “t-Test, Chi-Square, ANOVA, Regression, Correlation...” Accessed: May 27, 2025. [Online]. Available: https://datatab.net/tutorial/chi-square-distribution

Appendix

Appendix A – Algorithm written in Python to connect to a SQL database and perform reliability calculations.

```python
import tkinter as tk
from tkinter import messagebox
import numpy as np
import matplotlib.pyplot as plt
import math
from pyodbc import connect
from datetime import datetime
from scipy.stats import beta
import pandas as pd

# Initialize the global variables
dat_ini_clb_list = []
dat_objeto = None
time_differences = []

def fetch_data():
    global dat_ini_clb_list, dat_objeto, time_differences

    try:
        # Database connection settings
        #CONNECTION_STRING = 'DRIVER={ODBC Driver 17 for SQL Server};SERVER=(local)\\sqlexpress;DATABASE=***;UID=***;PWD=***'
        CONNECTION_STRING = 'DRIVER={ODBC Driver 17 for SQL Server};SERVER=(local)\\sqlexpress;DATABASE=***;Trusted_Connection=yes;'


        # Connect to the database
        connection = connect(CONNECTION_STRING)
        cursor = connection.cursor()

        # Query 1: Initial date and time of WO
        query1 = """
        SELECT DatIniClb
        FROM Calibra as ots
        JOIN TipTrabalho ON TipTrabalho.CodTipTrb = ots.CodTipTrb
        WHERE TipTrabalho.FlgPlando = 0 AND CodObjeto = 'DIV-0256'
        """

```

```
        cursor.execute(query1)
        results = cursor.fetchall()
        dat_ini_clb_list = [row[0] for row in results if row[0] is not None]
        dat_ini_clb_list.sort()

        # Query 2: Object Date
        query2 = """
        SELECT DatObjeto
        FROM Objectos
        WHERE CodObjeto = 'TRAS-0257'
        """

        cursor.execute(query2)
        dat_objeto_result = cursor.fetchone()
        dat_objeto = dat_objeto_result[0] if dat_objeto_result else None

        # Close the cursor and connection
        cursor.close()
        connection.close()

        # Calculate time differences in hours
        time_differences = []
        for i in range(1, len(dat_ini_clb_list)):
            difference = dat_ini_clb_list[i] - dat_ini_clb_list[i - 1]
            time_differences.append(difference.total_seconds() / 3600)

        # Update the status label
        status_label.config(text="Data fetched successfully")

    except Exception as e:
        messagebox.showerror("Error", str(e))

```

```
def calculate_parameters():
    if not time_differences:
        messagebox.showerror("Error", "No data available. Please fetch the data first.")
        return

    TTF = time_differences
    i = len(TTF)
    TTF.sort()
    # Convert to DataFrame
    #df = pd.DataFrame(TTF)

    # Export to Excel
    #df.to_excel("TTF3.xlsx", index=False)  # index=False to skip writing row numbers
    # Calculate Medium Ranks
    MR = [(n - 0.3) / (i + 0.4) for n in range(1, i + 1)]

    # Determine shape and scale parameters
    X = [math.log(ttf) for ttf in TTF]
    Y = [math.log(-math.log(1 - mr)) for mr in MR]

    par = np.polyfit(X, Y, 1)
    beta_param = par[0]  # Shape parameter
    bb = par[1]    # Intercept
    eta = 1 / math.exp(bb / beta_param)  # Scale parameter

    # Update the parameters in the UI
    beta_param_value_label.config(text=f"{beta_param:.4f}")
    eta_value_label.config(text=f"{eta:.4f}")

    # Calculate and display MTBF
    mttf = calculate_mtbf(eta, beta_param)
    mttf_value_label.config(text=f"{mttf:.4f}")

    # Calculate and display correlation coefficient (rho)
    rho = np.corrcoef(X, Y)[0, 1]
    rho_value_label.config(text=f"{rho:.4f}")
```

```
105
106     # Update the number of TTFs
107     ttf_count_label.config(text=f"{len(TTF)}")
108
109     return beta_param, eta, TTF, MR
110
111 def plot_graphs():
112     beta_param, eta, TTF, MR = calculate_parameters()
113
114     # Time values for plotting
115     t_value = np.linspace(0, max(TTF), 500)
116
117     # Probability Density Function (pdf)
118     def pdf(t):
119         return (beta_param / eta) * (t / eta) ** (beta_param - 1) * math.exp(-(t / eta) ** beta_param)
120
121     pdf_values = [pdf(t) for t in t_value]
122
123     # Reliability Function
124     def R(t):
125         return math.exp(-(t / eta) ** beta_param)
126
127     R_values = [R(t) for t in t_value]
128
129     # Failure Probability Function
130     def F(t):
131         return 1 - R(t)
132
133     F_values = [F(t) for t in t_value]
134
135     # Failure Rate Function
136     def gamma(t):
137         return pdf(t) / R(t)
138
139     gamma_values = [gamma(t) for t in t_value]
140
141      # Confidence levels
142      n = len(TTF)
143      F_5 = [beta.ppf(0.05, i, n - i + 1) for i in range(1, n + 1)]
144      F_95 = [beta.ppf(0.95, i, n - i +1) for i in range (1, n + 1)]
145
146      CL_lower_F = [eta*[math.log(1/(1-f))]**(1/beta_param) for f in F_5]
147      CL_upper_F = [eta*[math.log(1/(1-f))]**(1/beta_param) for f in F_95]
148
149      CL_lower_R = [eta*[math.log(1/(f))]**(1/beta_param) for f in F_5]
150      CL_upper_R = [eta*[math.log(1/(f))]**(1/beta_param) for f in F_95]
151
152      # Plotting graphs
153      fig, axs = plt.subplots(2, 2, figsize=(12, 10))
154
155      axs[0, 0].plot(t_value, F_values)
156      axs[0, 0].plot(CL_lower_F, MR, linestyle='--', label='Lower Bound (90%)', color='red',)
157      axs[0, 0].plot(CL_upper_F, MR, linestyle='--', label='Upper Bound (90%)', color='red',)
158      axs[0, 0].set_title('Probability of Failure vs. Time')
159      axs[0, 0].set_xlabel('Time to Failure [h]')
160      axs[0, 0].set_ylabel('Probability of Failure')
161
162      axs[0, 1].plot(t_value, R_values)
163      axs[0, 1].set_title('Reliability vs. Time')
164      axs[0, 1].plot(CL_lower_R, MR, linestyle='--', label='Lower Bound (90%)', color='red',)
165      axs[0, 1].plot(CL_upper_R, MR, linestyle='--', label='Upper Bound (90%)', color='red',)
166      axs[0, 1].set_xlabel('Time to Failure [h]')
167      axs[0, 1].set_ylabel('Reliability')
168
169      axs[1, 0].plot(t_value, pdf_values)
170      axs[1, 0].set_title('Probability Density Function (pdf)')
171      axs[1, 0].set_xlabel('Time to Failure [h]')
172      axs[1, 0].set_ylabel('Density')
173
```

```
    axs[1, 1].plot(t_value, gamma_values)
    axs[1, 1].set_title('Failure Rate vs. Time')
    axs[1, 1].set_xlabel('Time to Failure [h]')
    axs[1, 1].set_ylabel('Failure Rate [fail/h]')

    plt.tight_layout()
    plt.show()

def calculate_mtbf(eta, beta_param):
    return eta * math.gamma(1 + 1/beta_param)

def calculate_conditional_reliability():
    try:
        # Check if DatObjeto is retrieved
        if dat_objeto is None:
            messagebox.showerror("Error", "DatObjeto not available. Please fetch the data first.")
            return

        # Retrieve delta_t from the input entry
        delta_t = float(delta_t_entry.get())

        # Calculate T as the difference between current time and DatObjeto
        current_time = datetime.now()
        time_difference = current_time - dat_objeto
        T = time_difference.total_seconds() / 3600  # Convert time difference to hours

        beta_param, eta, TTF, MR = calculate_parameters()

        # Reliability Function
        def R(t):
            return math.exp(-(t / eta) ** beta_param)


        # Calculate conditional reliability
        R_T = R(T)
        R_T_plus_delta_t = R(T + delta_t)
        conditional_reliability = R_T_plus_delta_t / R_T

        # Update the conditional reliability in the UI
        conditional_reliability_label.config(text=f"{conditional_reliability:.4f}")

    except ValueError:
        messagebox.showerror("Error", "Invalid value for delta t. Please enter a numeric value.")

# Setup Tkinter window
root = tk.Tk()
root.title("Reliability Analysis")

# Create a frame for the buttons
frame = tk.Frame(root)
frame.pack(pady=10)

# Create and place the fetch button
fetch_button = tk.Button(frame, text="Fetch Data", command=fetch_data)
fetch_button.pack(side=tk.LEFT, padx=5)

# Create and place the calculate button
calculate_button = tk.Button(frame, text="Calculate Parameters", command=calculate_parameters)
calculate_button.pack(side=tk.LEFT, padx=5)

# Create and place the plot button
plot_button = tk.Button(frame, text="Plot Graphs", command=plot_graphs)
plot_button.pack(side=tk.LEFT, padx=5)

# Create a frame for displaying the parameters
param_frame = tk.Frame(root)
param_frame.pack(pady=10)
```

```
240
241     # beta_param parameter
242     tk.Label(param_frame, text="Shape Parameter (β):").grid(row=0, column=0, padx=5, pady=5)
243     beta_param_value_label = tk.Label(param_frame, text="N/A")
244     beta_param_value_label.grid(row=0, column=1, padx=5, pady=5)
245
246     # Eta parameter
247     tk.Label(param_frame, text="Scale Parameter (η):").grid(row=1, column=0, padx=5, pady=5)
248     eta_value_label = tk.Label(param_frame, text="N/A")
249     eta_value_label.grid(row=1, column=1, padx=5, pady=5)
250
251     # MTTF parameter
252     tk.Label(param_frame, text="Mean Time Between Failure (MTBF):").grid(row=2, column=0, padx=5, pady=5)
253     mttf_value_label = tk.Label(param_frame, text="N/A")
254     mttf_value_label.grid(row=2, column=1, padx=5, pady=5)
255
256     # Correlation coefficient (rho)
257     tk.Label(param_frame, text="Correlation Coefficient (ρ):").grid(row=3, column=0, padx=5, pady=5)
258     rho_value_label = tk.Label(param_frame, text="N/A")
259     rho_value_label.grid(row=3, column=1, padx=5, pady=5)
260
261     # Number of TTF values
262     tk.Label(param_frame, text="Number of TTF values:").grid(row=4, column=0, padx=5, pady=5)
263     ttf_count_label = tk.Label(param_frame, text="N/A")
264     ttf_count_label.grid(row=4, column=1, padx=5, pady=5)
265
266     # Create a frame for the conditional reliability
267     conditional_frame = tk.Frame(root)
268     conditional_frame.pack(pady=10)
269
270     # Delta t input
271     tk.Label(conditional_frame, text="Enter Δt:").grid(row=0, column=0, padx=5, pady=5)
272     delta_t_entry = tk.Entry(conditional_frame)
273     delta_t_entry.grid(row=0, column=1, padx=5, pady=5)
274
275 # Conditional reliability button
276 conditional_reliability_button = tk.Button(conditional_frame, text="Calculate Conditional Reliability", command=calculate_conditional_reliability)
277 conditional_reliability_button.grid(row=0, column=2, padx=5, pady=5)
278
279 # Conditional reliability result label
280 tk.Label(conditional_frame, text="Conditional Reliability R(Δt|T):").grid(row=1, column=0, padx=5, pady=5)
281 conditional_reliability_label = tk.Label(conditional_frame, text="N/A")
282 conditional_reliability_label.grid(row=1, column=1, padx=5, pady=5)
283
284 # Create and place the status label
285 status_label = tk.Label(root, text="")
286 status_label.pack(pady=10)
287
288 # Run the Tkinter event loop
289 root.mainloop()
```

Appendix B – Chi-square critical values table (adapted from [132], [133], [134]).

$\nu \backslash \alpha$	0,995	0,975	0,2	0,1	0,05	0,025	0,01	0,005
1	0,000	0,001	1,642	2,706	3,841	5,024	6,635	7,879
2	0,010	0,051	3,219	4,605	5,991	7,378	9,21	10,597
3	0,072	0,216	4,642	6,251	7,815	9,348	11,345	12,838
4	0,207	0,484	5,989	7,779	9,488	11,143	13,277	14,86
5	0,412	0,831	7,289	9,236	11,07	12,833	15,086	16,75
6	0,676	1,237	8,558	10,645	12,592	14,449	16,812	18,548
7	0,989	1,690	9,803	12,017	14,067	16,013	18,475	20,278
8	1,344	2,180	11,03	13,362	15,507	17,535	20,09	21,955
9	1,735	2,700	12,242	14,684	16,919	19,023	21,666	23,589
10	2,156	3,247	13,442	15,987	18,307	20,483	23,209	25,188
11	2,603	3,816	14,631	17,275	19,675	21,92	24,725	26,757
12	3,074	4,404	15,812	18,549	21,026	23,337	26,217	28,3
13	3,565	5,009	16,985	19,812	22,362	24,736	27,688	29,819
14	4,075	5,629	18,151	21,064	23,685	26,119	29,141	31,319
15	4,601	6,262	19,311	22,307	24,996	27,488	30,578	32,801
16	5,142	6,908	20,465	23,542	26,296	28,845	32,000	34,267
17	5,697	7,564	21,615	24,769	27,587	30,191	33,409	35,718
18	6,265	8,231	22,76	25,989	28,869	31,526	34,805	37,156
19	6,844	8,907	23,9	27,204	30,144	32,852	36,191	38,582
20	7,434	9,591	25,038	28,412	31,41	34,17	37,566	39,997
25	10,520	13,120	30,675	34,382	37,652	40,646	44,314	46,928
30	13,787	16,791	36,25	40,256	43,773	46,979	50,892	53,672
35	17,192	20,569	43,77	46,059	49,802	53,203	57,342	60,275
40	20,707	24,433	47,269	51,805	55,758	59,342	63,691	66,766

ν – degrees of freedom

α – significance level